Functional Nanocellulose from Oil Palm Empty Fruit Bunches Pulp

ノビトリ, ハスツチ

https://doi.org/10.15017/2534497

Functional Nanocellulose

from Oil Palm Empty Fruit Bunches Pulp

by

Novitri Hastuti

A Ph.D Thesis Submitted to Faculty of Agriculture
Department of Agro-Environmental Sciences
Graduate School of Bioresource and Bioenvironmental Sciences
Kyushu University, Japan
in partial fulfillment of the requirements for the degree of

Doctor of Philosophy

in

Agricultural Science

Prof. Takuya Kitaoka, Chair
Prof. Tetsuo Kondo
Assoc. Prof. Hirofumi Ichinose

Fukuoka, September 2019

Thesis Summary

The use of agricultural residues as inexpensive raw materials to produce high-value natural nanomaterials such as nanocellulose is aligned with the concept of Sustainable Development Goals (SDGs) by pioneering its promising functions in several applications. Nanocellulose derived from oil palm empty fruit bunches (OPEFB) pulp has been successfully extracted by hydrochloric acid hydrolysis and 2,2,6,6-Tetramethylpiperidine 1-oxyl (TEMPO) -mediated oxidation, respectively, affording cellulose nanocrystals (CNCs) and TEMPO-oxidized cellulose nanofibers (TOCNs). The CNC suspensions prepared from OPEFB by HCl hydrolysis remained stable without any sedimentation over 6 months. The OPEFB-derived CNCs exhibited high aspect ratios and superior thermal stability compared with those of woody CNCs. Very fine TOCNs in 3-nm thickness obtained from OPEFB pulps possessed high aspect ratios rather than 40 with various contents of carboxylates (1.0–1.5 mmol/g-TOCN), and showed good thermal stability.

Furthermore, highly-charged TOCNs from OPEFB were very effective in extractive fermentation to enhance butanol production. TOCNs were successfully applied to extractive fermentation using *Clostridium saccharoperbutylacetonicum* N1-4 as a butanol-producing strain. The butanol yield from free and immobilized cells remarkably increased in the presence of OPEFB-derived TOCNs. In the immobilized cell method, crosslinking of anionic carboxylate groups of TOCNs and alginate *via* Ca^{2+} ions to form alginate beads induced favorable 3-D networks for cell entrapment, and possibly provided better microenvironment for bacterial growth. The combination of OPEFB-derived TOCNs and alginate eventually yielded the highest total butanol production up to 37 g/L-broth.

From another viewpoint, the composite films of OPEFB-derived TOCNs and alginate performed as a pervaporation membrane for water/ethanol mixture, showing high flux as compared to PTFE commercial membrane. By applying pressure ranging from 30–40 hPa during the pervaporation, there was no micro-cracks observed on the membrane surface. Cross-linking between TOCNs and alginate presumably induced the change of pore sizes and surface areas, which are significant for adsorption capacity.

The use of CNCs and TOCNs from OPEFB as a reinforcing filler was tried to make polymer composites with poly(methylvinyl ether-*co*-maleic acid)–polyethylene glycol, and revealed different properties in surface roughness, optical transmittance, contact angles of water droplets, total color differences, thermal stability and mechanical properties. Fiber length of TOCNs affected the film properties, and induced higher mechanical performance as compared to other agricultural residues, confirming that the character of raw materials and the extraction process may play a critical role in forming nanocellulose properties.

Overall, this work revealed the potential of low cost biomass, OPEFB pulp, as a source of functional nanocellulose in bioenergy applications and as additives in various polymer composites. The obtained findings could open up a wider utilization of agricultural residues and unused biomass into novel value-added products by advanced nanocellulose technology.

Acknowledgements

First, I would like to express my grateful, it has been a great privilege for me to work under the supervision and counsel of Prof. Takuya Kitaoka, Ph.D and also for his warm welcome, a great support during my stay in Kyudai. My sincere thanks are go to Assoc. Prof. Hirofumi Ichinose, Ph.D, during my stay in Bioresources Chemistry (BRC) Laboratory. Throughout my time as graduate student, they been consistent and taking much attention in my research work, have never failed to provide support whenever possible. I especially thank them both for their kind patient and endurance for the rather slow of my work in doing Ph.D research and other assignments. I also deeply appreciate Prof. Tetsuo Kondo, Ph.D, for his critical review of my Ph.D thesis.

I am indeed grateful to Kyohei Kanomata, Ph.D for his hardwork, patient and endurance to teach me everything, regarding the laboratory works, reviewing my manuscript for several months, meaningful critics in every single word in my manuscript. I also wish to thank Mayumi Hatakeyama, Ph.D for her warm welcome and her kindly support and assistance of my son's daycare submission, daily business that need translation of Japanese documents and so on. I am useless without your help.

I also deliver my sincere thanks to Director of Forest Products Research and Development Center, FPRDC, Dr. Ir Dwi Sudharto, M.Si for giving the recommendation for me to pursue my doctoral degree in Kyushu University. I also would like to express my gratitude to Head of Dissemination and Collaboration Division, FPRDC, Dr. Wening Wulandari for meaningful support and discussions; and to my senior colleague, Prof. Gustan Pari, for encouraging me to do a research in nanocellulose. My deeply thanks also go to Kurnia Wiji Prasetyo from Biomaterial Research Institute, Indonesia, for helping me to provide empty fruit bunches pulp.

I deliver my thanks to my colleagues Dian Anggraini, Lisna Efiyanti and Santiyo Wibowo for giving support by beneficial discussion and providing the images of oil palm empty fruit bunches waste.

I will be remiss without thank to my colleague of most frequent talks, a Ph.D candidate from Madagascar, when I always did a mistake to spell his long name, my partner in talking, to remind my French. Merci beacoup Jessi. Tu me manqué. Je'espere que tu vais obtenir les meilleurs resultats pour ton doctorat. My sincere thanks go to Tsutsumi-san whom taught me how to prepare CNC at the early time when I started my Ph.D research. I also thank to other Ph.D candidate Xin Habaki, he has assisted me a lot over the years, everytime when I asked him, he always been there. I also thank to Hiroya Kimora, eventhough we do not have much interaction time, but he always been there for giving me a help. I thank you who were together at BRC lab: Uemura-san the most-friendly colleague during my first enrollment in Kyudai, Ardi and Saimura-san who picked me up at first time I came to Japan; and also for Ishihara-san, Tatebayashi-san, Kumamaru-san, Yukumitsu-san, Ukeba-san, Tamura-san, Miyata-san, Nakamura-san, Yoshida-san, Ichibakase-san. May good luck always along with you. I have been fortunate to work in the same lab with all BRC members: Yusaku Hirayama, the person who most entertained me over the years, Koki Ozono, Yurika Nagatomo, Naoya Fukuda, Natsuki Masunaga, Megumu Honda, Tomoka Noda and Haruka Sato for their help and friendship over the days and years. I express my sincere thanks to Midori Watanabe Sensei and Yumi Fukunaga, Ph.D for all meaningful assistance during my analysis at Center of Advanced Analysis and at the Ultramicroscopy Research Center of Kyushu University. I also deliver my sincere thanks to Sonomoto Sensei, Zendo Sensei, Goto Sensei, Yokota Sensei, Hasegawa Sensei, Shiratori Sensei for providing their laboratory apparatus to me then I can

complete my analysis. My partners in research collaborator, Rizki Fitria, Safrina Dyah and Hendrik Setiawan. Thank you very much for all your support then I can finish my experiment with supporting analysis.

To my family, My Dad in immortality, my beloved Mom, my siblings Dedi and Feri, there are not enough words how lucky I am to be your daughter and sister. Your prayers and encouragements are very meaningful to build up my spirit in my hardest time in Japan. To my dearest husband, Imam Budiman, I dedicate this work to you because you have travelled this road alongside me, with love, patient and devotion. My little angles, Syahida and Syauqi, for your sincere understanding of mama's time. You are truly heroes for mama. Thank you for enduring the long hours I have spent away and all the tough time we have been through. May Allah always bless you. All my colleagues from Indonesia, there are too many names to mention individually, but I deeply thanks to you all.

The last but the most important, for my God, Allah SWT, who granted me healthy, patience, guidance and bless during my Ph.D time. Alhamdulillah tsumma Alhamdulillah.

Fukuoka, September 2019

Novitri Hastuti

Table of Contents

List of Figures

List of Tables

List of Abbreviations

ABE	Acetone-Ethanol-Butanol
ACC	Aqueous Collision Counter
ADP	Adenosine diphosphate
AFM	Atomic Force Microscopy
AK	Acetate Kinase
ATP	Adenosine triphosphate
BADH	Butyraldehyde dehydrogenase
BC	Bacterial Cellulose
BDH	Butanol Dehydrogenase
BET	Brunauer-Emmett-Teller
BK	Butyrate Kinase
BNC	Bacterial Nanocellulose
BuOH	Butanol
CNFs	Cellulose Nanofibrils
cm	centimeter
CoA	Coenzyme A
CoAT	CoA Transferase
CNCs	Cellulose Nanocrystals
CO	Film of CNC from Oil Palm Empty Fruit Bunches
CPO	Crude Palm Oil
CrI	Crystallinity Index
DCW	Density Cell Weight
DI	Deionized
DMAc	Dimethylacetamide
DP	Degree Polymerization
DTG	Differential Thermogravimetry
EFB	Empty Fruit Bunches
FFBs	Fresh Fruit Bunches
FTIR	Fourier Transform Infrared
g	gram
HCl	Hydrochloric Acid
H_2SO_4	Sulfuric Acid
i.e	id est
IR	Infrared
IUPAC	International Union of Pure and Applied Chemistry

KBr	Potassium Bromide
K_d	Coefficient Distribution
kPa	kiloPascal
kV	kilovolt
mm	millimeter
mL	milliliter
mM	millimolar
µm	micrometer
µL	microliter
MPa	MegaPascal
NaBr	Sodium Bromide
$NaBH_4$	Sodium Borohydride
NaCl	Sodium Chloride
NaClO	Sodium Hypochlorite
NAD^+	Nicotinamide Adenine Dinucleotide (oxidized form)
NADH	Nicotinamide Adenine Dinucleotide (reduced form)
$NADP^+$	Nicotinamide Adenine Dinucleotide Phosphate (oxidized form)
NADPH	Nicotinamide Adenine Dinucleotide Phosphate (reduced form)
NaOH	Sodium Hydroxide
NC	Nanocellulose
NCC	Nanocrystalline Cellulose
nm	nanometer
OD	Optical Density
OPEFB	Oil Palm Empty Fruit Bunches
op-TOCN	TOCN derived from oil palm empty fruit bunches
op-TOCN-A	op-TOCN in Alginate Matrix
Pa	Pascal
PB	Phosphate Buffer
PCA	Poly (Acrylamide)
PEG	Poly (Ethylene Glycol)
PLA	Poly (Lactic Acid)
PMVEMA	Poly (Methyl Vinyl Ether Maleic Acid)
PVA	Poly (Vynil Alcohol)
POME	Palm Oil Mill Effluent
PTA	Phospotransacetylase
PTB	Phospotransbutyrylase
PTFE	Polytetrafluoroethylene

RH	Relative Humidity
SDGs	Sustainable Development Goals
SEM	Scanning Electron Microscopy
TCL	TOCN from company (long)
TCS	TOCN from company (short)
TEM	Transmission Electron Microscopy
TEMPO	2,2,6,6-tetramethylpiperidine 1-oxyl
TG	Thermogravimetry
TGA	Thermogravimetric Analysis
TO	Film of TOCN from oil palm empty fruit bunches
TOCNs	TEMPO-Oxidized Cellulose Nanofibers
T_{on}	Temperature of initial degradation (ºC)
T_{max}	Temperature of maximum degradation (ºC)
TYA	Tryptone-Yeast extract-Acetate
UV/Vis	Ultra Violet/Visible
w-TOCN	TOCN derived from Wood (commercial TOCN)
w-TOCN-A	w-TOCN in Alginate Matrix
XRD	X-ray Diffraction

Chapter 1

Introduction

1.1 Oil Palm Empty Fruit Bunches

Oil palm (*Elaeis guineensis*) is one of the major plantation commodities in Indonesia [1]. Total area of oil palm plantation in 2017 reached 13.20 million Ha, with the total production of crude palm oil (CPO) around 34.47 million ton and the total export value reached US$ 21 billion [2]. Almost half of the fruit mass of *E. guineensis* is considered as byproduct or waste and is burned in mill boilers or is discarded in the stabilization ponds as palm oil mill effluent (POME) [3]. The process of fresh fruit bunches (FFBs) into CPO results in biomass wastes in large amount of oil palm empty fruit bunches (OPEFB). This OPEFB, which is wastes in palm oil factories, is quite abundant, are often incinerated at the plant site which causes some air pollution [4]. Along with the unprecedented increase in the palm oil industry in Indonesia, the generation of OPEFB is increasing every year [5]. The palm oil industry must dispose about 1.1 ton of OPEFB for every ton of CPO produced [1].

Practically, some of byproducts from oil palm industries are used as fuel in boiler to generate steam to run a turbine to generate electricity [6]. OPEFB is byproduct of agricultural production and processes, so they do not require additional land, energy or water to produce them [7]. Empty fruit bunch is the fibrous mass left behind after separating the fruits from sterilized (steam treatment at 294 kPa for 1 h) FFB [8]. Nowadays, OPEFB residues have not been optimally used, because they are wet, bulky and voluminous which are unfavorable for handling and transportation [9]. However, biomass of OPEFB is still underutilized due to the limited application and gain attention over their disposal management [10]. Therefore, the utilization of OPEFB as

agricultural waste for functional biomaterials production is attracting attention as an effort to use biomass as raw materials to be converted as added value/novel products.

Figure 1.1 Optical images of huge amount of oil palm empty fruit bunches waste

The utilization of bio-based renewable materials is increasing from consumers and industry. This is driven by the environmental issue such as *green life-style* and *green consumer* which have been encouraged by global and/or local acts and regulations to support the sustainable development goals (SDGs). In addition, the petroleum market fluctuations and the realization that petroleum is finite resource make the utilization of biomaterials from biomass is becoming important. Furthermore, the wastes from biomass such as agricultural wastes and forest residues have high potential for reuse as fuel or feedstock for production of high value-added materials without the competition with human and animal food chains [11]. OPEFB is one of promising biomass to be proceed as functional biomaterials. The potential products from abundance amount of OPEFB [12] which have been reported previously such as for activated carbon, fermentable sugars, reinforcing agent in polymer composite, biogas production, sustainable acoustic absorber, as media for fungus cultivation and nanocellulose [13–18]. Oil palm empty fruit bunches fibers are extracted from EFB by

retting process. The available retting processes are mechanical retting (hammering), chemical retting (boiling with chemicals), steam/vapor retting and water/microbial retting [8].

OPEFB typically comprises of three part of chemical component which are: cellulose (44%–59%), hemicellulose (12%–31%) and lignin (14%–25%) [19,20] is still considered as an under-utilized resource. In view of its high cellulose content, cellulose from OPEFB is attracting interest because cellulose has attractive properties and can be processed as a new functional material by chemical modifications and can be applied to enormous industrial applications. Cellulose was extracted from OPEFB by chlorite bleaching, alkali treatment and acid hydrolysis. Chlorite bleaching has the function of extracting holocellulose from raw cellulose fiber, to remove most of the lignin present in the fibers and leads the defibrillation, alkali treatment is a process used to solubilize the lignin and the remaining pectins and hemicellulose, and acid hydrolysis is used to degrade the amorphous cellulose [21]. The pulp of OPEFB after bleaching and alkali treatment showed rough surface. Furthermore, the smoother surface was observed after pre-treated in hot water as described in **Fig. 1.2**.

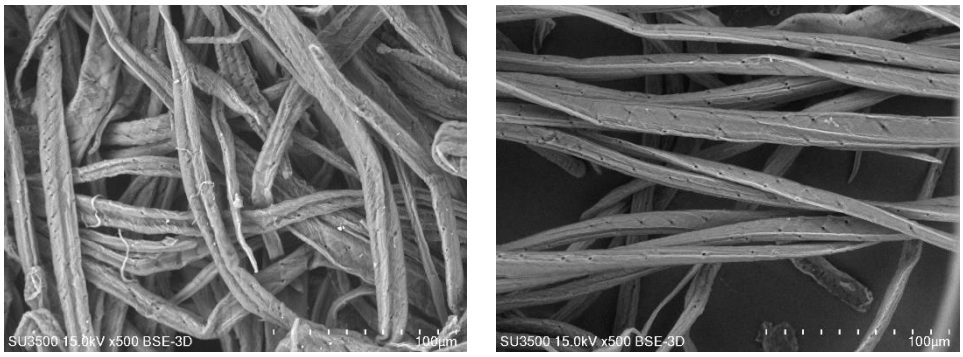

Figure 1.2 SEM images of OPEFB pulp after bleaching and alkali treatment (left) and OPEFB pulp after pre-treated in hot water (right)

1.2 Cellulose and Nanocellulose

Plant biomass resources are complex materials that generally consist of 3 major organic fractions: lignin, cellulose, and hemicellulose. Lignin is a complex, high-molecular-weight structure containing cross-linked polymers of phenolic monomers. Lignin in the primary cell wall provides structural support, impermeability, and resistance against microbial attack. Cellulose is the main structural constituent in plant cell walls and is composed of long chains of cellobiose units that are linked to D-glucose subunits through β-(1,4)-glycosidic bonds. These linkage bonds are broken by hydrolysis, which are catalyzed by cellulase or acids. Hemicellulose consists of branches of short lateral monosaccharides such as pentose (xylose, rhamnose, and arabinose), hexose (glucose, mannose, and galactose), and uronic acid. Cellulose in cell walls are packed into microfibrils by the long-chain cellulose polymers linked by hydrogen and van der Waals bonds, which are protected by hemicellulose and lignin [22]. There are several sources of cellulose which had been widely acknowledged such as: wood, plant, tunicate, algae and bacterial [23]. Native cellulose consists of crystalline microfibrils 3−10 nm in width and several microns in length depending on

the origins [24]. In cellulose structure, each glucose residue is rotated by 180° relative to its neighbours, so that the basic repeating unit is in fact cellobiose. Chain length varies between 100 and 14000 residues. The chains are oriented in parallel and highly ordered, crystalline domain interspersed by more disordered, amorphous region [25]. This amorphous region makes the cellulose susceptible to acid hydrolysis and breakdown into individual crystallite [26]. Cellulose chains aggregate into the repeated crystalline structure to form microfibrils in the plant cell wall, which also aggregate into larger macroscopic fibres. This hierarchical structure that is essentially deconstructed in order to generate cellulose nanofibres from plants [27].

The crystal part of cellulose cannot be broken due to strong hydrogen bond of hydroxy groups in cellulose. Rather cellulose crystalline has several polymorphs: cellulose I, II, III, IV. Cellulose I is the crystalline cellulose that is naturally produced by a variety of organisms, which is sometimes referred to as natural cellulose. Its structure is thermodynamically metastable and can be converted to either cellulose II or III. Cellulose II is the most stable crystalline structure and can be produced by regeneration and mercerization [28].

There are two polymorphs of cellulose I, which are cellulose I_α and I_β. Both are present in native cellulose structures but their ratio depends on the source of cellulose. There are slightly differences of cellulose geometry between cellulose I_α and I_β. In cellulose Iα the alternation is down in the same chain, in cellulose I_β the alternation is between conformationally distinct chains [29]. The Iα structure is the dominant polymorph for most algae and bacteria, while I_β is dominant polymorph for higher plant cell wall and in tunicates [30,31]. Hydrogen (H) bonds in intra and inter chain of cellulose chains play a key role in determining thermostability and stiffness properties of cellulose composite. The H-bonding network in cellulose contributed to the

plasticity properties of cellulose due to frustration and redundancy in the replacement of H-bonds that give rise to stability over a wide range of temperatures [32].

Cellulose belongs to renewable sustainable biological resources that little affect the environment and humans and do not cause risks to health and safety in the industries [33]. Cellulose is the most abundant natural polymer which can be used to propose rational solutions for replacing fossil oil-based products with bio-based ones and resolve numerous issues of environmental pollution, carbon footprint and sustainability [34,35].

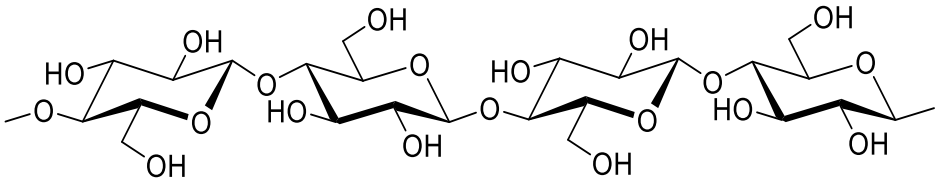

Figure 1.3 The repeat unit of cellulose

Cellulose is one of the most important natural polymers, an almost inexhaustible raw material, and a key source of sustainable materials on an industrial scale. Therefore, the study of cellulose in order to extract nanocellulose form its bulk microfibrils is generating much activity. Nanocellulose has received considerable interest during the last decade. Isogai had concluded that there are several reasons for the greatly interest in nanocellulose: (1) nanocelluloses can be produced from abundant wood biomass partly using conventional and already established pulping/ bleaching technologies; (2) recent advances in nanotechnology-related science and engineering such as carbon nanotubes and graphene have opened up new applications in high-tech material fields; (3) nanocelluloses originating from reproducible wood biomass are thought to be much more preferential and beneficial in terms of production process, energy consumption, and environmental and safety issues; (4) pulp and paper industry particularly in

developed countries has been looking for new application of wood fibers and therefore (5) nanocelluloses have great potential to be used as new bio-based nanomaterials [36].

Novel methods have been developed to produce nanocellulose in range of top-down methods involving enzymatic/chemical/physical methodologies for their isolation from wood and forest/agricultural residues to the bottom-up production of cellulose nanofibrils from glucose by bacteria [37]. The special attention is the size of nanocellulose fiber which generally contains less than 100 nm in diameter and several micrometers in length [11].

Typically, two main types of nanocellulose are distinguished: (i) the one obtained by acid treatment referred to as cellulose nanocrystals (CNCs) and (ii) produced mainly by mechanical disintegration called cellulose nanofibrils (CNFs) [34]. In addition, some literatures included other type of nanocellulose derived from bacteria which called as bacterial nanocellulose (BNC) [37]. CNCs are subject to nanocellulose extraction by acid hydrolysis assisted by ultrasonication/ mechanical treatments. It has a rod-like-shape or whisker shape (can be denoted as cellulose nanowhiskers) and have a high aspect ratio with 3–5 nm wide and 50–500 nm in length. Cellulose nanocrystals produced by sulfuric acid hydrolysis have negatively charged (anionic) sulfonate ester groups leading to easily disperse in aqueous solvents due to electrostatic repulsion. However, CNCs can be generated using hydrochloric acid, although a weaker charge density results from this processing route, leading to poorer dispersion in organic solvents [26]. In addition, increasing the acid to fibers ratio and hydrolysis time reduced the dimension of CNCs [38].

CNFs is usually extracted by mechanical disintegration and has longer fibril shapes compared with CNCs. CNFs are reminiscent of elementary fibrils in the wood and plant cellulose biosynthesis process and are considered to consist of 36 cellulose

chains arranged in Iß crystal structure with a high aspect ratio by having 4-20 nm in wide and 500-2000 nm in length [23]. Recently, the extraction of individual nanofibers in 3-4 nm wide has been developed by low energy in mild condition using TEMPO (2,2,6,6-tetramethylpiperidine-1-oxyl radical)-mediated oxidation and denoted as TEMPO-oxidized cellulose nanofibers (TOCNs). TEMPO-mediated oxidation was first applied by de Nooy and co-authors in various substrate of glucans and its derivatives in TEMPO/NaClO/NaBr system using water as solvent [39]. This method made the oxidation selectively occurred on primary hydroxyl groups of polysaccharides under mild and aqueous condition, significant amounts of C6 carboxylate groups are selectively formed [40,41]. The oxidation proceeded throughout the fibers but occurred only at the surface of microfibrils therefore become negatively charged without change the original fibers morphology [24,42]. Classical technique to extract CNFs by mechanical treatment to disrupt the association of microfibrils is not enough to suspend the microfibrils in water. TEMPO-mediated oxidation induced the microfibrils disintegration become faster due to the electric repulsion between microfibrils and loosening the adhesion between microfibrils by the significant amount of carboxylate groups introduced on the microfibrils surface [42]. Condition of TEMPO-mediated oxidation influenced the obtained nanofibrils. Longer time of oxidation revealed higher amount of carboxylate content and nanofibrils yield [24]. However, Saito and Isogai reported that prolong the reaction time induced higher carboxylate or aldehyde content and decreased the degree of polymerization (DP); but the amount of carboxylate content at certain reaction time level reached plateau level and leveling off-DP occurred. This fact due to the periodical distribution of disordered regions present along cellulose structure has probably brought about such leveling-off DP [40].

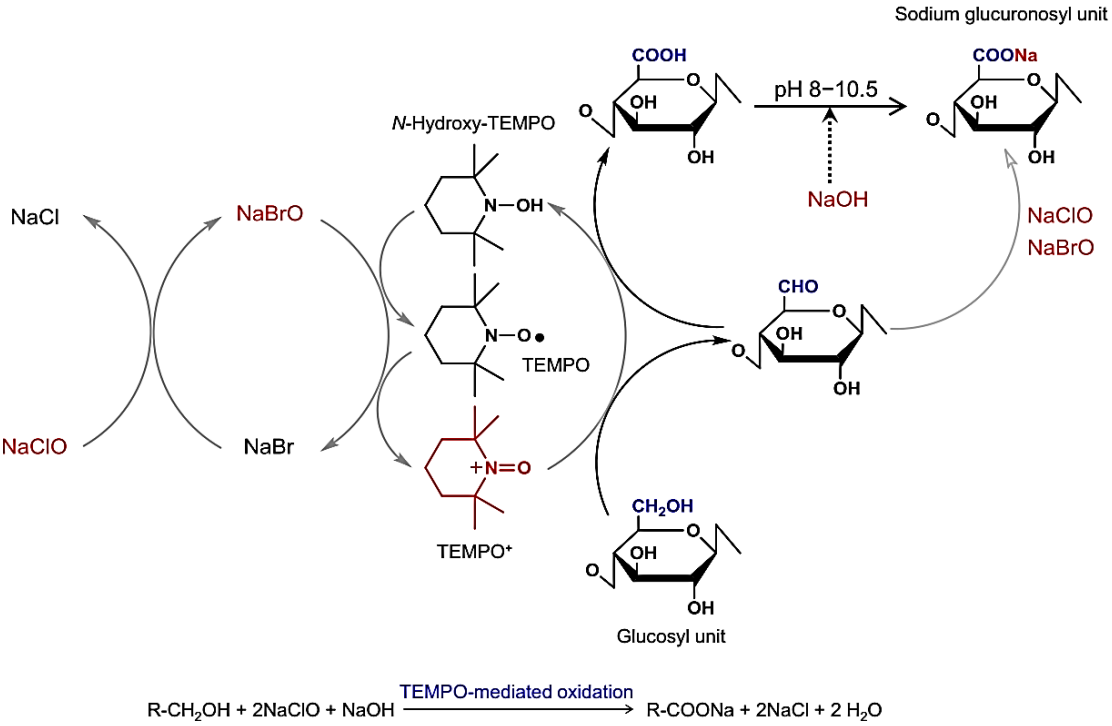

Figure 1.4. Mechanism of TEMPO-mediated oxidation for the conversion of primary hydroxy groups in cellulose into sodium C6-carboxylate groups using TEMPO/NaBr/NaClO in water at pH 10 (Reprinted from the Ref. 43 with the license from Elsevier)

The novel method invented by Kondo et al. (2008) is known as wet-pulverizing of polysaccharides method using aqueous counter collision (ACC) scheme also effective to produce bionanofibers without chemical modification including depolymerization [44]. This method works by ejecting a liquid suspension of the sample containing polysaccharide through a pair of nozzles under high pressure ranging from 70 to 270 MPa forms a pair of water jets. The diameter of nozzles is 100-200 µm and angle of collision between two jets is typically in range 95°-178°. The number of ejection steps and ejection pressure may be adjusted to desired quantity of

pulverizing cycles or “pass” which potentially can be repeated between 1-180 passes. The properties of nanofibers of microcrystalline cellulose obtained by ACC method revealed nanoscale dimension by having diameter ranging from 14-20 nm and length ranged from 0.72-1.3 μm [44,45].

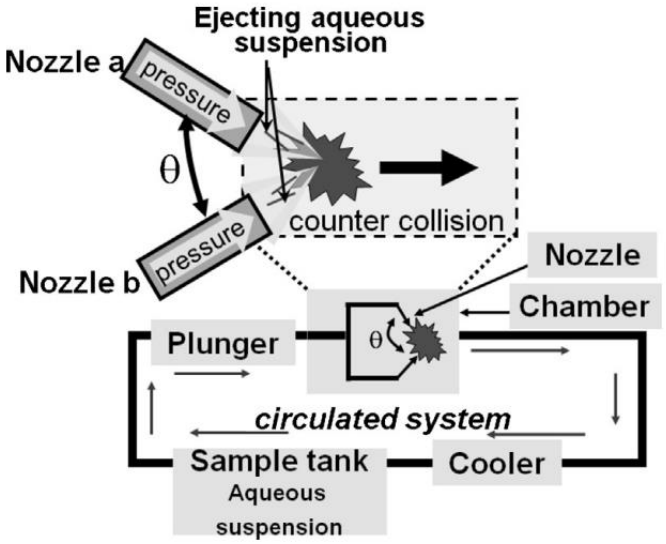

Figure 1.5. The dual water jet in aqueous collision counter (ACC) system. Reprinted from Ref 45 with the license from Elsevier

Combination of TEMPO-mediated oxidation and ACC method had been applied to produce CNF from hardwood and softwood. The study reported that by combining TEMPO-mediated oxidation time in range 1-3 h with 5 passes of ACC generated nanocellulose with high aspect ratio > 40 [46]. The ACC method was successfully applied to produce nanofibers from pellicle secreted by Gluconoacetobacter xylinus, a strain of cellulose-producing bacteria, yielded nanofibers with the crystallinity ~70% [47]. Cellulose produced from bacteria then grouped as bacterial cellulose (BC).

Bacterial cellulose (BC) is mainly produced from those belonging to the genus Gluconoacetobacter, produce a very peculiar form of cellulose with mechanical

andstructural properties can be applied in various applications [48]. The characteristics of CNCs, CNFs and BNC can be distinguished from their differences in morphology and physical properties. CNCs are 100-250 nm; CNFs are 0.1-2 μm and BNC has different types of nanofibers networks in lenght. CNC has degree polymerization (DP) ranged from 500-15000, meanwhile the DP of CNF is ≥ 500 and BNC is 4000 – 10000. The degree of crystallinity of BNC is highest by having crystal structure of cellulose Iα (shell) and Iß (core). CNC has medium degree of crystallinity and composed of primarily cellulose Iß and sometimes cellulose Iα. In addition, CNF is considered as the lowest degree of crystallinity and its crystal structure is primarily cellulose Iß [49].

Nanocellulose has outstanding properties compared with the original cellulosic fiber but also when compared with other materials normally used as reinforcements in composite materials such as Kevlar or steel wires [23]. The present of hydroxyl groups on the surface of nanocellulose favors the formation hydrogen bonding and plays a critical role in the nature of adhesion between nanocellulose and other polymeric materials [50]. The study of nanocellulose is not only about its extraction from biomass, but also the new applications in various fields [11]. The high demand for nanocellulose by market in 2017 is coming from several sectors such as: pulp and paper 14%; composites 30%; paints-films-coatings 15%; rheological modifiers 8%; filtration 8%; medicine and life sciences 7%; aerogels 5%; construction 4% and oil 2% [51]. The impressive mechanical properties, reinforcing capabilities, abundance, low density, and biodegradability of nanocellulose make them ideal candidates for the processing of polymer nanocomposites [52]. Recently, the utilization of nanocellulose has been intensively reported such as in medical applications for tissue engineering scaffold and fibroblast cells growth, in composite as reinforcing agent, metal nanoparticle

deposition, polymer brushes and so on [49,53]. Therefore, the study of functional nanocellulose, particularly nanocellulose derived from agricultural residue is being important.

1.3 Utilization of Nanocellulose from Oil Palm Biomass

Cellulose was extracted from OPEFB by chlorite bleaching, alkali treatment and acid hydrolysis. Chlorite bleaching has the function of extracting holocellulose from raw cellulose fiber, to remove most of the lignin present in the fibers and leads the defibrillation, alkali treatment is a process used to solubilize the lignin and the remaining pectins and hemicellulose, and acid hydrolysis is used to degrade the amorphous cellulose [21].

Nanocellulose preparation derived from OPEFB have been reported by a few researchers. Cellulose nanofibers of OPEFB prepared by chemo-mechanical treatments (grinding and high pressure homogenization) revealed nanoscale dimension by having diameter ranged from 5-40 nm and was narrower than that of nanofibers isolated from the rubberwood (10-90 nm) [16]. CNF of OPEFB isolated by 64 wt% sulfuric acid hydrolysis assisted by sonication showed that the degree of polymerization (DP) and CNF length decreased as the hydrolysis time was increased from 15 min to 90 min [54]. In addition, the preparation of CNC from OPEFB via chemical and ultrasonication showed high degree crystallinity and thermal stability [20,55]. Highly stable and dispersible nanocrystalline cellulose (NCC) was successfully isolated from OPEFB microcrystalline cellulose (OPEFB-MCC), with yields of 93% via a sono-assisted TEMPO-oxidation and a subsequent sonication process [56].

Utilization of nanocellulose derived from oil palm biomass had been reported by Elias and co-authors as reinforcing agent in chitosan-nanocellulose beads to immobilize Candida rugosa lipase for efficient production of butyl butyrate. The raw materials were oil palm frond leaves [57,58]. Haafiz et al. reported the use of cellulose nanowhiskers from microcrystalline OPEFB using chemical swelling method in polylactic acid (PLA) composite [59]. The study about nanocellulose utilization from OPEFB is still limited compared to thus the reported studies about the nanocellulose extraction.

The studies about nanocellulose extraction from OPEFB is mostly reported the use of sulfuric acid as the solvent for hydrolysis. Therefore, in this study, hydrochloric acid was chosen as the solvent for hydrolysis. Application of nanocellulose of OPEFB from the previous reported studies demonstrated the limited information about its utilization in wider applications.

In this work, functional nanocellulose from OPEFB is presented, including production of nanocellulose and the application of nanocellulose derived from OPEFB.

Moreover, the wastes from biomass such as agricultural wastes and forest residues have high potential for reuse as fuel or feedstock for production of high value-added products without the competition with human and animal food chains [11].

1.4 Research Goals

The first goal of this study is to produce nanocellulose derived from OPEFB. Two main pathways to produce nanocellulose were chosen: (a) using hydrochloric acid hydrolysis and (b) 2,2,6,6-tetramethylpiperidine 1-oxyl (TEMPO) in TEMPO/NaClO/NaBr system at pH 10 by modifying the amount of oxidant to produce TOCNs with different amounts of carboxylate content. The second goal is to observe

the OPEFB nanocellulose in several applications. The following specific activities were set to accomplish the research goals:

a) Evaluate the characteristics and properties of obtained nanocellulose from OPEFB produced by hydrochloric acid and TEMPO-mediated oxidation using different amount of oxidant (NaClO).
b) Evaluate the performance of obtained nanocellulose from OPEFB in extractive fermentation to produce bio-butanol and pervaporation membrane
c) Evaluate the performance of obtained nanocellulose from OPEFB as reinforcing agent in polymeric matrix.

1.5 Outline of Dissertation

General information related to OPEFB as agricultural residue, a literature review about cellulose and nanocellulose, in which we address multiple aspects of cellulose structure, nanocellulose terms and reported studies of OPEFB nanocellulose utilization is in Chapter 1.

In Chapter II, preparation and characterization of nanocellulose using hydrochloric acid hydrolysis and TEMPO-mediated oxidation is presented. The pretreatment of OPEFB pulps before acid hydrolysis and varying the amount of oxidants used in oxidation as treatments are demonstrated.

Application of nanocelulose in bioenergy applications as enhancer in extractive fermentation to produce biobutanol and water-ethanol mixture separation are in Chapter 3.

Futhermore, in other view of point, application of nanocellulose as reinforcing agent in polymeric matrices is presented. A comparison of other agricultural residues

as reinforcing agent is also discussed in Chapter 4. Overall conclusions regarding the nanocellulose production and applications are given in Chapter 5.

1.6 References

[1] K. Myrtha, H. Onggo, A.D. Abdullah, A. Syampurwadi, Effect of oil palm empty fruit bunch fiber on the physical and mechanical properties of fiber glass reinforced polyester resin, J. Biol. Sci. 8 (2008) 101–106.

[2] BPS-Statistics Indonesia, Indonesian Oil Palm Statistics, BPS-Statistics Indonesia, Jakarta, 2018.

[3] N.F. Souza, J.A. Pinheiro, A.I.S. Brígida, J.P.S. Morais, M. de sá M. de Souza Filho, M. de Freitas Rosa, Fibrous residues of palm oil as a source of green chemical building blocks, Ind. Crops Prod. 94 (2016) 480–489. doi:10.1016/j.indcrop.2016.09.012.

[4] Y. Sudiyani, D. Styarini, E. Triwahyuni, Sudiyarmanto, K.C. Sembiring, Y. Aristiawan, H. Abimanyu, M.H. Han, Utilization of biomass waste empty fruit bunch fiber of palm oil for bioethanol production using pilot–scale unit, Energy Procedia. 32 (2013) 31–38. doi:10.1016/j.egypro.2013.05.005.

[5] N. Razali, M.S. Hossain, O.A. Taiwo, M. Ibrahim, N.W. Mohd Nadzri, N. Razak, N.F. Mohammad Rawi, M. Mohd Mahadar, M.H. Mohamad Kassim, Influence of acid hydrolysis reaction time on the isolation of cellulose nanowhiskers from oil palm empty fruit bunch microcrystalline cellulose, BioResources. 12 (2017) 6773–6788. doi:10.15376/biores.12.3.6773-6788.

[6] S. Vijaya, a N. Ma, Y.M. Choo, N.I.K. Meriam, Life Cycle Inventory of the Production of Crude Palm Oil, J. Oil Palm Res. 20 (2008) 484–494. http://palmoilis.mpob.gov.my/publications/joprv20june-vijaya.pdf.

[7] J. Kudakasseril Kurian, G. Raveendran Nair, A. Hussain, G.S. Vijaya Raghavan, Feedstocks, logistics and pre-treatment processes for sustainable lignocellulosic biorefineries: A comprehensive review, Renew. Sustain. Energy Rev. 25 (2013) 205–219. doi:10.1016/j.rser.2013.04.019.

[8] S. Shinoj, R. Visvanathan, S. Panigrahi, M. Kochubabu, Oil palm fiber (OPF) and its composites: A review, Ind. Crops Prod. 33 (2011) 7–22. doi:10.1016/j.indcrop.2010.09.009.

[9] J.D. Coral Medina, A.L. Woiciechowski, A. Zandona Filho, L. Bissoqui, M.D. Noseda, L.P. de Souza Vandenberghe, S.F. Zawadzki, C.R. Soccol, Biological activities and thermal behavior of lignin from oil palm empty fruit bunches as potential source of chemicals of added value, Ind. Crops Prod. 94 (2016) 630–637. doi:10.1016/j.indcrop.2016.09.046.

[10] M.A. Hassan, M.A.A. Farid, Y. Shirai, H. Ariffin, M.R. Othman, M.H. Samsudin, M.Y. Hasan, Oil palm biomass biorefinery for sustainable production of renewable materials, Biotechnol. J. (2019) 1800394. doi:10.1002/biot.201800394.

[11] P. Phanthong, P. Reubroycharoen, X. Hao, G. Xu, A. Abudula, G. Guan, Nanocellulose: Extraction and application, Carbon Resour. Convers. 1 (2018) 32–43. doi:10.1016/j.crcon.2018.05.004.

[12] S.S. Mohtar, T.N.Z. Tengku Malim Busu, A.M. Md Noor, N. Shaari, H. Mat, An ionic liquid treatment and fractionation of cellulose, hemicellulose and lignin from oil palm empty fruit bunch, Carbohydr. Polym. 166 (2017) 291–299. doi:10.1016/j.carbpol.2017.02.102.

[13] S. Palamae, P. Dechatiwongse, W. Choorit, Y. Chisti, P. Prasertsan, Cellulose and hemicellulose recovery from oil palm empty fruit bunch (EFB) fibers and

production of sugars from the fibers, Carbohydr. Polym. 155 (2017) 491–497. doi:10.1016/j.carbpol.2016.09.004.

[14] M.A. Abdullah, M.S. Nazir, M.R. Raza, B.A. Wahjoedi, A.W. Yussof, Autoclave and ultra-sonication treatments of oil palm empty fruit bunch fibers for cellulose extraction and its polypropylene composite properties, J. Clean. Prod. 126 (2016) 686–697. doi:10.1016/j.jclepro.2016.03.107.

[15] D.C. Nieves, K. Karimi, I.S. Horváth, Improvement of biogas production from oil palm empty fruit bunches (OPEFB), Ind. Crops Prod. 34 (2011) 1097–1101. doi:10.1016/j.indcrop.2011.03.022.

[16] M. Jonoobi, A. Khazaeian, P.M. Tahir, S.S. Azry, K. Oksman, Characteristics of cellulose nanofibers isolated from rubberwood and empty fruit bunches of oil palm using chemo-mechanical process, Cellulose. 18 (2011) 1085–1095. doi:10.1007/s10570-011-9546-7.

[17] A. Arum Sari, A. Kristiani, S. Tachibana, Y. Sudiyani, H. Abimanyu, Mechanisms and optimization of oil palm empty fruit bunch as a pre-grown source for white-rot fungus to degrade DDT, J. Environ. Chem. Eng. 2 (2014) 1410–1415. doi:10.1016/j.jece.2014.07.018.

[18] N.B. Osman, N. Shamsuddin, Y. Uemura, Activated carbon of oil palm empty fruit bunch (EFB); core and shaggy, Procedia Eng. 148 (2016) 758–764. doi:10.1016/j.proeng.2016.06.610.

[19] R. Sun, J. Bolton, L. Mott, J. Fang, Fractional isolation and characterization of polysaccharides from oil palm trunk and empty fruit bunch fibres, Holzforschung. 53 (1999) 253–260. doi:10.1515/HF.1999.043.

[20] Z.A.Z. Azrina, M.D.H. Beg, M.Y. Rosli, R. Ramli, N. Junadi, A.K.M.M. Alam, Spherical nanocrystalline cellulose (NCC) from oil palm empty fruit bunch pulp

via ultrasound assisted hydrolysis, Carbohydr. Polym. 162 (2017) 115–120. doi:10.1016/j.carbpol.2017.01.035.

[21] Y.C. Ching, T.S. Ng, Effect of Preparation Conditions on Cellulose from Oil, BioResources. 9 (2014) 6373–6385. doi:10.15376/biores.9.4.6373-6385.

[22] J. Pérez, J. Muñoz-Dorado, T. De La Rubia, J. Martínez, Biodegradation and biological treatments of cellulose, hemicellulose and lignin: An overview, Int. Microbiol. 5 (2002) 53–63. doi:10.1007/s10123-002-0062-3.

[23] R.J. Moon, A. Martini, J. Nairn, J. Simonsen, J. Youngblood, Cellulose nanomaterials review: structure, properties and nanocomposites., 2011. doi:10.1039/c0cs00108b.

[24] T. Isogai, T. Saito, A. Isogai, Wood cellulose nanofibrils prepared by TEMPO electro-mediated oxidation, Cellulose. 18 (2011) 421–431. doi:10.1007/s10570-010-9484-9.

[25] P. Béguin, J. Paul Aubert, The biological degradation of cellulose, FEMS Microbiol. Rev. 13 (1994) 25–58.

[26] S.J. Eichhorn, Cellulose nanowhiskers: Promising materials for advanced applications, Soft Matter. 7 (2011) 303–315. doi:10.1039/c0sm00142b.

[27] S.J. Eichhorn, A. Dufresne, M. Aranguren, N.E. Marcovich, J.R. Capadona, S.J. Rowan, C. Weder, W. Thielemans, M. Roman, S. Renneckar, W. Gindl, S. Veigel, J. Keckes, H. Yano, K. Abe, M. Nogi, A.N. Nakagaito, A. Mangalam, J. Simonsen, A.S. Benight, A. Bismarck, L.A. Berglund, T. Peijs, Review: current international research into cellulose nanofibres and nanocomposites, J. Mater. Sci. 45 (2010) 1–33. doi:10.1007/s10853-009-3874-0.

[28] J.H. Kim, B.S. Shim, H.S. Kim, Y.J. Lee, S.K. Min, D. Jang, Z. Abas, J. Kim, Review of nanocellulose for sustainable future materials, Int. J. Precis. Eng. Manuf. - Green Technol. 2 (2015) 197–213. doi:10.1007/s40684-015-0024-9.

[29] Y. Nishiyama, J. Sugiyama, H. Chanzy, P. Langan, Crystal Structure and Hydrogen Bonding System in Cellulose Iα from Synchrotron X-ray and Neutron Fiber Diffraction, J. Am. Chem. Soc. 125 (2003) 14300–14306. doi:10.1021/ja037055w.

[30] P. Belton, S. Tanner, N. Cartier, H. Chanzy, High-resolution solid-state carbon-13 nuclear magnetic resonance spectroscopy of tunicin, an animal cellulose, Macromolecules. 22 (1989) 1615–1617. doi:10.1021/ma00194a019.

[31] H. Yamamoto, F. Horii, In situ crystallization of bacterial cellulose I. Influences of polymeric additives, stirring and temperature on the formation celluloses Iα and Iβ as revealed by cross polarization/magic angle spinning (CP/MAS)13C NMR spectroscopy, Cellulose. 1 (1994) 57–66. doi:10.1007/BF00818798.

[32] T. Shen, S. Gnanakaran, The stability of cellulose: A statistical perspective from a coarse-grained model of hydrogen-bond networks, Biophys. J. 96 (2009) 3032–3040. doi:10.1016/j.bpj.2008.12.3953.

[33] S.I. Kuzina, I.A. Shilova, V.F. Ivanov, A.I. Mikhailov, Molecular mobility of nanocellulose hydrogels, Russ. J. Phys. Chem. B. 10 (2016) 839–843. doi:10.1134/s1990793116050067.

[34] O. Nechyporchuk, M.N. Belgacem, J. Bras, Production of cellulose nanofibrils: A review of recent advances, Ind. Crop. Prod. 93 (2016) 2–25. doi:10.1016/j.indcrop.2016.02.016.

[35] J. Tang, J. Sisler, N. Grishkewich, K.C. Tam, Functionalization of cellulose nanocrystals for advanced applications, J. Colloid Interface Sci. 494 (2017) 397–409. doi:10.1016/j.jcis.2017.01.077.

[36] A. Isogai, Wood nanocelluloses: Fundamentals and applications as new bio-based nanomaterials, J. Wood Sci. 59 (2013) 449–459. doi:10.1007/s10086-013-1365-z.

[37] D. Klemm, D. Klemm, F. Kramer, S. Moritz, T. Lindström, M. Ankerfors, D. Gray, A. Dorris, Nanocelluloses : A New Family of Nature-Based Materials Angewandte, Angew. Chemie. 50 (2011) 5438–5466. doi:10.1002/anie.201001273.

[38] S.-B. Candanedo, M. Roman, D.G. Gray, Effect of reaction conditions on the properties and behavior of wood cellulose nanocrystal suspension, Biomacromolecules. 6 (2005) 1048–1054. doi:10.1021/bm049300p.

[39] A.E.J. de Nooy, A.C. Besemer, H. van Bekkum, Highly selective nitroxyl radical-mediated oxidation of primary alcohol groups in water-soluble glucans, Carbohydr. Res. 269 (1995) 89–98. doi:10.1016/0008-6215(94)00343-E.

[40] T. Saito, A. Isogai, TEMPO-mediated oxidation of native cellulose. The effect of oxidation conditions on chemical and crystal structures of the water-insoluble fractions, Biomacromolecules. 5 (2004) 1983–1989. doi:10.1021/bm0497769.

[41] A. Isogai, T. Saito, H. Fukuzumi, TEMPO-oxidized cellulose nanofibers, Nanoscale. 3 (2011) 71–85. doi:10.1039/c0nr00583e.

[42] T. Saito, Y. Nishiyama, J.L. Putaux, M. Vignon, A. Isogai, Homogeneous suspensions of individualized microfibrils from TEMPO-catalyzed oxidation of native cellulose, Biomacromolecules. 7 (2006) 1687–1691. doi:10.1021/bm060154s.

[43] A. Isogai, L. Bergström, Preparation of cellulose nanofibers using green and sustainable chemistry, Curr. Opin. Green Sustain. Chem. 12 (2018) 15–21. doi:10.1016/j.cogsc.2018.04.008.

[44] T. Kondo, M. Morita, K. Hayakawa, Y. Onda, Wet pulverizing of polysaccharides, US 7357339 B2, 2008.

[45] T. Kondo, R. Kose, H. Naito, W. Kasai, Aqueous counter collision using paired water jets as a novel means of preparing bio-nanofibers, Carbohydr. Polym. 112 (2014) 284–290. doi:10.1016/j.carbpol.2014.05.064.

[46] L. Van Hai, L. Zhai, H.C. Kim, J.W. Kim, E.S. Choi, J. Kim, Cellulose nanofibers isolated by TEMPO-oxidation and aqueous counter collision methods, Carbohydr. Polym. 191 (2018) 65–70. doi:10.1016/j.carbpol.2018.03.008.

[47] R. Kose, I. Mitani, W. Kasai, T. Kondo, "Nanocellulose" as a single nanofiber prepared from pellicle secreted by gluconacetobacter xylinus using aqueous counter collision, Biomacromolecules. 12 (2011) 716–720. doi:10.1021/bm1013469.

[48] A.F.S. Costa, F.C.G. Almeida, G.M. Vinhas, L.A. Sarubbo, Production of bacterial cellulose by Gluconacetobacter hansenii using corn steep liquor as nutrient sources, Front. Microbiol. 8 (2017) 1–12. doi:10.3389/fmicb.2017.02027.

[49] D. Klemm, E.D. Cranston, D. Fischer, M. Gama, S.A. Kedzior, D. Kralisch, F. Kramer, T. Kondo, T. Lindström, S. Nietzsche, K. Petzold-Welcke, F. Rauchfuß, Nanocellulose as a natural source for groundbreaking applications in materials science: Today's state, Mater. Today. 21 (2018) 720–748. doi:10.1016/j.mattod.2018.02.001.

[50] M. Börjesson, G. Westman, Crystalline nanocellulose -Preparation, Modification, and Properties, in: M. Poletto, H.L.O. Junior (Eds.), Cellul. - Fundam. Asp. Curr. Trends, IntechOpen, London, 2015: pp. 159–191. doi:10.5772/61899.

[51] Pratima Bajpai, Pulp and Paper Industry Nanotechnology in Forest Industry, Elsevier, 2017.

[52] A. Dufresne, Nanocellulose: A new ageless bionanomaterial, Mater. Today. 16 (2013) 220–227. doi:10.1016/j.mattod.2013.06.004.

[53] J. Tang, J. Sisler, N. Grishkewich, K.C. Tam, Journal of Colloid and Interface Science Functionalization of cellulose nanocrystals for advanced applications, J. Colloid Interface Sci. 494 (2017) 397–409. doi:10.1016/j.jcis.2017.01.077.

[54] F. Fahma, S. Iwamoto, N. Hori, T. Iwata, A. Takemura, Isolation , preparation , and characterization of nanofibers from oil palm empty-fruit-bunch (OPEFB), Cellulose. 17 (2010) 977–985. doi:10.1007/s10570-010-9436-4.

[55] M.K.M. Haafiz, A. Hassan, Z. Zakaria, I.M. Inuwa, M.S. Islam, Physicochemical characterization of cellulose nanowhiskers extracted from oil palm biomass microcrystalline cellulose, Mater. Lett. 113 (2013) 87–89. doi:10.1016/j.matlet.2013.09.018.

[56] R. Rohaizu, W.D. Wanrosli, Sono-assisted TEMPO oxidation of oil palm lignocellulosic biomass for isolation of nanocrystalline cellulose, Ultrason. Sonochem. 34 (2017) 631–639. doi:10.1016/j.ultsonch.2016.06.040.

[57] N. Elias, S. Chandren, N. Attan, N.A. Mahat, F.I.A. Razak, J. Jamalis, R.A. Wahab, Structure and properties of oil palm-based nanocellulose reinforced chitosan nanocomposite for efficient synthesis of butyl butyrate, Carbohydr. Polym. 176 (2017) 281–292. doi:10.1016/j.carbpol.2017.08.097.

[58] N. Elias, S. Chandren, F.I.A. Razak, J. Jamalis, N. Widodo, R.A. Wahab, Characterization, optimization and stability studies on Candida rugosa lipase supported on nanocellulose reinforced chitosan prepared from oil palm biomass, Int. J. Biol. Macromol. 114 (2018) 306–316. doi:10.1016/j.ijbiomac.2018.03.095.

[59] M.K.M. Haafiz, A. Hassan, H.P.S.A. Khalil, M.R.N. Fazita, M.S. Islam, I.M. Inuwa, M.M. Marliana, M.H. Hussin, Exploring the effect of cellulose nanowhiskers isolated from oil palm biomass on polylactic acid properties, Int. J. Biol. Macromol. 85 (2016) 370–378. doi:10.1016/j.ijbiomac.2016.01.004.

Chapter 2

Preparation and Characterization of Nanocellulose from Oil Palm Empty Fruit Bunches (OPEFB) Pulp

2.1 Introduction

Oil palm (*Elaeis guineensis*) plantations have spread rapidly over the last decade to fulfill increasing demand for crude palm oil. In 2015, the total area of oil palm plantations in Indonesia reached 11 Mha, representing an increase of *ca.* 77% since 2006 [1]. The production of crude palm oil from fresh fruit bunches causes by-products and large amounts of biomass waste, which is referred to as oil palm empty fruit bunches (OPEFB) [2]. The utilization of OPEFB waste from oil palm industries has been studied intensively, and various applications have been tested, including biogas production [3], bioethanol production [2], acoustic absorbers [4], activated carbon [5], and nanomaterials such as nanocelluloses [6,7].

Figure 2.1. Optical image of empty fruit bunches fibers (left) and its bleached pulp (right)

The utilization of OPEFB for nanocelluloses has attracted considerable interest because raw OPEFB contains *ca.* 59% cellulose, 12% of hemicellulose and 25% of lignin [8]. Furthermore, non-woody plants such as oil palm are an attractive source of cellulose because their lignin content is less than that of woody plants. This enables easier and more energy efficient delignification and subsequent nanofibrillation [9]. Thus, the use of oil palm waste as a source of raw materials for nanocellulose production is a promising approach for turning agricultural waste into valuable products [10]. Nanocellulose materials have many beneficial properties, such as renewability, low toxicity, biocompatibility, bio-degradability, low cost, and easy availability, together with superior physicochemical properties, which make them ideal for a wide range of applications [11].

Nanocellulose has been determined as cellulose nanocrystals (CNCs) and cellulose nanofibrils (CNFs) based on their morphological characteristics. Furthermore, CNCs are produced by chemical treatments, followed by mechanical disintegration, with needle-like morphologies. CNFs are obtained by either mechanical or chemical treatments with individual nanofibrils up to several microns. CNCs are highly crystalline with length less than 500 nm and CNFs are consist of mixture amorphous and crystalline [12].

The preparation of CNCs from oil palm biomass has been reported by some researchers, with the use of sulfuric acid hydrolysis. Lamaming et al. reported the isolation of CNCs from oil palm trunk by sulfuric and hydrochloric acid hydrolysis [10,13,14]. Azrina et al. combined sulfuric acid hydrolysis with ultrasonication to isolate CNC from OPEFB pulp [8]. Chen et al. applied one pot sequential oxidative−hydrolysis to raw OPEFB biomass [15]. Haafiz et al. used microcrystalline cellulose of OPEFB as a starting material, in which CNC was produced by *N,N*-

dimethylacetamide (DMAc)/LiCl-swelling and a subsequent ultrasonic treatment [16]. In addition, the preparation of CNFs from OPEFB via mechanical treatments revealed that nano-grinding treatments does not give significant changes on chemical and thermal behavior compared to cellulose and CNF sheets from OPEFB showed translucent and high performance in mechanical and thermal properties compared to CNF prepared from mesocarp of oil palm [17,18].

In case of nanocellulose preparation, the use of sulfuric acid in CNC production has both advantages and disadvantages. The main advantage is that highly stable CNC suspensions can be obtained, because negatively charged sulfate groups are introduced onto the surface of the CNC during hydrolysis [19]. However, sulfuric acid is strongly oxidizing, and sometimes causes degradation of cellulose because sulfate groups behave as a catalyst for oxidative decomposition. This decomposition has a negative effect on large-scale production and applications of CNCs [20]. Thus, strong hydrolyzing acids, other than sulfuric acid, and particularly hydrochloric acid, have been widely used to prepare CNCs. Unlike sulfuric acid hydrolysis, hydrochloric acid hydrolysis affords unmodified charge-neutral CNCs. CNCs isolated by hydrochloric acid hydrolysis show some superior features compared with sulfated CNCs; CNCs prepared by hydrochloric acid treatments form stable oil/water interfaces, so-called Pickering emulsions, whereas sulfated CNCs do not show this interfacial behavior [21,22].

Furthermore, the CNF preparation using mechanical treatments requires high energy by providing high mechanical shear and high pressure homogenization [23]. Among ever reported, nanocellulose produced by 2,2,6,6-tetramethylpiperidine-1-oxyl (TEMPO)-catalyzed oxidation, namely TEMPO-oxidized cellulose nanofibers (TOCNs), has attracted considerable attention since it requires low energy in its

production, affording the narrowest nanofiber ever reported [24]. Besides, the TOCNs bear anionic carboxylate groups on their surfaces as the result of TEMPO-mediated selective oxidation of surface-exposed primary alcohols to carboxylates [25]. These carboxylates induce negative zeta potential as low as –70 mV on the solid surfaces, resulting in high dispersibility of TOCNs in water by electrical repulsion [26], and high dispersant effects for various suspended solid matters [27]. Therefore, in this study the nanocellulose preparation from OPEFB pulp using hydrochloric acid (HCl) to produce CNC and using TEMPO-mediated oxidation to produce CNF are presented.

However, to the best of our knowledge, the preparation of CNCs from OPEFB pulps with hydrochloric acid has not been reported. In this study, we successfully isolated CNCs from OPEFB pulp with high purity by hydrochloric acid hydrolysis. The obtained CNCs were fully characterized by microscopy, spectroscopy, and thermal analyses. We compared these features with those of a woody CNC and some other reported CNCs obtained from different types of agricultural waste. In CNF preparation, using TEMPO-mediated oxidation, the different amount of oxidant, NaClO, was applied by estimating the different carboxy content of obtained CNF will be produced. Oxidation using TEMPO/NaBr/NaClO system at pH 10 was examined and characterized. The results of this study can be a benefit to get deep understanding in nanocellulose properties prepared by different methods.

2.2 Cellulose Nanocrystals Produced by Hydrochloric Acid Hydrolysis

2.2.1 Materials

Bleached kraft OPEFB pulp was kindly supplied by Biomaterial Research Center, Indonesian Institute of Sciences (Bogor, Indonesia). Sodium hydroxide

(NaOH), hydrochloric acid (35.0–37.0% HCl aq.), acetic acid 99.7% (w/w) and potassium bromide (KBr) were purchased from Wako Pure Chemical Industries Ltd. (Osaka, Japan), sodium phosphotungstate from Nacalai Tesque Inc. (Kyoto, Japan), and cellulose nitrate tube from Nippon Medical and Chemical Instrument Co. Ltd. (Osaka, Japan). NaOH and HCl aq. were diluted by water to afford solutions of designated concentration. KBr was dried at 100°C overnight prior to use. Cellulose nitrate tube was soaked in hot water to remove glycerol prior to use. The water used in this study was purified with an Arium Ultrapure Water System (Sartorius Co., Ltd., Tokyo, Japan).

2.2.2 Preparation of Cellulose Nanocrystals

A raw fibers of OPEFB were pulped and bleached by kraft method using NaOH and Na_2S as employed for wood pulping. Bleached kraft OPEFB pulp (pulp-A) was purified with 4% NaOH at 60°C for 4 h to remove hemicellulose and other impurities, and then washed with deionized water until the pH was neutral. The resultant pulp was denoted as pulp-B. Pulp-B was then treated with hot water. The pulp was swelled

by soaking in deionized water at 60°C for 2 h, and the resultant pulp was denoted as pulp-C (**Fig. 2.2**).

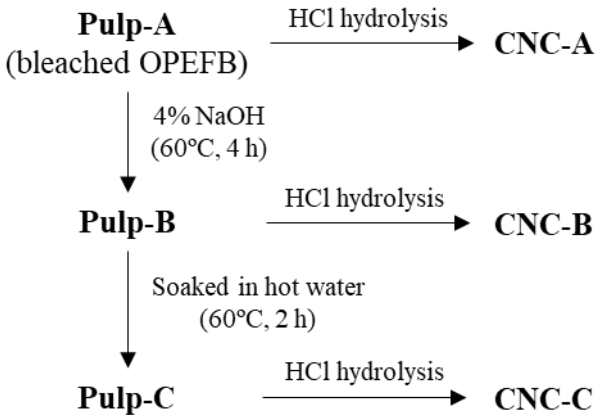

Figure 2.2 Preparation of the treated pulps and cellulose nanocrystals (CNCs) from oil palm empty fruit bunches (OPEFB)

The three different pulps (pulp-A, -B, and -C) were hydrolyzed with hydrochloric acid. A 5.0-g portion of each pulp was suspended in 100 mL of 3 M HCl at 80°C, and the mixture was continuously stirred for 2 h while the temperature was maintained at 80°C [13]. The hydrolysis was quenched by adding 500 mL of cold deionized water. The resultant suspensions were filtered through a Buchner funnel, and then washed with approximately 2.5 L of deionized water until the pH became neutral. The residue was re-suspended in 500 mL of deionized water and treated in a household blender for 30 min at 10,000 rpm. The as-prepared cellulose suspension was centrifuged at 4,000 *g* for 20 min (Kubota Table Top Centrifuge Model 4000, Kubota Corporation, Tokyo, Japan) at room temperature to remove micrometer-sized fractions, and the turbid supernatant was collected as a CNC suspension. The suspension was then centrifuged at 11,400 *g* for 20 min (TOMY Hybrid Refrigerated Centrifuge CAX-571, TOMY Digital Biology Co. Ltd., Tokyo, Japan) at 25°C to

obtain concentrated CNCs. The collected CNCs were then dialyzed with a cellulose nitrate tube for 3 days. Subsequently, 300-mL portions (0.5 wt%) of the CNC suspensions were treated with an ultrasonic homogenizer (VP-5S, Taitec, Saitama, Japan) at 19.5 kHz with a 100% output power for 30 min. All the resulting suspensions were freeze-dried to afford white aerogels. The yields were calculated based on the dry weight of the starting pulps. The resulting CNCs were denoted as CNC-A, CNC-B and CNC-C, corresponding to the starting pulps. For comparison, a CNC derived from wood pulp (denoted as CNC-wood) was also analyzed, which was kindly supplied by Paper Company in Japan.

2.2.3 Characterization Methods

2.2.3.1 Scanning Electron Microscopy (SEM)

The morphology of the raw pulps and CNCs were observed on a scanning electron microscope equipped with a navigation camera (SEM-SU3500, Hitachi Ltd., Tokyo, Japan) at the Center of Advanced Instrumental Analysis, Kyushu University. Samples were mounted on carbon tape and observed at an acceleration voltage of 15 kV.

2.2.3.2 Elemental Analysis

Elemental analysis was performed with an Organic Micro Element Analyzer (CHN) Yanaco CHN CORDER MT-6 (Yanaco, Co. Ltd., Tokyo, Japan) at The Service Centre of the Elementary Analysis of Organic Compounds (Faculty of Science, Kyushu University).

2.2.3.3 Determination of α-Cellulose Content

About 1 g of each cellulose sample was added into 17.5% NaOH (25 mL) and the mixture was kept constant at 20°C for 30 min. After that, about 25 mL of pure water

was added, stirred for 1 min, and then left for 5 min. Dried glass filter was weighed prior to use. The treated cellulose sample was filtered with the glass filter, and thoroughly washed with 600 mL of pure water, followed by vacuum filtration with about 40 mL of 10% (v/v) acetic acid and 1-L boiled water. The filtrated residue was dried in an oven at 105°C to evaporate the water. α-Cellulose content was determined by measuring the increase in weight of the glass filter.

2.2.3.4 Birefringence Observation

Birefringence was observed by putting 0.8% (w/v) of the CNC suspensions between crossed polarizers under stirring at room temperature.

2.2.3.5 Fourier Transform Infrared Spectroscopy (FTIR)

The FTIR spectra were recorded on a JASCO FT/IR-620 spectrophotometer (JASCO International Co. Ltd., Tokyo, Japan). Prior to analysis, a 100-mg portion of the sample was mixed and ground with 5 mg of KBr. The resulting mixtures were pressed into transparent pellets and analyzed in the spectral range of 400–4000 cm^{-1} with a resolution of 2 cm^{-1} for each sample.

2.2.3.6 Transmission Electron Microscopy (TEM)

The morphology and size of the CNCs were observed on a JEM-2100 HC (JEOL Ltd., Tokyo, Japan) operated at an accelerating voltage of 120 kV at The Ultramicroscopy Research Center Kyushu University. A 5-μL portion of the CNC suspension (0.1 %) was dropped onto a carbon-coated TEM grid (ELS-C10, Oukenshouji, Tokyo, Japan) and a drop of 1% (w/v) sodium phosphotungstate was added prior to drying. Extra liquid was wicked off with a filter paper. The grids were then dried under vacuum for 30 min. The lengths of 50 isolated crystals were measured on TEM images with image processing software (Image-J version 1.51s).

2.2.3.7 X-Ray Diffraction (XRD)

X-Ray diffraction (XRD) data were recorded on a Rigaku X-ray Diffractometer (Rigaku Denki Co. Ltd., Tokyo, Japan) operated at 40 kV and 20 mA. Freeze-dried samples were pressed to make a pellet with a KBr disk apparatus for IR spectroscopy. The specimens were step-wise scanned over a range of scattering angles (2θ) from 5° to 40°, at a scan speed of 0.6 deg/min with CuK_α radiation (λ = 1.541 Å). The crystallinity index, CrI (%), was calculated using the method reported by Segal et al. [28].

2.2.3.8 Thermogravimetric (TG) Analysis

The thermal stability of the CNCs was analyzed with a thermogravimetric analyzer (TG/DTA 7300, Hitachi Ltd., Tokyo, Japan) with a thermogravimetric sensitivity of 0.2 μg at the Center of Advanced Instrumental Analysis, Kyushu University. A 0.7–1-mg portion of the specimens was scanned from 30 to 500°C at a rate of 20°C/min under a nitrogen atmosphere.

2.2.4 Results and Discussion

2.2.4.1 Morphology of the Raw Pulps and CNCs

The morphologies of the raw pulps and the obtained CNCs were observed by scanning electron microscopy (SEM). SEM images of the raw pulps revealed morphological changes induced by the alkali and hot water treatments. Untreated pulp-A exhibited rough and twisted surfaces accompanied by surrounding thin wires, probably indicating the presence of impurities, such as hemicellulose (**Fig. 2.3a**). Alkali-treated pulp-B showed smooth surfaces, which implied the removal of impurities (**Fig. 2.3b**). The following hot water treatment had a less notable effect on morphology of the pulp (**Fig. 2.3c**). Small holes on the surface of all the OPEFB

pulps were induced by the strong chemicals used during the pulping process [8]. CNCs obtained by acid hydrolysis were also observed after freeze-drying. All the pulps were successfully fibrillated into nano-ordered fibers (**Fig. 2.3 d, e and f**).

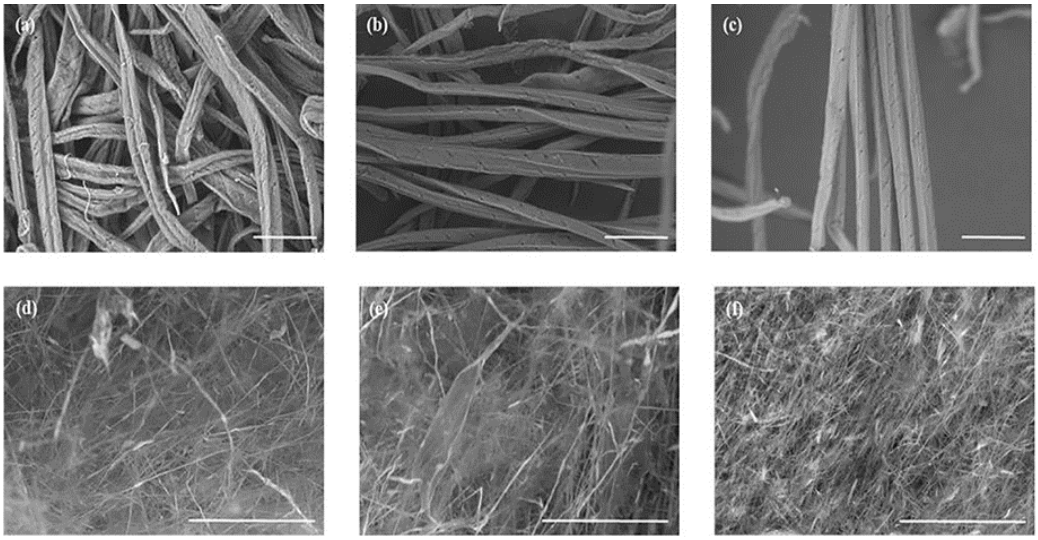

Figure 2.3 SEM images of (a) pulp-A, (b) pulp-B, (c) pulp-C, (d) CNC-A, (e) CNC-B, and (f) CNC-C (scale bars: 50 μm)

2.2.4.2 Yields of CNCs

Initial screening of hydrolysis conditions revealed that treatment of pulps with 3 M HCl at 80°C for 2 h was optimal, which is identical to those applied to oil palm trunk samples in literature [14]. The yields of the CNC-A, B, and C from the three pulps, i.e., pulp-A, -B, and -C, were 21%, 18%, and 19%, respectively. Other different conditions for acid concentrations, temperatures, and reaction times resulted in lower yield of CNCs with unclear birefringence in this work. Although purer pulps were obtained by alkali treatments (see the section Elemental Analysis), the yields of the resultant CNCs remained almost unchanged (CNC-A vs CNC-B and -C). While sulfuric acid is the most commonly used in acid hydrolysis of cellulose resources, its strong oxidizing property sometimes results in partial degradation of CNCs, which

would be a serious problem in large-scale production and application of CNCs [20]. The yields of the CNCs in the present study were compared with some literature data. The yields of our pulps were comparable or even higher than those of CNCs from other types of agricultural wastes, which were prepared by sulfuric acid hydrolysis: oil palm trunk (24%−27%) [10]; banana pseudostem (19%) [29]; garlic straw (20%) [30]; barley straw and husk (12%) [31]; corncob (6%) [32] groundnut shell (12%) [33]. However, the yields were lower than those isolated from sugarcane bagasse prepared by ammonium persulfate oxidation (27%−54%) [34].

2.2.4.3 Elemental Analysis

Elemental analysis was performed to compare the purity of each pulp sample and the resultant CNCs, and the CNC obtained from wood (**Table 2.1**). Treating the pulps with sodium hydroxide increased the carbon content, suggesting that residual impurities were partially removed (pulp-A vs pulp-B and -C). These results were in agreement with the α-cellulose contents of the pulps used. Pulp-A had a lower α-cellulose content (77.7%) as compared to those of pulp-B and -C (89.3% and 81.8%, respectively). The resultant CNCs after acid hydrolysis showed remarkably higher carbon content compared with the corresponding raw pulps. The carbon contents of all CNCs obtained from OPEFB were in the range of 43%–44%, which is close to the theoretical value calculated from the chemical composition (44.44%), although CNC-C had a slightly lower carbon content. The α-cellulose contents of CNC-A, -B, and -C are 94.6%, 96.0%, and 90.8%, respectively, which were in good agreement with the increase in carbon contents for all the CNCs as compared to the original pulps, and with slightly lower carbon content of CNC-C among them. These results suggested that highly pure CNCs were obtained by hydrochloric acid hydrolysis of

OPEFB [35]. The CNC-wood sample showed a lower carbon content compared with those of the OPEFB, indicating that some impurities remained in CNC-wood.

Table 2.1 Elemental analysis of raw pulps and resultant CNCs

Elements	pulp-A	pulp-B	pulp-C	CNC-A	CNC-B	CNC-C	CNC-wood
H (%)	6.29	6.38	6.36	5.94	5.95	5.91	5.85
C (%)	38.80	40.13	40.04	44.11	44.03	43.44	42.91

2.2.4.4 Birefringence Observations

Birefringence was observed to evaluate the nano-scale dispersibility of the CNCs in water. When CNCs are nano-dispersed in certain solvents, they show shear birefringence between crossed polarizers under stirring [36]. In general, CNCs prepared by hydrochloric acid hydrolysis have low dispersibility because they lack charged functional such as sulfate ester to induce electrostatic repulsion, which is introduced in the case of sulfuric acid hydrolysis [37]. Accordingly, some CNCs prepared by hydrochloric acid hydrolysis cannot be homogeneously dispersed in water and do not show birefringence [38]. Nevertheless, the CNC suspensions obtained from OPEFB in this study showed clear birefringence, confirming that nano-scale ordered dispersions were achieved. Mechanical disintegration by house blender followed by ultrasonication was effective to get the obtained CNC in nano-scale dimension (**Fig. 2.4a**). Furthermore, the suspensions were allowed to stand and remained stable without any sedimentation over 6 months (**Fig. 2.4b**).

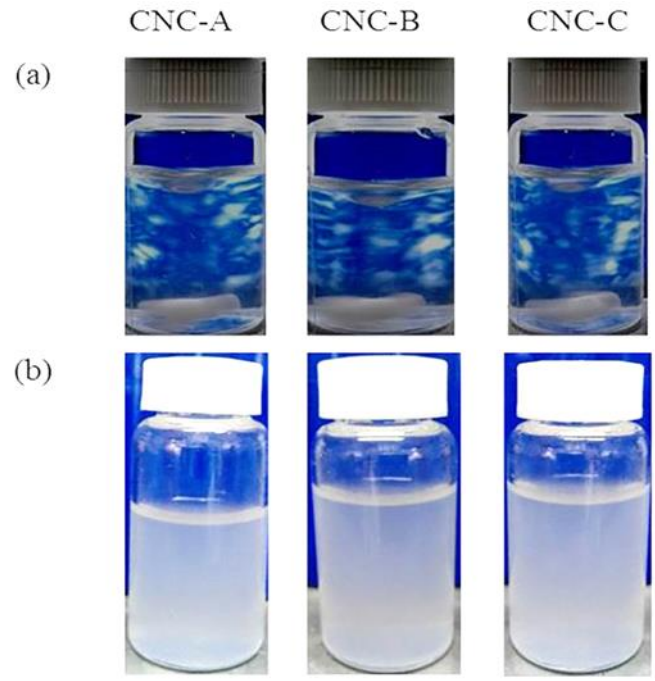

Figure 2.4 (a) Birefringence images of the prepared CNCs and (b) photographs taken after standing for 6 months

2.2.4.5 Fourier Transform Infrared Spectroscopy (FTIR)

The FTIR spectra of pulps and the resultant CNCs were measured to investigate changes in the chemical structures induced by acid hydrolysis (**Fig. 2.5**). The spectra of the prepared CNCs exhibited narrower absorption bands compared with those of the starting OPEFB pulps in the region of 3200–3500 cm^{-1}, which corresponds to the stretching vibration of the hydroxy group (F**ig. 2.5 d, e, f vs a, b, c**). The absorption band at 2901 cm^{-1}, which is associated with the stretching vibration of the C–H bond of cellulose, was not affected by hydrolysis. The absorption band at 1641–1644 cm^{-1} for both raw pulps and the CNCs is attributed to the stretching vibration of adsorbed water [16,39]. We noted a difference in the appearance of a weak peak at 1725 cm^{-1} for the CNCs prepared from OPEFB. The corresponding peak was not observed in the starting pulps and CNC-wood. These peaks were assigned to the free carboxy (-

COOH) group [40]. These results suggest that trace amounts of carboxy groups were formed during acid hydrolysis. By comparing the intensity of these peaks with a characteristic reference peak at 1160 cm^{-1} (glycosidic stretching vibration), the relative intensities of the carboxy peaks were determined to be 0.20, 0.20, and 0.21 for CNC-A, B, and C, respectively. The bands at 1160 and 896 cm^{-1} were associated with the C–O and C–H stretching of glycosidic linkages, respectively, both of which are typical of cellulose [20]. The results of the FTIR measurements suggested that the changes in the chemical structure of cellulose were negligible during the alkali/hot water-pretreatment and acid hydrolysis.

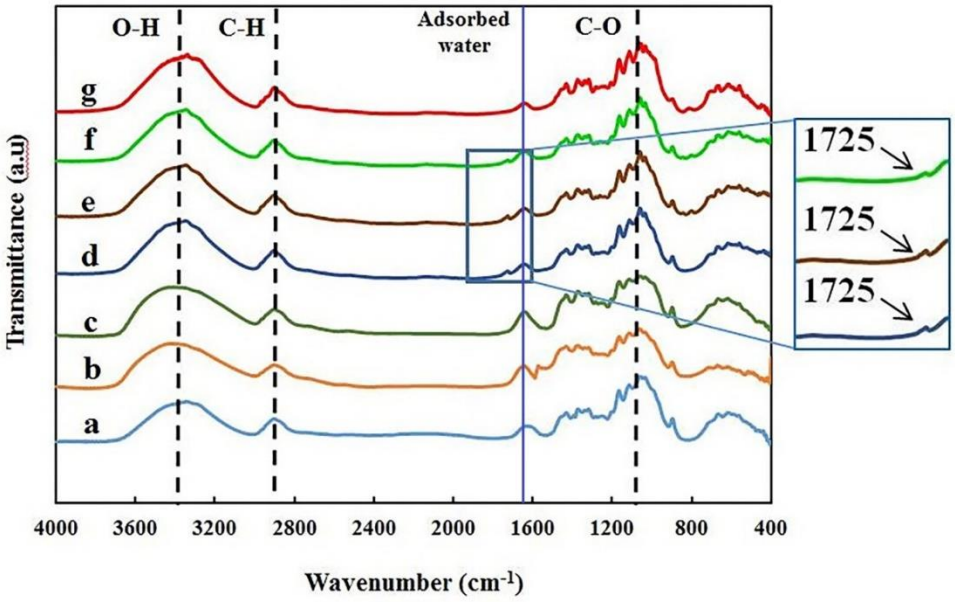

Figure 2.5 FTIR spectra of (a) pulp-A, (b) pulp-B, (c) pulp-C, (d) CNC-A, (e) CNC-B, (f) CNC-C, and (g) CNC-wood

2.2.4.6 Morphology and Size of CNCs

Morphological features of the CNCs were observed by TEM. The CNCs from OPEFB pulps, and CNC-wood, showed a needle-like morphology (**Fig. 2.6**). All CNCs prepared by hydrochloric acid hydrolysis formed bundled structures (**Fig. 2.6**

a–c), indicating assembly of the rod-like CNCs. Similar aggregation phenomenon has been previously reported [37,41]. Such aggregation could occur in the drying process for TEM sample preparation, because the nano-ordered dispersibility of CNCs prepared from OPEFB was clearly confirmed by birefringence observations (see the section Birefringence Observations).

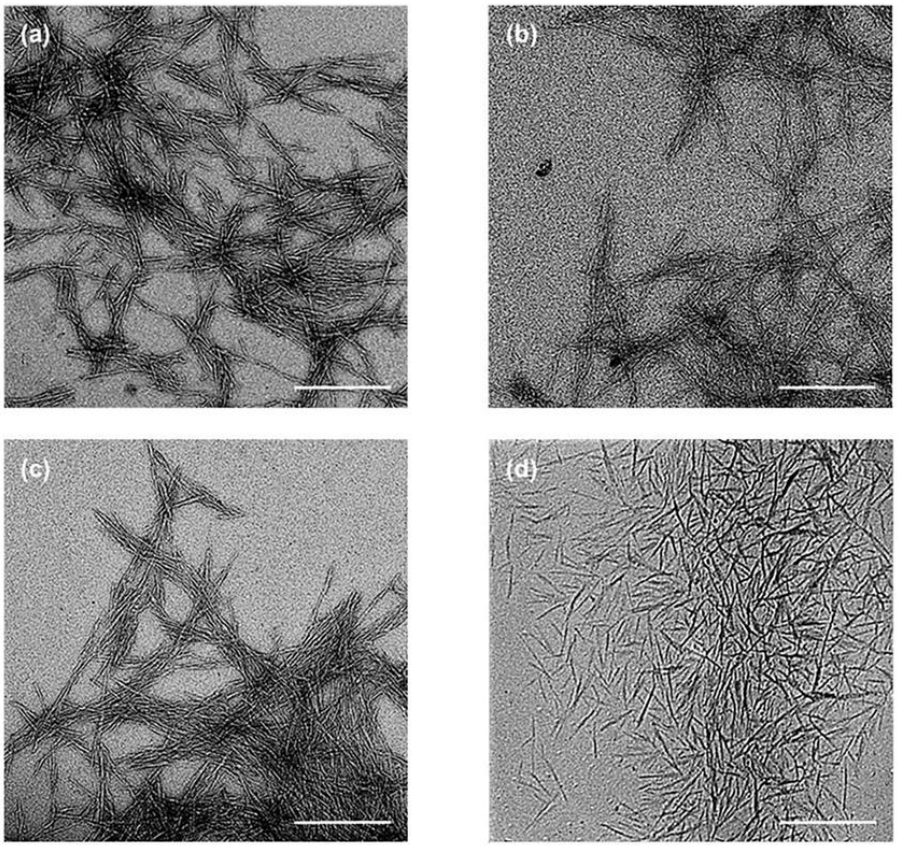

Figure 2.6 TEM images of: (a) CNC-A, (b) CNC-B, (c) CNC-C, and (d) CNC-wood (scale bars: 500 nm)

The aspect ratio of each sample was evaluated and compared with literature data (**Table 2.2**), because the aspect ratio is one of the most important factors for CNC applications, particularly for use as reinforcing materials in nanocomposites [42]. The aspect ratios of the three CNCs prepared from OPEFB pulps in this study were comparable in the range of 23–29. Notably, the aspect ratios of these CNCs

from OPEFB were higher than that of CNC-wood (23–29 vs 15). The CNCs prepared in this study showed a comparable aspect ratio to that of CNCs obtained from the same OPEFBs prepared by ultrasonication-assisted 2,2,6,6-tetramethylpiperidine-1-oxyl (TEMPO)-oxidation [43]. The aspect ratios of our CNCs were even higher than that of other OPEFB-derived CNCs prepared by chemical swelling with DMAc/LiCl followed by sonication [16] or ultrasound-assisted sulfuric acid hydrolysis [8], and that of CNCs from oil palm mesocarp by sulfuric acid hydrolysis [44]. Some CNCs with higher aspect ratios have been prepared from oil palm trunk [10,14]; however, our CNCs were comparable with other CNCs obtained from empty fruit bunches.

Table 2.2 Dimensions of CNCs prepared from oil palm biomass and wood by various method.

Origin of CNCs	Size of CNCs (nm)		Aspect ratio	Preparation	References
	Length	Width			
CNC-A (OPEFB)	264 ± 43	12 ± 2	23 ± 18	3 M HCl	This study
CNC-B (OPEFB)	301 ± 58	13 ± 3	24 ± 19	3 M HCl	This study
CNC-C (OPEFB)	285 ± 58	10 ± 2	29 ± 9	3 M HCl	This study
CNC-wood	190 ± 22	13 ± 3	15 ± 5	–[a]	This study
MCC of OPEFB	122 ± 45	4 ± 2	30.5	TEMPO oxidation + sonication	[35]
MCC of OPEFB	300	<20	>15	Chemical swelling + sonication	[15]
OPEFB	–[b]	30–40[b]	1[b]	64% H_2SO_4 + sonication	[8]

continued

Oil palm trunk	361.70[c] 397.03[d]	7.67[c] 7.97[d]	47[c] 49[d]	64% H_2SO_4	[10]
Oil palm trunk	82.81[e] 361.81[f]	3.58[e] 7.68[f]	23[e] 47[f]	3 M HCl	[13]
Oil palm mesocarp	104 ± 52	9 ± 6	12	6 M H_2SO_4	[36]

[a] CNC prepared by sulfuric acid hydrolysis was supplied by a paper company; [b] CNCs are spherical; [c] CNCs from raw fiber; [d] CNCs from hot-water treated fiber; [e] without pre-hydrolysis; [f] with pre-hydrolysis.

Furthermore, all the CNCs prepared from OPEFB in this study showed higher aspect ratios compared with those of other types of agricultural waste, such as grain straws [45], rice straws [46], and rice husk [47] (**Table 2.3**). The aspect ratios of our CNCs were lower than those of CNCs prepared from garlic straw by sulfuric acid hydrolysis [30].

Table 2.3 Dimensions of CNCs prepared from OPEFB, wood, and other types of agricultural waste

Origin of CNCs	Size of CNCs (nm)		Aspect ratio	Preparation	References
	Length	Width			
CNC A–C (OPEFB)	264–301	10–13	23–29	3 M HCl	This study
Grain straws	120–800	10–25	16–19	64% H_2SO_4	[37]
Garlic straws	480	6	80	64% H_2SO_4	[22]
Rice straws	117[a] 270[b]	11.2[a] 30.7[b]	10.5[a] 8.8[b]	64% H_2SO_4	[38]
Rice husk	n.d.[c]	15–20	10–15	64% H_2SO_4	[39]

[a] CNC from 45-min sulfuric acid hydrolysis; [b] CNC from 30-min sulfuric acid hydrolysis; [c] not determined

2.2.4.7 X-Ray Diffraction (XRD) Analysis

The XRD profiles revealed three distinct peaks at 2θ of 15–17°, 22.8°, and 34.6° (**Fig. 2.7**).

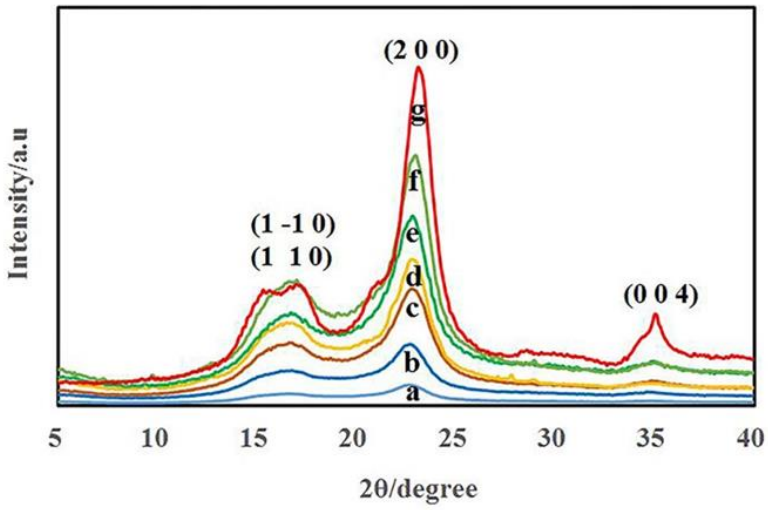

Figure 2.7 X-ray diffraction patterns of (a) pulp-C, (b) CNC-C, (c) pulp-B, (d) CNC-B, (e) pulp-A, (f) CNC-A, and (g) CNC-wood

These peaks are characteristics of native cellulose I crystals assigned to (1–10)/(110), (200), and (004) planes, respectively [48]. The crystallinity indices (CrIs) of the starting OPEFB pulps and resultant CNCs, together with that of CNC-wood, are summarized in **Table 2.4**.

Table 2.4. CrI of raw pulps and CNCs

	CrI (%)		CrI (%)
pulp-A	62	CNC-A	65
pulp-B	61	CNC-B	60
pulp-C	56	CNC-C	53
wood-pulp	n.d	CNC-wood	77

n.d = not determined

The CrI of the starting pulp was slightly decreased by the hot water treatment (pulp-A, -B vs -C). The Cr.I of wood-pulp was not determined because there is no information from the company which provided the CNC-wood. The CrIs were maintained through the preparation of CNCs, i.e., the CrIs of the CNCs were almost identical to those of the corresponding starting pulp. CNCs have potential for reinforcing agents in composites, due to their highly crystalline nature. The addition of cellulose nanocrystals is expected to enhance interfacial stress transfer and increase the modulus of elasticity of the composites [42]. It was reported that the addition of CNCs obtained from non-wood agricultural wastes, such as sugarcane bagasse, improved the mechanical properties of starch films [49]. In this regard, CNC-A, having the highest CrI among our CNCs, would be suitable for nanocomposite applications.

The CrIs of the OPEFB-derived CNCs were lower than that of CNC-wood. This finding was attributed to the non-wood OPEFB pulps having a relatively low crystallinity compared with the wood pulps. The CrIs of the CNCs prepared from OPEFB in this study were comparable to those of oil palm biomass or other non-wood agricultural wastes reported in literature, namely: OPEFB with sulfuric acid hydrolysis (54%–59%) [6]; oil palm fiber with NaOH/urea pretreatment and subsequent high-pressure homogenization (59%–69%) [50]; rice husk with sulfuric acid hydrolysis (59%) [47]; garlic skin with sulfuric acid hydrolysis (63%) [51]; waste cotton cloth with mixed acid of sulfuric acid and hydrochloric acid (56%) [20]. Although some OPEFB-derived CNCs reported in the literature have higher CrIs in range of 70%–88% [7,8,16,43,44], the CrI values in the present study (53%–65%) are reasonable because they remained almost unchanged from those of the starting pulps (56%–62%) after acid hydrolysis, indicating successful downsizing of the

pulps to nano-scale CNCs, while maintaining their original crystalline structures. CNCs prepared in this study had higher CrIs than those produced from the same type of raw materials, i.e. OPEFB, by sulfuric acid hydrolysis, probably because strong sulfuric acid partially destroyed the crystalline regions of CNCs [6]. In addition, while the CrIs remained almost unchanged even after 2-h hydrochloric acid hydrolysis in this study, they gradually decreased under prolonged reaction times in sulfuric acid hydrolysis [6]. Thus, hydrochloric acid hydrolysis is operationally simple and favorable in CNC production from OPEFB pulps, as compared to sulfuric acid hydrolysis in which the reaction time must be strictly controlled.

2.2.4.8 Thermal Degradation Behavior

Thermal degradation behavior was analyzed by thermogravimetry (TG) and differential thermogravimetry (DTG) for the obtained CNCs (CNC-A, B, and C) and CNC-wood (**Fig. 2.8**). A slight weight loss below 150°C was observed for all samples, which was attributed to evaporation of adsorbed water [20]. The CNCs obtained from OPEFB began to degrade at 230°C, and the weight gradually decreased. Conversely, CNC-wood started to decompose at 280°C, and the weight sharply decreased. Small shoulders of the OPEFB-derived CNCs at 180–275°C appeared in the DTG curves, which were attributed to degradation of residual hemicellulose in the CNCs [52]. The amounts of residues over 400°C were lower for OPEFB-derived CNCs compared with that of CNC-wood (**Table 2.5**). The larger amount of residue for CNC-wood indicated the presence of lignin as an impurity, which requires high temperatures for decomposition [53].

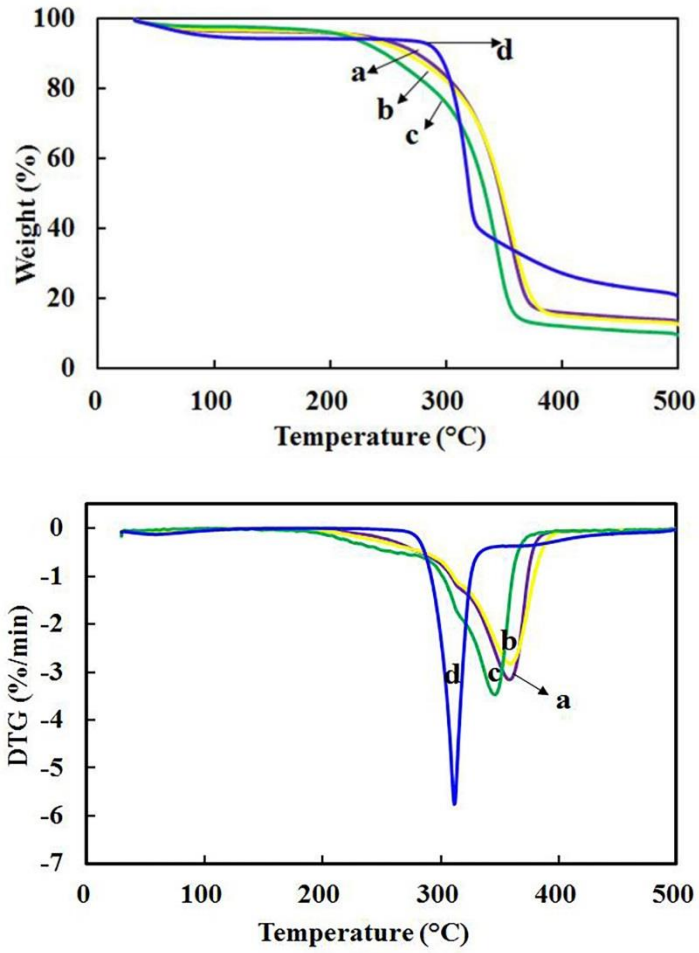

Figure 2.8 TG (top) and DTG (bottom) curves of (a) CNC-A, (b) CNC-B, (c) CNC-C, and (d) CNC-wood

The onset temperatures (T_{on}) and maximum degradation temperatures (T_{max}) are summarized in **Table 2.5**. The T_{max} of CNC-C was lower by 12°C compared with those of CNC-A and CNC-B. This result is consistent with the lower crystallinity index of CNC-C (see the section X-Ray Diffraction Analysis), because crystallinity is a main factor determining thermal stability. The lower T_{on} values of the OPEFB-derived CNCs, especially CNC-C, were attributed to the lower thermal stability of hemicellulose, which remained as a minor impurity in the CNCs [8,52]. As previously shown (see the section Elemental Analysis), CNC-C had the lowest α-cellulose content among as-

prepared samples, indicating that the CNC-C contained higher amount of hemicellulosic impurity. On the other hand, CNC-wood showed a considerably lower T_{max} value than those of the OPEFB-derived CNCs. This is because sulfate groups introduced on the CNC surface during sulfuric acid hydrolysis catalyzed the thermal degradation of cellulose [20]. Accordingly, hydrochloric acid hydrolysis can produce more thermally stable CNCs than those produced by sulfuric acid hydrolysis. High thermal resistances of CNCs are promising as a filler in thermoplastic polyurethane composites, which are commonly used in manufacturing of thermoplastic devices. The thermoplastic polyurethane–CNC nanocomposites exhibited higher thermal stability [54]. In this regard, CNC-A and -B, which had higher degradation temperatures than CNC-C, would be suitable for potential applications in thermoplastic devices.

Table 2.5 Thermal properties of resultant CNCs (OPEFB and wood) and from oil palm biomass pulp

Materials	**Preparation**	T_{on} **(°C)**	T_{max} **(°C)**	**Residual char (%)**	**References**
CNC-A (OPEFB)	3 M HCl	261.8	358.5	13	This study
CNC-B (OPEFB)	3 M HCl	252.2	359.2	12	This study
CNC-C (OPEFB)	3 M HCl	244.0	346.5	9	This study
CNC-wood	–[a]	282.9	311.4	20	This study
Oil palm trunk	3 M HCl	322.54[c] 323.53[d]	345.13[c] 341.37[d]	5.88[c] 2.33[d]	[13]
OPEFB[b]	TEMPO oxidation	200	280	7	[35]
OPEFB	64% H_2SO_4 + sonication	362.17	357.08	30	[8]
OPEFB[b]	Chemical swelling + sonication	329	418	< 5	[15]

Materials	Preparation	T_{on} (°C)	T_{max} (°C)	Residual char (%)	References
Grain straws	64% H_2SO_4	265–271	312–329	10–20	[37]
Corn husk	64% H_2SO_4, ultrasonication, TEMPO oxidation	229–278	279–351	8–27	[45]

[a] A CNC prepared by sulfuric acid hydrolysis was supplied by a paper company; [b] In microcrystalline cellulose form; [c] without pre-hydrolysis; [d] with pre-hydrolysis; TEMPO: 2,2,6,6-tetramethylpiperidine 1-oxyl

The T_{max} values of CNCs prepared from OPEFB in this study were comparable or even higher than those of oil palm biomass or other agricultural wastes reported in literature: 341–345°C for oil palm trunk [14]; 280°C for OPEFB-derived microcrystalline cellulose [43]; 357°C for OPEFB [8]; 312–329°C for grain straws [45]; 279–351°C for corn husk [55]. The difference in each thermal property was affected by the difference of preparation methods. Our CNCs exhibited higher T_{max} than TEMPO-oxidized CNCs [43], because decarboxylation takes place at lower temperatures for the TEMPO-CNCs [56]. CNCs produced by sulfuric acid hydrolysis tend to have lower degradation temperatures, because of sulfate groups introduced to the surfaces of CNCs [45,55]. CNCs with high CrIs (88% and 84%) produced from OPEFB by using swelling agent and sulfuric acid revealed better thermal properties [7,16]. While a CNC with an even higher T_{max} has been reported (418°C), such high thermal stability strongly depended on its high crystallinity [16]. Our simple method can provide high-quality CNCs from low-quality OPEFB pulps.

2.3 Cellulose Nanofibers Produced by TEMPO-Mediated Oxidation

2.3.1 Materials

Bleached kraft pulp of oil palm empty fruit bunches (OPEFB) was kindly supplied from Biomaterial Research Institute, Indonesian Institute of Sciences (Bogor, Indonesia). 2,2,6,6-Tetramethylpiperidine 1-oxyl (TEMPO), sodium bromide, sodium hypochlorite, and sodium borohydride were purchased from Sigma-Aldrich (Tokyo, Japan) and used without further purification. The water used in this study was purified with an Arium Ultrapure Water System (Sartorius Co., Ltd., Tokyo, Japan).

2.3.2 Preparation of TOCN

The bleached kraft pulp of OPEFB was soaked in a 0.01 M HCl solution for 30 min for demineralization. TOCN was prepared by TEMPO/NaBr/NaClO system at pH 10 according to the literatures [25,57]. In brief, a 2.5-g of dry weight of demineralized OPEFB pulp (about 85% of cellulose content) was suspended in water (250 mL) containing TEMPO (16 mg/g-cellulose) and NaBr (100 mg/g-cellulose). Oxidation reaction was initiated by adding 2 M NaClO aq as oxidant (10, 15, 20 mmol/g-cellulose). The pH of suspension was maintained at 10 by adding 0.5 M aqueous NaOH with a pH titrator (Mitsubishi Chemical Analytech, Yamato, Japan) during the reaction. After 2 h, the reaction was quenched by adding ethanol (2 mL), followed by addition of $NaBH_4$ (100 mg/g-cellulose), and the resultant mixture was further stirred for 1 h. The obtained suspension was thoroughly washed using deionized water by centrifugation and then sonicated by an ultrasonic homogenizer for 5 min (US-300E, Nihonseiki Ltd., Tokyo, Japan). Residual unfibrillated fibers were removed by further centrifugation at 12000 *g* for 10 min. Obtained TOCNs, denoted as T10, T15, and T20 corresponding to the amount of NaClO used in the oxidation, were kept at 4°C until further use.

2.3.3 Characterization of TOCNs

Elemental analysis was performed with an Organic Micro Analyzer CHN CORDER MT-6 (Yanaco Ltd., Tokyo, Japan). The surface morphology of original OPEFB pulp was observed using a scanning electron microscope (SEM SU-3500, Hitachi Ltd., Tokyo, Japan) at the Center of Advanced Instrumental Analysis, Kyushu University. Samples were mounted on carbon tape without any coating, and the machine was operated at an acceleration voltage of 15 kV and pressure of 30 Pa. The length and width of TOCNs were measured by a transmission electron microscopy (TEM) (JEM 2100-HC, JEOL Ltd., Tokyo, Japan) operated at an acceleration voltage of 120 kV at the Ultramicroscopy Research Center, Kyushu University. The size was measured using Image-J version 1.51s. Structural analysis was observed by X-ray diffraction (XRD), Fourier Transform Infrared (FTIR) and thermogravimetric analysis (TGA) of TOCNs were conducted as described in our previous work [58]. The carboxylate contents were measured by conductometric titration [25]. Determination of α-cellulose content as described in the previous section (**See section 2.2.3.3**). Zeta potential was measured using Zetasizer nanoseries MAL 109300 (Malvern, UK) by

placing 0.05 % (w/v) of TOCN solution in folded capillary cells DTS1070 (Malvern Instrument Ltd., UK).

2.3.4 Results and Discussion

2.3.4.1 Yields and birefringence

Yields of obtained TOCNs for T10, T15 and T20 were 37%, 34% and 47%, respectively. Birefringence of obtained TOCNs as described in **Fig. 2.9**.

Figure 2.9 Birefringence test of T10 (left); T15 (middle) and T20 (right)

Birefringence was observed to evaluate the nano-scale dispersibility of the TOCNs in water. OPEFB-derived TOCNs showed nano-scale dispersibility. The nano-scale dispersibility is important for TOCNs uses in several applications, particularly in aqueous media.

2.3.4.2 Elemental analysis, carboxylate content and zeta potential

Elemental analysis revealed that the carbon content (C%) of obtained TOCNs decreased as compared to the starting pulp (**Table 2.6**). Higher amounts of oxidant applied in this study revealed that the C% almost unchanged by increasing the oxidant, indicating that TEMPO-mediated oxidation selectively occurred on the primary

hydroxy groups of cellulose and did not affect cellulose polymorph. Carboxylate content increased by increasing the amount of oxidant. Saito and Isogai reported that the increase of carboxylate content is not exceeds a certain level even by the excess NaClO addition [25]. The presence of carboxylate groups induce negative zeta potential on the solid surfaces, resulting in high dispersibility of TOCNs in water by electrical repulsion [26], and high dispersant effects for various suspended solid matters [27].

Table 2.6 Carbon contents, carboxylate contents and zeta potential

Sample	Carbon content (C%)	α – cellulose content (%)	Carboxylate content (mmol/g)	Zeta potential (mV)
Raw pulp	40.13	85	n.d.	n.d
T-10	38.32	91	1.08	-37
T-15	38.67	93	1.34	-41
T-20	37.77	90	1.50	-43

n.d. = not determined

2.3.4.3 Optical image and morphology of TOCNs

Optical image and morphology of obtained TOCNs as shown in **Fig. 2.10**. Microscopy analysis of original pulp showed that TEMPO-mediated oxidation, followed by ultrasonication successfully afforded nanofibrillated fibers from OPEFB pulp. The length of resultant TOCNs was more than 200 nm, and the width was 3–9 nm. The aspect ratios were 40 ± 22 for T-10, 41 ± 19 for T-15, and 41 ± 14 for T-20 (**Fig. 2.10**). Notably, the aspect ratios of resultant TOCNs were almost unchanged by increasing the amount of oxidant. The oxidation occurred only on C6 primary hydroxy groups on the surfaces of fibrils in cellulose fibers, therefore no significant changes in the fibrous morphology [57]. The aspect ratios of obtained TOCNs were much higher

than those reported in previous study, in which TOCNs were produced from microcrystalline cellulose (MCC) of OPEFB [43]. Larger length of TOCNs can be obtained when holocellulose was used as starting materials in TEMPO-mediated oxidation at pH 10 compared to thermomechanical pulp as raw material [59].

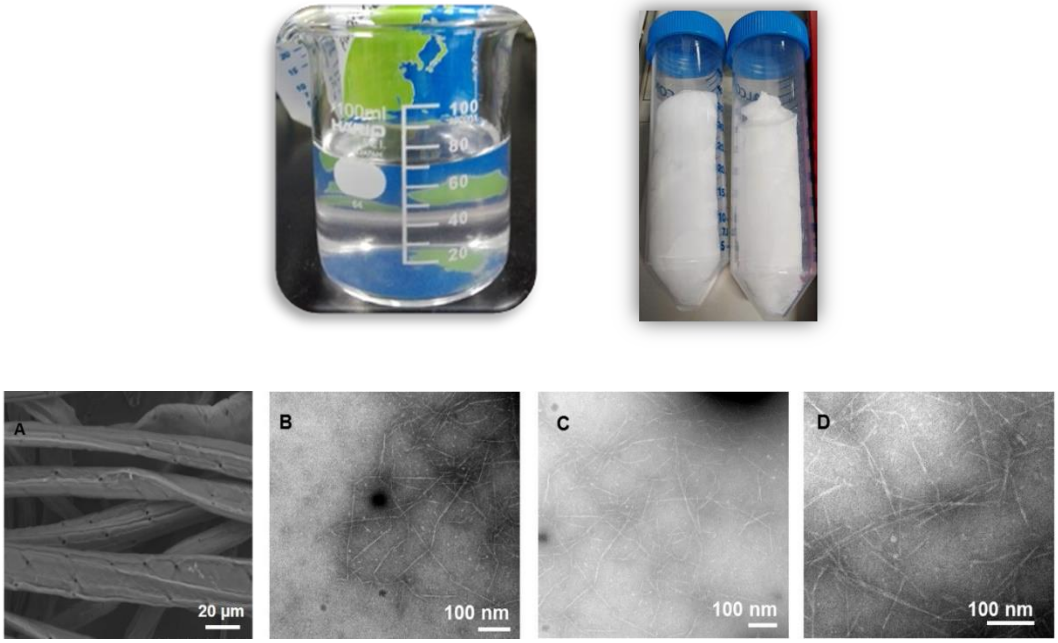

Figure 2.10 Optical images of viscous TOCNs and freeze-dried TOCNs (upper) and SEM image of raw OPEFB pulp (A) and TEM images of the resultant TOCN T-10 (B), T-15 (C), and T-20 (D) (bottom)

2.3.4.4 Structural Analysis

The FTIR and XRD analyses of the starting pulp and resultant TOCNs are shown in **Fig. 2.11**. In FTIR spectra, the peaks at 1618 cm^{-1} of resultant TOCNs are attributed to carboxylate groups, and small absorption bands at 1720 cm^{-1} are C=O groups in the protonated carboxy groups [60]. This absorption band was not found on the starting pulp spectra. The FTIR spectra justified that during the oxidation process, significant amount of carboxylate groups were introduced into nanocellulose surface [57].

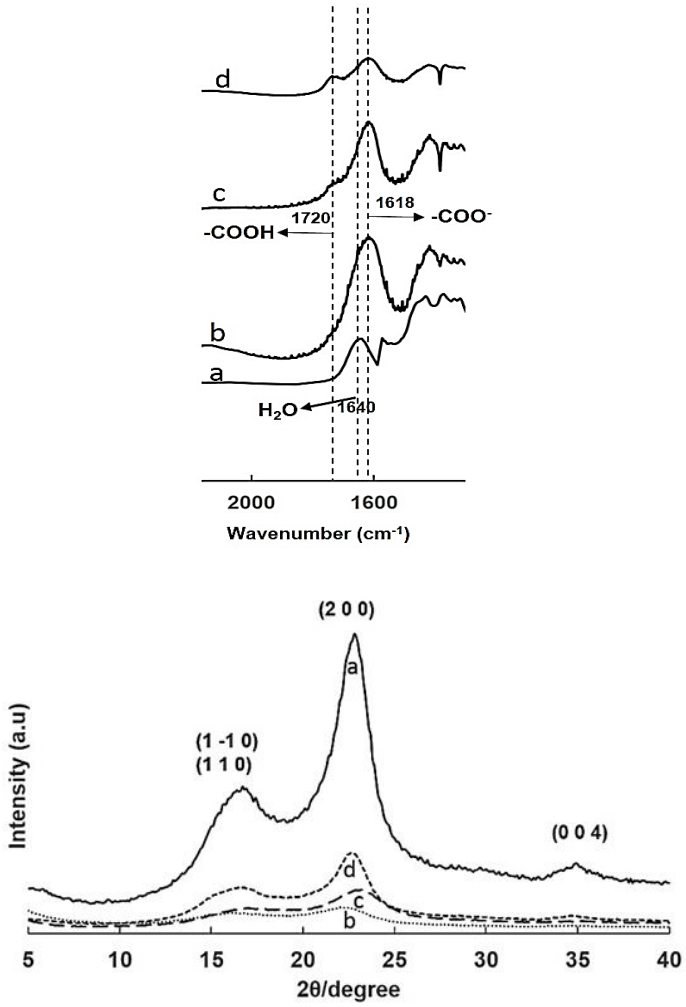

Figure 2.11 FTIR spectra (upper) and XRD patterns (bottom) of: (a) raw pulp of OPEFB (b) T-10; (c) T-15 and (d) T-20

XRD profiles showed that crystallinity indices (Cr.I) of resultant TOCNs decreased after oxidation process (**Fig. 2.11**). It might be caused by the regio-selective conversion of primary hydroxy groups at the C6 position of raw pulp (cellulose) to carboxylate ones by having sodium glucuronosyl units and made the crystallinity index become lower [57,61]. However, the 200 and 110 diffraction peak positions of TOCNs changed after oxidation, it may indicate the introduction of carboxylate and aldehyde groups on the surface of cellulose I [25]. The Cr.I of raw pulp was 61% and for T-10,

T-15 and T-20 were: 34%, 46% and 55%, respectively. Higher amount of oxidant added in the oxidation decreased the Cr.I compared to the raw pulp. Presumably, the carboxylate groups formed by oxidation present on the surfaces of crystalline cellulose [24,25]. However, the Cr.I of obtained TOCN increased by increasing the amount of oxidant. It was assumed that the more crystalline region was extracted with the addition of oxidant. The Cr.I values of resultant TOCNs were lower than previous study conducted by Rohaizu and co-author (60.5%). This lowering is affected by the difference of starting cellulose source, whereas microcrystalline cellulose of OPEFB was used in previous study which was relatively highly crystalline [43].

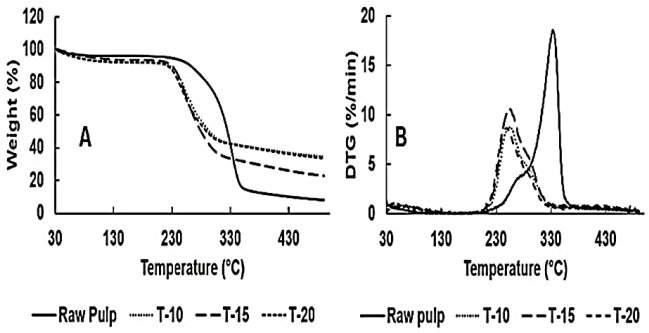

C

Sample	T_{on} (°C)	T_{max} (°C)
Raw pulp	252.2	359.2
T-10	220.1	251.2
T-15	215.4	252.1
T-20	211.5	250.1

Figure 2.12 TG curves (A); DTG curves (B); and thermal properties of raw pulp and resultant TOCNs (C)

Thermal analysis was performed by thermogravimetry (TG) and differential thermogravimetry (DTG); the onset temperature (T_{on}) and the maximum degradation temperature (T_{max}) as shown in **Fig. 2.12**. Thermal stability of resultant TOCNs was sharply decreased compared to the starting pulp, because carboxylate groups trigger rapid decomposition of polysaccharides at lower temperature [16]. The amount of oxidant in the preparation of TOCN did not affect the thermal properties of resultant TOCNs, indicates that the oxidation occurred on the surfaces on primary hydroxyl

groups, instead of crystallite area [25]. On the other hand, the char residue remaining after 500°C of resultant TOCNs was much higher compared to that with the starting pulp. It indicates that carboxylate groups on TOCNs have a flame retardant effect [43]. These thermal properties parameters were close to TOCNs made of MCC OPEFB but lower than TOCNs made from corn husk pulp [43,55].

2.4 Conclusion

Cellulose nanocrystals (CNCs) and TEMPO-oxidized cellulose nanofibers (TOCNs) were successfully prepared from oil palm empty fruit bunches (OPEFB) pulp. CNCs were prepared by hydrochloric acid hydrolysis, followed by ultrasonic homogenization and TOCNs were prepared using TEMPO-mediated oxidation by modifying the amount of oxidant, NaClO. The CNCs prepared here formed dispersions in water that remained stable for more than 6 months, and showed clear birefringence, indicating excellent nano-dispersibility. The TEM observations revealed the aspect ratios of our OPEFB-derived CNCs were higher than that of a woody CNC sample. Furthermore, thermogravimetric analysis revealed that the present CNCs had higher thermal stability than that of the woody CNC. The thermal stability of our CNCs was comparable to that of previously reported oil palm biomass-derived CNCs prepared by other methods. Hydrochloric acid hydrolysis is one of the simplest treatments for preparing CNCs; thus, the findings of this study will be useful for providing a simple protocol to produce pure CNCs from waste of OPEFB and other bioresources.

The differences in applying amount of primary oxidant in TOCNs preparation, NaClO, were not affected the TOCNs morphologies which were observed by microscopy and XRD analysis. Higher amount of oxidant slightly increased the

carboxylate content and induced lower thermal stability of TOCNs OPEFB than raw pulp. High aspect ratios and the presence of carboxylate groups of TOCNs are promising properties for further application such as reinforcing agents in plastics and nanoparticle anchor in catalytic reactions.

2.5 References

[1] Directorat General of Estate Crops, Tree Crop Estate Statistics of Indonesia 2014-2016, Jakarta, 2015. doi:http://ditjenbun.pertanian.go.id/tinymcpuk/gambar/file/statistik/2016/SAWIT 2014-2016.pdf.

[2] Y. Sudiyani, D. Styarini, E. Triwahyuni, Sudiyarmanto, K.C. Sembiring, Y. Aristiawan, H. Abimanyu, M.H. Han, Utilization of biomass waste empty fruit bunch fiber of palm oil for bioethanol production using pilot–scale unit, Energy Procedia. 32 (2013) 31–38. doi:10.1016/j.egypro.2013.05.005.

[3] D.C. Nieves, K. Karimi, I.S. Horvath, Improvement of biogas production from oil palm empty fruit bunches (OPEFB), Ind. Crop. Prod. 34 (2011) 1097–1101. doi:10.1016/j.indcrop.2011.03.022.

[4] K.H. Or, A. Putra, M.Z. Selamat, Oil palm empty fruit bunch fibres as sustainable acoustic absorber, Appl. Acoust. 119 (2017) 9–16. doi:10.1016/j.apacoust.2016.12.002.

[5] N.B. Osman, N. Shamsuddin, Y. Uemura, Activated carbon of oil palm empty fruit bunch (EFB); core and shaggy, Procedia Eng. 148 (2016) 758–764. doi:10.1016/j.proeng.2016.06.610.

[6] F. Fahma, S. Iwamoto, N. Hori, T. Iwata, A. Takemura, Isolation , preparation , and characterization of nanofibers from oil palm empty-fruit-bunch (OPEFB), Cellulose. 17 (2010) 977–985. doi:10.1007/s10570-010-9436-4.

[7] M.K.M. Haafiz, A. Hassan, Z. Zakaria, I.M. Inuwa, Isolation and characterization of cellulose nanowhiskers from oil palm biomass microcrystalline cellulose, Carbohydr. Polym. 103 (2014) 119–125. doi:10.1016/j.carbpol.2013.11.055.

[8] Z.A.Z. Azrina, M.D.H. Beg, M.Y. Rosli, R. Ramli, N. Junadi, A.K.M.M. Alam, Spherical nanocrystalline cellulose (NCC) from oil palm empty fruit bunch pulp via ultrasound assisted hydrolysis, Carbohydr. Polym. 162 (2017) 115–120. doi:10.1016/j.carbpol.2017.01.035.

[9] O. Nechyporchuk, M.N. Belgacem, J. Bras, Production of cellulose nanofibrils: A review of recent advances, Ind. Crop. Prod. 93 (2016) 2–25. doi:10.1016/j.indcrop.2016.02.016.

[10] J. Lamaming, R. Hashim, O. Sulaiman, C.P. Leh, T. Sugimoto, N.A. Nordin, Cellulose nanocrystals isolated from oil palm trunk, Carbohydr. Polym. 127 (2015) 202–208. doi:10.1016/j.carbpol.2015.03.043.

[11] S. Mondal, Preparation, properties and applications of nanocellulosic materials, Carbohydr. Polym. 163 (2017) 301–316. doi:10.1016/j.carbpol.2016.12.050.

[12] N. Grishkewich, N. Mohammed, J. Tang, K.C. Tam, Recent advances in the application of cellulose nanocrystals, Curr. Opin. Colloid Interface Sci. 29 (2017) 32–45. doi:10.1016/j.cocis.2017.01.005.

[13] J. Lamaming, R. Hashim, C.P. Leh, O. Sulaiman, T. Sugimoto, M. Nasir, Isolation and characterization of cellulose nanocrystals from parenchyma and

vascular bundle of oil palm trunk (Elaeis guineensis), Carbohydr. Polym. 134 (2015) 534–540. doi:10.1016/j.carbpol.2015.08.017.

[14] J. Lamaming, R. Hashim, C.P. Leh, O. Sulaiman, Properties of cellulose nanocrystals from oil palm trunk isolated by total chlorine free method, Carbohydr. Polym. 156 (2017) 409–416. doi:10.1016/j.carbpol.2016.09.053.

[15] Y.W. Chen, H.V. Lee, S.B.A. Hamid, Facile production of nanostructured cellulose from Elaeis guineensis empty fruit bunch via one pot oxidative-hydrolysis isolation approach, Carbohydr. Polym. 157 (2017) 1511–1524. doi:10.1016/j.carbpol.2016.11.030.

[16] M.K.M. Haafiz, A. Hassan, Z. Zakaria, I.M. Inuwa, M.S. Islam, Physicochemical characterization of cellulose nanowhiskers extracted from oil palm biomass microcrystalline cellulose, Mater. Lett. 113 (2013) 87–89. doi:10.1016/j.matlet.2013.09.018.

[17] M.A.F. Supian, K.N.M. Amin, S.S. Jamari, S. Mohamad, Production of cellulose nanofiber (CNF) from empty fruit bunch (EFB) via mechanical method, J. Environ. Chem. Eng. (2019) 103024. doi:10.1016/j.jece.2019.103024.

[18] Y. Okahisa, Y. Furukawa, K. Ishimoto, C. Narita, K. Intharapichai, H. Ohara, Comparison of cellulose nanofiber properties produced from different parts of the oil palm tree, Carbohydr. Polym. 198 (2018) 313–319. doi:10.1016/j.carbpol.2018.06.089.

[19] J. Araki, Electrostatic or steric? -preparations and characterizations of well-dispersed systems containing rod-like nanowhiskers of crystalline polysaccharides, Soft Matter. 9 (2013) 4125–4141. doi:10.1039/c3sm27514k.

[20] Z. Wang, Z. Yao, J. Zhou, Y. Zhang, Reuse of waste cotton cloth for the extraction of cellulose, Carbohydr. Polym. 157 (2017) 945–952. doi:10.1016/j.carbpol.2016.10.044.

[21] I. Kalashnikova, H. Bizot, B. Cathala, I. Capron, Modulation of cellulose nanocrystals amphiphilic properties to stabilize oil/water interface, Biomacromolecules. 13 (2012) 267–275. doi:10.1021/bm201599j.

[22] I. Kalashnikova, H. Bizot, P. Bertoncini, B. Cathala, I. Capron, Cellulosic nanorods of various aspect ratios for oil in water Pickering emulsions, Soft Matter. 9 (2013) 952–959. doi:10.1039/C2SM26472B.

[23] N. Amiralian, P.K. Annamalai, P. Memmott, D.J. Martin, Isolation of cellulose nanofibrils from Triodia pungens via different mechanical methods, Cellulose. 22 (2015) 2483–2498. doi:10.1007/s10570-015-0688-x.

[24] A. Isogai, T. Saito, H. Fukuzumi, TEMPO-oxidized cellulose nanofibers, Nanoscale. 3 (2011) 71–85. doi:10.1039/c0nr00583e.

[25] T. Saito, A. Isogai, TEMPO-mediated oxidation of native cellulose. The effect of oxidation conditions on chemical and crystal structures of the water-insoluble fractions, Biomacromolecules. 5 (2004) 1983–1989. doi:10.1021/bm0497769.

[26] Y. Okita, T. Saito, A. Isogai, Entire surface oxidation of various cellulose microfibrils by TEMPO-mediated oxidation, Biomacromolecules. 11 (2010) 1696–1700. doi:10.1021/bm100214b.

[27] Y. Li, H. Zhu, F. Shen, J. Wan, S. Lacey, Z. Fang, H. Dai, L. Hu, Nanocellulose as green dispersant for two-dimensional energy materials, Nano Energy. 13 (2015) 346–354. doi:10.1016/j.nanoen.2015.02.015.

[28] L. Segal, J. Creely, A. Martin, C. Conrad, An empirical method for estimating the degree of crystallinity of native cellulose using the X-Ray diffractometer, Text. Res. J. 29 (1959) 786–794.

[29] A.L.S. Pereira, D.M.D. Nascimento, M.D.S.M.S. Filho, J.P.S. Morais, N.F. Vasconcelos, J.P.A. Feitosa, A.I.S. Brígida, M. de F. Rosa, Improvement of polyvinyl alcohol properties by adding nanocrystalline cellulose isolated from banana pseudostems, Carbohydr. Polym. 112 (2014) 165–172. doi:10.1016/j.carbpol.2014.05.090.

[30] F. Kallel, F. Bettaieb, R. Khiari, A. García, J. Bras, S.E. Chaabouni, Isolation and structural characterization of cellulose nanocrystals extracted from garlic straw residues, Ind. Crop. Prod. 87 (2016) 287–296. doi:10.1016/j.indcrop.2016.04.060.

[31] E. Fortunati, P. Benincasa, G.M. Balestra, F. Luzi, A. Mazzaglia, D.D. Buono, D. Puglia, L. Torre, Revalorization of barley straw and husk as precursors for cellulose nanocrystals extraction and their effect on PVA_CH nanocomposites, Ind. Crops Prod. 92 (2016) 201–217. doi:10.1016/j.indcrop.2016.07.047.

[32] F.I. Ditzel, E. Prestes, B.M. Carvalho, I.M. Demiate, L.A. Pinheiro, Nanocrystalline cellulose extracted from pine wood and corncob, Carbohydr. Polym. 157 (2017) 1577–1585. doi:10.1016/j.carbpol.2016.11.036.

[33] S. Bano, Y.S. Negi, Studies on cellulose nanocrystals isolated from groundnut shells, Carbohydr. Polym. 157 (2017) 1041–1049. doi:10.1016/j.carbpol.2016.10.069.

[34] K. Zhang, P. Sun, H. Liu, S. Shang, J. Song, D. Wang, Extraction and comparison of carboxylated cellulose nanocrystals from bleached sugarcane

bagasse pulp using two different oxidation methods, Carbohydr. Polym. 138 (2016) 237–243. doi:10.1016/j.carbpol.2015.11.038.

[35] M. Labet, W. Thielemans, Improving the reproducibility of chemical reactions on the surface of cellulose nanocrystals: ROP of ε-caprolactone as a case study, Cellulose. 18 (2011) 607–617. doi:10.1007/s10570-011-9527-x.

[36] H. Okura, M. Wada, T. Serizawa, Dispersibility of HCl-treated cellulose nanocrystals with water-dispersible properties in organic solvents, Chem. Lett. 43 (2014) 601–603. doi:10.1246/cl.131181.

[37] J. Araki, M. Wada, S. Kuga, T. Okano, Flow properties of microcrystalline cellulose suspension prepared by acid treatment of native cellulose, Colloids Surfaces A Physicochem. Eng. Asp. 142 (1998) 75–82. doi:PII S0927-7757(98)00404-X.

[38] O. van den. Berg, J.R. Capadona, C. Weder, Preparation of homogeneous dispersions of tunicate cellulose whiskers in organic solvents, Biomacromolecules. 8 (2007) 1353–1357. doi:10.1021/bm061104q.

[39] M. Jonoobi, A. Khazaeian, P.M. Tahir, S.S. Azry, K. Oksman, Characteristics of cellulose nanofibers isolated from rubberwood and empty fruit bunches of oil palm using chemo-mechanical process, Cellulose. 18 (2011) 1085–1095. doi:10.1007/s10570-011-9546-7.

[40] S. Fujisawa, Y. Okita, H. Fukuzumi, T. Saito, A. Isogai, Preparation and characterization of TEMPO-oxidized cellulose nanofibril films with free carboxyl groups, Carbohydr. Polym. 84 (2011) 579–583. doi:10.1016/j.carbpol.2010.12.029.

[41] S. Montanari, M. Roumani, L. Heux, M.R. Vignon, Topochemistry of carboxylated cellulose nanocrystals resulting from TEMPO-mediated oxidation, Macromolecules. 38 (2005) 1665–1671. doi:10.1021/ma048396c.

[42] S.J. Eichhorn, A. Dufresne, M. Aranguren, N.E. Marcovich, J.R. Capadona, S.J. Rowan, C. Weder, W. Thielemans, M. Roman, S. Renneckar, W. Gindl, S. Veigel, J. Keckes, H. Yano, K. Abe, M. Nogi, A.N. Nakagaito, A. Mangalam, J. Simonsen, A.S. Benight, A. Bismarck, L.A. Beglund, T. Peijs, Review : current international research into cellulose nanofibres and nanocomposites, J Mater Sci. 45 (2010) 1–33. doi:10.1007/s10853-009-3874-0.

[43] R. Rohaizu, W.D. Wanrosli, Sono-assisted TEMPO oxidation of oil palm lignocellulosic biomass for isolation of nanocrystalline cellulose, Ultrason. Sonochem. 34 (2017) 631–639. doi:10.1016/j.ultsonch.2016.06.040.

[44] A. de. Campos, A.R. de S. Neto, V.B. Rodrigues, B.R. Luchesi, F.K.V. Moreira, A.C. Correa, L.H.C. Mattoso, J.M. Marconcini, Bionanocomposites produced from cassava starch and oil palm mesocarp cellulose nanowhiskers, Carbohydr. Polym. 175 (2017) 330–336. doi:10.1016/j.carbpol.2017.07.080.

[45] A.A. Oun, J.W. Rhim, Isolation of cellulose nanocrystals from grain straws and their use for the preparation of carboxymethyl cellulose-based nanocomposite films, Carbohydr. Polym. 150 (2016) 187–200. doi:10.1016/j.carbpol.2016.05.020.

[46] P. Lu, Y. Hsieh, Preparation and characterization of cellulose nanocrystals from rice straw, Carbohydr. Polym. 87 (2012) 564–573. doi:10.1016/j.carbpol.2011.08.022.

[47] N. Johar, I. Ahmad, A. Dufresne, Extraction, preparation and characterization of cellulose fibres and nanocrystals from rice husk, Ind. Crop. Prod. 37 (2012) 93–99. doi:10.1016/j.indcrop.2011.12.016.

[48] A.D. French, Idealized powder diffraction patterns for cellulose polymorphs, Cellulose. 21 (2014) 885–896. doi:10.1007/s10570-013-0030-4.

[49] A.M. Slavutsky, M.A. Bertuzzi, Water barrier properties of starch films reinforced with cellulose nanocrystals obtained from sugarcane bagasse, Carbohydr. Polym. 110 (2014) 53–61. doi:10.1016/j.carbpol.2014.03.049.

[50] X. Luo, X. Wang, Preparation and characterization of nanocellulose fibers from NaOH/Urea pretreatment of oil palm fibers, Bioresources. 12 (2017) 5826–5837.

[51] J.P. Reddy, J.W. Rhim, Isolation and characterization of cellulose nanocrystals from garlic skin, Mater. Lett. 129 (2014) 20–23. doi:10.1016/j.matlet.2014.05.019.

[52] T. Taflick, L.A. Schwendler, S.M.L. Rosa, C.I.D. Bica, S.M.B. Nachtigall, Cellulose nanocrystals from acacia bark–Influence of solvent extraction, Int. J. Biol. Macromol. 101 (2017) 553–561. doi:10.1016/j.ijbiomac.2017.03.076.

[53] P. Ninduangdee, V.I. Kuprianov, E. Young Cha, R. Kaewrath, P. Youngyen, W. Attawethworawuth, Thermogravimetric studies of oil palm empty fruit bunch and palm kernel shell: TG/DTG analysis and modeling, Energy Procedia. 79 (2015) 453–458. doi:10.1016/j.egypro.2015.11.518.

[54] J. Liu, D.J. Martin, R.J. Moon, J.P. Youngblood, Enhanced thermal stability of biomedical thermoplastic polyurethane with the addition of cellulose nanocrystals, J. Appl. Polym. Sci. 132 (2015) 1–8. doi:10.1002/app.41970.

[55] X. Yang, F. Han, C. Xu, S. Jiang, L. Huang, L. Liu, Z. Xia, Effects of preparation methods on the morphology and properties of nanocellulose (NC) extracted from corn husk, Ind. Crops Prod. 109 (2017) 241–247. doi:10.1016/j.indcrop.2017.08.032.

[56] H. Fukuzumi, T. Saito, Y. Okita, A. Isogai, Thermal stabilization of TEMPO-oxidized cellulose, Polym. Degrad. Stab. 95 (2010) 1502–1508. doi:10.1016/j.polymdegradstab.2010.06.015.

[57] T. Saito, S. Kimura, Y. Nishiyama, A. Isogai, Cellulose nanofibers prepared by TEMPO-mediated oxidation of native cellulose, Biomacromolecules. 8 (2007) 2485–2491. doi:10.1021/bm0703970.

[58] N. Hastuti, K. Kanomata, T. Kitaoka, Hydrochloric Acid Hydrolysis of Pulps from Oil Palm Empty Fruit Bunches to Produce Cellulose Nanocrystals, J. Polym. Environ. 0 (2018) 0. doi:10.1007/s10924-018-1248-x.

[59] R. Kuramae, T. Saito, A. Isogai, TEMPO-oxidized cellulose nanofibrils prepared from various plant holocelluloses, React. Funct. Polym. 85 (2014) 126–133. doi:10.1016/j.reactfunctpolym.2014.06.011.

[60] M. Shimizu, H. Fukuzumi, T. Saito, A. Isogai, Preparation and characterization of TEMPO-oxidized cellulose nanofibrils with ammonium carboxylate groups, Int. J. Biol. Macromol. 59 (2013) 99–104. doi:10.1016/j.ijbiomac.2013.04.021.

[61] B. Puangsin, Q. Yang, T. Saito, A. Isogai, Comparative characterization of TEMPO-oxidized cellulose nanofibril films prepared from non-wood resources, Int. J. Biol. Macromol. 59 (2013) 208–213. doi:10.1016/j.ijbiomac.2013.04.016.

Chapter 3

Application of Oil Palm Empty Fruit Bunches Nanocellulose in Bio-alcohol Production

3.1. Introduction

Indonesia is the world's largest producer and exporter of palm oil in the world [1] Therefore, oil palm (*Elaeis guineensis*) is the mainstay of estate crop commodity in Indonesia and its contribution to the national economy tends to increase from year to year and expected to strengthen overall national development [2]. In addition, the crude palm oil (CPO) production left abundant supply of palm-press fibres and oil palm empty fruit bunches (OPEFB) which are regarded as wastes and have not been utilized satisfactorily [3]. The palm oil industry must dispose about 1.1 ton of OPEFB for every ton of CPO produced [4]. The huge amount of OPEFB is essential to be proceed as added-value products because OPEFB relatively contain high amount of cellulose about 59% of cellulose [5]. Cellulose is an abundant natural polymer and can be extracted from plant, animal, algae and bacteria [6]. Cellulosic fibers have gained consideration because of their following promising characteristics such as: biodegradability, renewability and high mechanical properties due to its own crystalline organization [7]. In view of its relatively high content of cellulose, OPEFB is a potential source as nanocellulose raw materials. In general term “nanocellulose” refers to cellulosic extracts or processed materials and having nano-scale structural dimensions [6]. One of useful method that enables cellulose fibers to be completely converted to individual cellulose nanofibrils is catalytic oxidation using 2,2,6,6-tetramethylpiperidine 1-oxyl (TEMPO). By using TEMPO/NaBr/NaClO oxidation system, this process can convert selectively the primary hydroxy groups of

polysaccharides into carboxylates; fully individualized TEMPO-oxidized cellulose fibrils can be obtained by approximately 4 nm in width and at least a few micrometers in length; with carboxylate contents of more than about 1 mmol/g by mild mechanical disintegration in water [8,9]. Nanocellulose produced by 2,2,6,6-tetramethylpiperidine-1-oxyl (TEMPO)-catalyzed oxidation, namely TEMPO-oxidized cellulose nanofibers (TOCNs), has attracted considerable attention since it requires low energy in its production, affording the narrowest nanofiber ever reported [10]. Besides, the TOCNs bear anionic carboxylate groups on their surfaces as the result of TEMPO-mediated selective oxidation of surface-exposed primary alcohols to carboxylates [11]. These carboxylates induce negative zeta potential as low as –70 mV on the solid surfaces, resulting in high dispersibility of TOCNs in water by electrical repulsion [12], and high dispersant effects for various suspended solid matters [13].

Recently, the use of TOCNs has been applied in several applications such as for green reinforcement in polymer composite, adsorbent for metal removal, gels component for medical application (drug delivery) [14–17]. Although nanocellulose has been extensively studied for developing reinforcing agents in composite plastics and films [18,19], enhancers in emulsion systems [20,21], functional hydrogels for environmental remediation [22,23], and carriers for metal catalysts and enzyme immobilization [24–26], its application in microbial systems remains limited. Yu and co-workers have reported effects of the size of nanocellulose on microalgal flocculation and lipid metabolism; cellulose nanofibrils effectively induced microalgal flocculation *via* a mechanical interaction based on geometric properties such as nanocellulose morphology and hydrogen bonding [27]. Sun and co-workers also observed aggregation of *Pseudomonas fluorescens* and *Escherichia coli* K12 in the presence of nanocellulose; they found that bacterial aggregation and adhesion to solid

surfaces were significantly affected by the surrounding solution chemistry [28,29]. The electrostatic interaction promoted by the charged cellulose nanocrystals could give rise to clustering, phase separation and rapid aggregation of negatively charged bacteria [28,30,31]. Clustering and phase separation of bacteria are very important for product recovery in microbial biofuel production.

Practical applications of microbial systems in the production of biofuels from renewable resources attract much attention for environmental and economic reasons [32]. Biobutanol produced by microbial fermentation is of significant interest as demand for butanol as an industrial intermediate is rapidly increasing, and it can be used directly in gasoline engines without any modification and/or substitution [33]. Butanol is the most attractive biofuel alternative to ethanol because it has numerous desirable properties, including lower vapor pressure, higher calorific value, less corrosive properties, and a non-hygroscopic nature [34]. Butanol can be produced from renewable resources through acetone-butanol-ethanol (ABE) fermentation [35] using *Clostridia* as a high-performance butanol-producing strain [36]. The metabolic pathway of typical ABE fermentation of butanol-producing *Clostridia* strain as summarized in **Fig 3.1** [37].

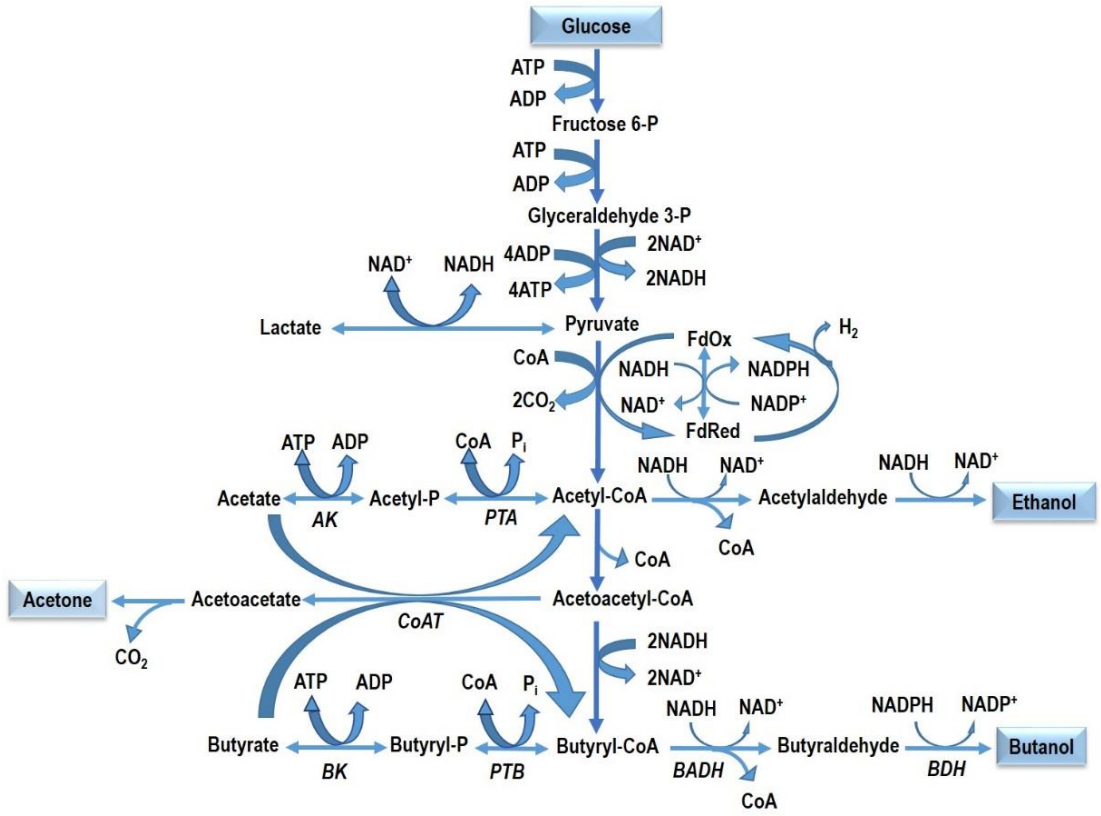

Figure 3.1. Metabolic pathway of acetone-butanol-ethanol (ABE) fermentation in butanol-producing strain. Several enzymes involved in ABE fermentation are described in italics. These abbreviations are: *AK*, acetate kinase; *PTA*, phospotransacetylase; *CoAT*, CoA transferase; *PTB*, phospotransbutyrylase; *BK*, butyrate kinase; *BADH*, butyraldehyde dehydrogenase; *BDH*, butanol dehydrogenase

However, microbial butanol production has suffered from severe product inhibition in fermentation processes and high cost of product recovery, resulting in low butanol productivity. Studies have been conducted to overcome these obstacles by integrating a butanol separation step, such as cell immobilization, extractive fermentation, pervaporation, or perstraction [38–40]. Among these, extractive fermentation (liquid–liquid extraction) has great potential to increase the product titer

if one can determine the most appropriate solvent for butanol selectivity that is compatible with the cells producing the butanol [40,41]. In extractive fermentation, the broth is in contact with an extracting solvent; therefore some inhibitory products become dissolved in the solvent, resulting in reduction of inhibitory effects on the culture [42]. However, the efficiency of this method depends on the affinity of solutes for the extraction solvent and the mixing ratio of the phases [43]. Extractive fermentation may result in inactivation of cells due to the extensive exposure of cells to extraction solvents and product toxicity [44]. Therefore, advanced technology to immobilize cells has been investigated to overcome such problems by using silica gel, pumice and Ca-alginate as microbial carriers and has been applied in microbial fermentation [45,46]. However, to the best of our knowledge, no study has reported an effective strategy using nanocellulose to improve microbial stability to enhance butanol productivity. Herein, we attempted to address microbial stability in biobutanol production by using in-broth TOCNs, which were produced from OPEFB waste. OPEFB-derived TOCNs have surface anionic carboxylate groups with high density (up to 1.5 mmol g^{-1}); these can promote electrostatic repulsion of negatively-charged bacteria producing biobutanol, which is important in microbial system stability by preventing bacterial aggregation and then enhancing microbial dispersibility [30,47]. Our strategy is illustrated in **Fig. 3.2.**

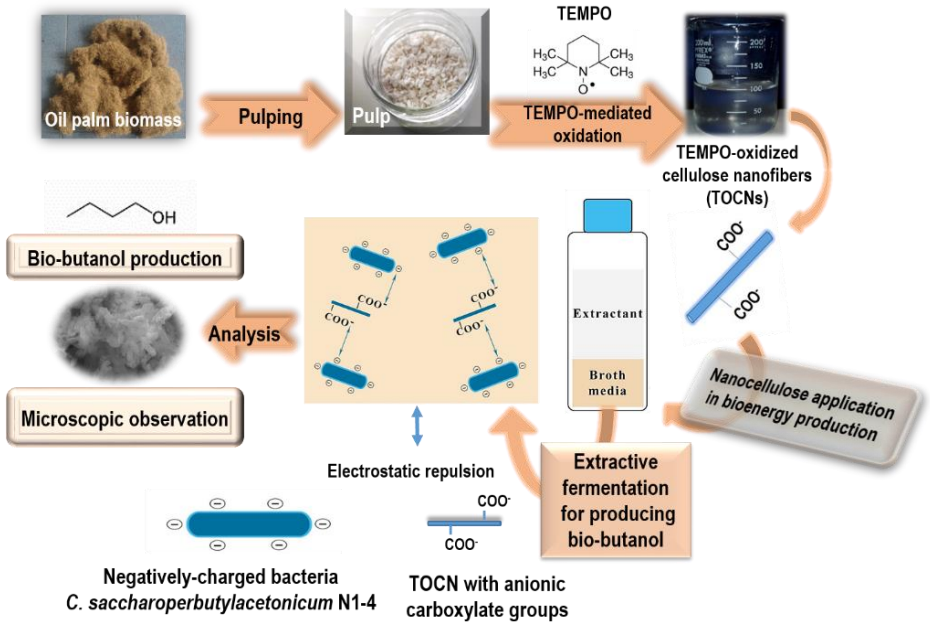

Figure 3.2. Overview of use of 2,2,6,6-tetramethylpiperidine-1-oxyl (TEMPO)-oxidized cellulose nanofibers (TOCNs) in microbial biobutanol production.

Furthermore, the application of nanocellulose in bioenergy can be applied as a filler or hydrophilic additive into membrane by blending or coating technique and applied as ultrafiltration and separation membrane for gas capturing and bioenergy recovery [48,49]. The use of nanocellulose in membrane composite also increase biofouling resistant of membrane by forming a thin layer on top of porous polymer matrix after coating [50]. Utilization of nanocellulose in membrane application was mostly derived from wood rather than non-wood [50,51], whereas nanocellulose extraction from non-wood was considered more efficient in delignification process due to the lignin content is less than that of woody plants [52]. The utilization of nanocellulose derived from non-wood material, oil palm empty fruit bunches (OPEFB), as an additive in membrane composite for bioenergy application is still unknown. Therefore, in this study, pervaporation membranes consisting of TOCN from OPEFB

and alginate that has not been studied previously was investigated. Nanocellulose derived from OPEFB was cross-linked with alginate and calcium chloride to produce a membrane and applied in pervaporation system for water-ethanol mixture separation. Pervaporation is a method for the separation of mixtures of liquids by partial vaporization through a non-porous membrane. The separation mechanism is a solution–diffusion model [53]. The method is particularly useful to separate liquid mixtures with close boiling points as well as azeotropic mixtures of water-ethanol. It is possible to separate the mixture components on the basis of liquid polarity and its interaction with the polymer membranes [54]. This process requires the feed liquid mixtures to contact one side of semi-permeable Among the reported of pervaporation membranes in water-ethanol separation, the alginate membranes gained much attention. It caused by their good membrane forming properties, high affinity toward water molecules, non-toxic, inexpensive, easy to use but lower mechanical strength [55]. Therefore, the utilization of nanocellulose in alginate membrane is suggested to conquer this disadvantage. Nanocellulose film prepared by TEMPO-mediated oxidation (TOCN) possess high aspect ratio and mechanical properties by tensile strength > 200 MPa [56]. The presence of anionic carboxylate groups on the surface of TOCN are responsible to improve hydrophilic properties of membrane. The presence of water increase membrane permeability and plasticity, it may undergo competitive sorption of other gas species which is important in the case of facilitated the membranes transport [49,57,58]. However, the study of pervaporation membrane using alginate and TOCN has not been reported yet. Meanwhile, the use of other polysaccharide such as chitosan for alcohol dehydration had been reported intensively [55,59–61]. The use of nanocellulose from OPEFB in bioenergy application can open

up the utilization of low cost agricultural residue to be an added-value and useful products.

3.2. Application of OPEFB Nanocellulose in Enhanced Microbial Bio-butanol Production

3.2.1. Materials

Bleached kraft pulp of oil palm empty fruit bunches (OPEFB) was kindly supplied from Biomaterial Research Institute, Indonesian Institute of Sciences (Bogor, Indonesia). 2,2,6,6-Tetramethylpiperidine 1-oxyl (TEMPO), sodium bromide, sodium hypochlorite, and sodium borohydride were purchased from Sigma-Aldrich (Tokyo, Japan) and used without further purification. The water used in this study was purified with an Arium Ultrapure Water System (Sartorius Co., Ltd., Tokyo, Japan). *Clostridium saccharoperbutylacetonicum* N1-4 ATCC 13564 was used in this study. TOCNs from Nippon Paper Company were used as comparison.

3.2.2. Method

3.2.2.1. Preparation of TEMPO-oxidized cellulose nanofibers (TOCNs) from OPEFB

The bleached kraft pulp of OPEFB was soaked in a 0.01 M HCl solution for 30 min for demineralization. TOCN was prepared using a TEMPO/NaBr/NaClO system. In brief, a 2.5-g portion of demineralized OPEFB pulp (about 85% cellulose content) was suspended in water (250 mL) containing TEMPO (16 mg/g-cellulose) and NaBr (100 mg/g-cellulose). Oxidation was initiated by adding 2 M NaClO aq. (20 mmol/g-cellulose), and the pH of the suspension was maintained at 10 by adding 0.5 M aqueous

NaOH with a pH titrator (Mitsubishi Chemical Analytech, Yamato, Japan) during the reaction. After 2 h, the oxidation was quenched by adding ethanol (2 mL), followed by the addition of $NaBH_4$ (100 mg/g-cellulose), and the resultant mixture was stirred for 1 h. The obtained suspension was thoroughly washed using deionized water and then centrifuged at 4000 × g for 10 min (five times) and sonicated using an ultrasonic homogenizer US-300E (Nihonseiki Ltd., Tokyo, Japan) at the maximum level for 5 min. Remaining floating fibers were removed by further centrifugation at 12000 × g for 10 min. Obtained TOCN was kept at 4°C until further use, and named TOCN-OPEFB (op-TOCN).

3.2.2.2. Characterization of TOCNs-derived OPEFB (op-TOCN)

Elemental analysis was performed with an Organic Micro Analyzer CHN CORDER MT-6 (Yanaco Ltd., Tokyo, Japan). The surface morphology of OPEFB pulp and TOCN-OPEFB were observed using a scanning electron microscope (SEM SU-3500, Hitachi Ltd., Tokyo, Japan) at the Center of Advanced Instrumental Analysis, Kyushu University. Samples were mounted on carbon tape; the machine was operated at an acceleration voltage 15 kV and the vacuum was set at 30 Pa. The length and width of TOCN-OPEFB were observed by transmission electron microscopy (JEM 2100-HC, JEOL Ltd., Tokyo, Japan) operated at an acceleration voltage of 120 kV at the Ultramicroscopy Research Center, Kyushu University. The size was measured using Image-J software version 1.51s. X-ray diffraction, Fourier-transform infrared spectroscopy and thermogravimetric analysis of TOCN were conducted as described in our previous work [62]. The carboxylate content of TEMPO-oxidized cellulose nanofibers was determined by conductometric titration [11]. Zeta potential was measured using Malvern Zetasizer Nanoseries (MAL1093000) (Malvern

Instrument Ltd., UK) by placing 1 mL of TOCNs solution *ca*.0.1% (w/v) in folded capillary cells DTS 1070 (Malvern Instrument Ltd., UK).

3.2.2.3. Microorganism inoculation

One milliliter of spore suspension of *C. saccharoperbutylacetonicum* N1-4 was transferred from sand stock and refreshed in 9 mL of fresh potato glucose medium (10% v/v) [38]. The spore suspension was heat-shocked in a water bath at 100°C for 1 min, and then refreshed at 30°C for 24 h anaerobically using an Anaeropack (Mitsubishi Gas Chemical, Co., Inc., Tokyo, Japan). The refreshed culture broth was then inoculated into tryptone–yeast extract–acetate (TYA) medium [54]. After inoculation, the culture broth was incubated anaerobically at 30°C for 15 h using an Anaeropack, and then used as a seed culture.

3.2.2.4. Extractive fed-batch fermentation with free cells

Fed-batch extractive fermentation with free cells was performed in a 25-mL portion of TYA broth and a 50-mL portion of extractant, which was composed of a 1:1 (*v*/*v*) mixture of oleyl alcohol and tributyrin; the volume ratio of extractant (V_e) to broth (V_b) was thus 2.0 ($V_e/V_b = 2.0$). In brief, seed culture (2.5 mL) was inoculated into a 25-mL portion of TYA medium, containing glucose (2.5 mL of 50 g/L solution), calcium carbonate (2.5 mL of 3 g/L solution), and TOCNs (5.0 mL of 0.5% *w*/*v* aqueous dispersion, 25 mg of TOCNs in dry weight; see the Supporting Information for preparation of TOCNs) in a 500-mL Erlenmeyer flask closed with a rubber seal, as an aqueous phase. The flask was then sparged with nitrogen gas for 10 min to obtain anaerobic conditions. The fed-batch cultures were grown at 30°C in a shaker (100 rpm)

and by feeding 1 g of glucose powder at 24, 48 and 72 h after seeding and maintained the anaerobic condition by sparging with N_2 after glucose feeding.

3.2.2.5. Extractive fed-batch fermentation with immobilized cells

A solution of sodium alginate (4% *w*/*v*) was prepared in boiling water and autoclaved at 115°C for 15 min. Precultured cells (2.5 mL) and TOCNs (0.5% *w*/*v*, 25 mg dry weight) were added into sterilized saline water (20 mL, 0.85% NaCl). The resultant suspension was then mixed with an equal volume of 4% sodium alginate solution (final concentration of sodium alginate, 2%). As-prepared mixture was then dropped into a 3% $CaCl_2$ solution using a syringe with continuous stirring to form alginate beads containing cells and TOCNs. The resultant beads were recovered by filtration. Cell-containing alginate beads without TOCNs were also prepared as a control. The diameters of beads were approximately 5 mm. Extractive fed-batch fermentation with immobilized cells was performed as described above (section 2.2).

3.2.2.6. Analytical Methods

Cell density was determined by measuring the optical density of the suspension at 562 nm (OD_{562}) using a UV/vis spectrophotometer (Bio-Spec, Shimadzu, Kyoto, Japan) after diluting the samples. The dry cell weight (DCW) was calculated according to a previously reported method [63] from the formula:

$$DCW = 0.301 \times OD_{562} \times D - 0.0008 \quad (1)$$

where D is the dilution rate.

The total butanol concentration ($[BuOH]_{Total}$) was defined as total amount of butanol produced in all the phases per broth volume (g/L-broth), and calculated as follows [64]:

$$[BuOH]_{Total} = ([BuOH]_b V_b + [BuOH]_c V_c + [BuOH]_e V_e) / V_b \quad (2)$$

where $[BuOH]_b$ and V_b are the butanol concentration (g/L) in the broth and the volume (L) of the broth, $[BuOH]_c$ and V_c are the butanol concentration in the cell beads and the volume of the beads, and $[BuOH]_e$ and V_e are the butanol concentration in the extractant and the volume of the extractant, respectively. V_c the volume of alginate beads, is 1.5 mL for every measurement because six beads were crushed in aqueous sodium citrate solution in a total volume of 1.5 mL.

The concentration of glucose was measured in the supernatant obtained by centrifugation of broth by using a high-performance liquid chromatograph (US-HPLC-1210, JASCO, Tokyo, Japan) equipped with a refractive index detector and SH-1011 column (Shodex, Tokyo, Japan). H_2SO_4 aq. (0.05 mM) was used as the mobile phase (1.0 mL/min, 50°C), using an injection volume of 20 μL. The concentration of butanol was measured in supernatant obtained by centrifugation of both extractant and broth using a gas chromatograph (6890A, Agilent Technologies, Palo Alto, CA, USA) equipped with a flame ionization detector and a 15-m capillary column (INNOWAX 19095N-121, Agilent Technologies) in previously reported conditions [36].

The distribution coefficient (K_d) of butanol between the extractant (oil phase) and broth (aqueous phase) was calculated as:

$$K_d = [BuOH]_e / [BuOH]_b \quad (3)$$

The treatments of free TOCNs and the presence of TOCNs was analyzed with analysis of variance (ANOVA) reported as *p*-values. *p*-values less than 0.05 suggested that differences were statistically significant.

3.2.2.7. Enzyme assay

Enzyme assay was performed as described by Gao (2015) by measuring butanol dehydrogenase (BDH) enzyme activity which determine the butanol yield in metabolic pathway of microbial butanol production. Cells grown in TYA medium of aqueous phase (broth) after 48 h and 72 h of fermentation were withdrawn at certain volume ~ 0.75-1 mL (V_H, mL) and collected aseptically into plastic centrifuge tubes and centrifuged at 8300 x *g* for 20 min at 4ºC. Discarded the supernatant carefully as much as possible and then exposured the plastic tubes containing the collected cells to liquid nitrogen for 5 seconds. The plastic tubes containing collected sample immediately were stored at -80ºC. The same method was applied for cells in alginate beads by collecting the beads in plastic tubes, disintegrated by 0.2 M sodium citrate, centrifuged and followed the same steps as described above.

The crude enzyme extract was prepared by cell disruption using 50 mM phosphate buffer (PB) (pH 6.0) as lysis buffer. The collected cells were suspended in 2 mL of 50 mM PB in 15 mL plastic centrifuge tubes. Then the tubes were placed in ice bath and the cells were disrupted using ultrasonication (Digital Sonifier 250, Branson, US) for 1 min (PULSE ON 0.2 sec; PULSE OFF 0.8 sec; AMPLITUDE 20%), stood for 3 min. Then disrupted for 1 min (PULSE ON 0.3 sec; PULSE OFF 0.7 sec; AMPLITUDO 30%), stood for 5 min. After that, the clarified supernatants were obtained by centrifuged at 20.000 x *g* for 30 min at 4ºC and considered as the crude enzyme extracts for BDH assays. The lysis buffer (50 mM PB buffer) composed of: $ZnSO_4.7H_2O$ 0.5 mM; DTT 2.5 mM; KH_2PO_4 50 mM; K_2HPO_4 50 mM. Substrate stock of 1 mL volume consist of 500 µL PB (pH 6.0); 100 µL of 500 mM butyraldehyde (dissolved in methanol); 100 µL of 4 mM NADPH and deionized water 290 µL.

The substrate stock was mixed in cuvette at room temperature for 1 min and reaction was initiated by addition of 10 µL of crude extract and the decrease in the adsorbance at 340 nm, indicative of NADPH oxidation was monitored. A blank measurement was prepared by using methanol instead of butyraldehyde as a substrate. The enzyme activity was defined as the amount of enzyme oxidation of 1 µmol NADPH per min and calculated using the equation below:

$$\text{BDH (U)} = \frac{(\triangle_{A340} - \triangle_{A340}\,\text{blank}) \times V_s \times 10^3)}{t \times \triangle\varepsilon_{340} \times V \times L} \qquad (4)$$

Where the unit of BDH is U (enzyme activity/ml, NADPH/min); $\triangle_{A340}$ is the decrease absorbance of sample test; $\triangle_{A340}$ blank is the decrease absorbance of blank sample; V_s is the volume of subtsrate stock (mL); t is the reaction time (min); V is the volume of cell (crude) extract (mL); L is the light path of cuvette (1 cm); $\triangle\varepsilon_{340}$ is the molar extinction coefficient of 6.22×10^3 $M^{-1}cm^{-1}$.

3.2.2.8. Microscopic analysis

Samples for scanning electron microscopy (SEM) analysis were prepared as follows. Samples of free cells were prepared by collecting a 1.5-mL portion of broth, which was centrifuged at 120 rpm for 20 min to obtain cells as the precipitate. For immobilized cells, several alginate beads were collected from the broth, and cut into smaller pieces. A 500-µL portion of broth from free cells or the cut beads containing immobilized cells were fixed by 2% formaldehyde (300 µL) and phosphate buffer (1 mL) at pH 5.5 and 4°C, overnight. Half of the fixed cells were then collected and washed with deionized water and centrifuged at 120 rpm for 10 min. The precipitate was stained by 1% OsO_4 solution for 4 h and washed with deionized water. The specimen was then washed successively with 50, 70, 80 and 99.5% ethanol, each for

5 min. As-prepared specimens were freeze-dried and observed using an SU-8000 apparatus (Hitachi, Tokyo, Japan) at the Center of Advanced Instrumental Analysis, Kyushu University.

The cells were also observed using a confocal laser scanning microscope (LSM 700, Carl Zeiss AG, Oberkochen, Germany). A 500-µL portion of culture medium containing free cells was collected in a 1.5-mL plastic tube and washed with phosphate buffer at pH 5.5 by centrifugation. The precipitate was stained with 4',6-diamidino-2-phenylindole (DAPI), and washed again with phosphate buffer by centrifugation. The cells in alginate beads were treated in the same manner after destroying the beads by treatment with 500 µL 0.2 M sodium citrate for 2 h. A 20-µL portion of prepared cells in phosphate buffer was put on an observation glass and observed under a 405-nm laser.

3.2.3. Results and Discussion

3.2.3.1. Characterization of op-TOCN

OPEFB-derived TOCNs (op-TOCN) used in this experimental was TOCNs with the carboxy content 1.5 mmol g^{-1}. Microscopy analysis of op-TOCN as described in **Fig 3.3.**

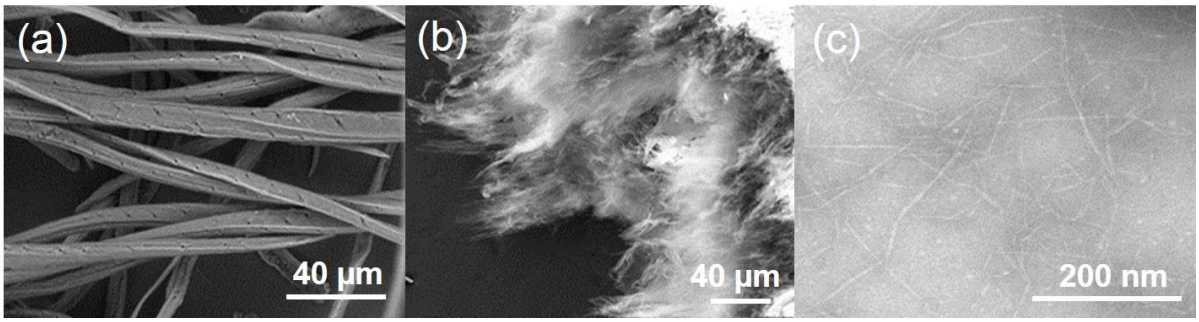

Figure 3.3 Microscopy images (SEM) of raw pulp OPEFB (a); op-TOCN (b) and TEM image of op-TOCN (c)

Aspect ratio of op-TOCN was 41 ± 14. High aspect ratio is preferred in TOCNs utilization as reinforcing filler. X-ray diffraction analysis, thermogravimetric (TG) analysis and FTIR of raw pulp OPEFB and op-TOCN as described in **Fig. 3.4.** Crystallinity index of op-TOCN was lower than original pulp, indicating that decrystallization took place to some extent on crystalline cellulose microfibrils during the oxidation [65]. The X-ray diffraction patterns were nearly unchanged even after the oxidation. The 200 and 110 diffraction peaks position of op-TOCN slightly changed after oxidation. These slightly changes may reflect the introduction of significant amounts of carboxylate and aldehyde groups on the cellulose I surfaces [11]. Thermal stability of op-TOCN also lower than original pulp, indicating that the presence of sodium carboxylate groups in TOCNs decreased the thermal decomposition temperature [66]. FTIR spectra showed the peaks at nearly 1600 cm^{-1} attributed to carboxylate groups, and small absorption bands at 1720 cm^{-1} are C=O groups in the protonated carboxyl groups [67]. This absorption band was not found on the starting pulp spectra. The FTIR spectra justified that during the oxidation process, significant amount of carboxylate groups were introduced into nanocellulose surface [68].

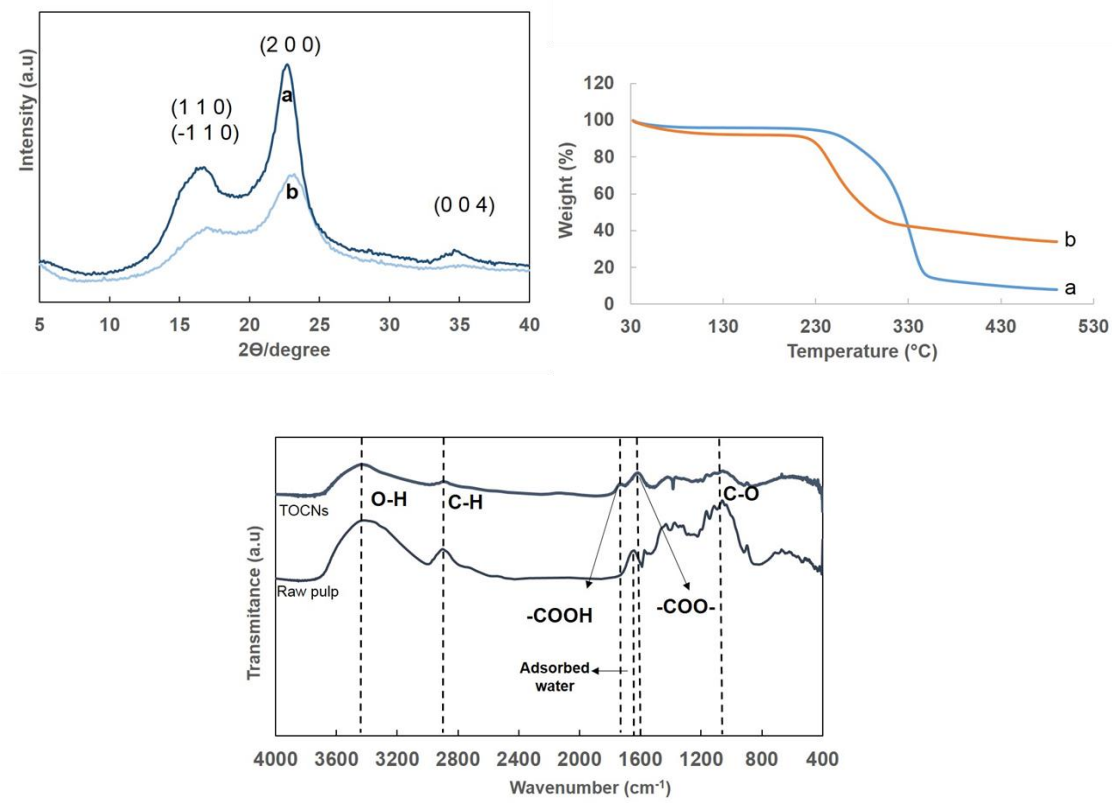

Figure 3.4. XRD pattern and TG curves of (a) raw pulp and (b) op-TOCN (upper); FTIR spectra of raw pulp and op-TOCN (bottom)

TOCN from Nippon Paper Company, as wood-derived TOCN, denoted as w-TOCN, was used as comparison. Microscopy characteristics of w-TOCN as shown in **Fig. 3.5**. TOCN from company had carboxylate content of 1.43 mmol/g with aspect ratio 44±16. Its characteristic was closer to op-TOCN (carboxylate content 1.5 mmol/g and aspect ratio 41±14.

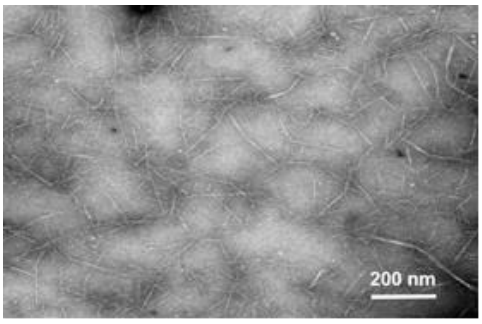

Figure 3.5. Transmission electron microscopy of TOCNs from company (w-TOCN)

3.2.3.2. Extractive fed-batch fermentation with free cells

Fermentation behavior of free cells was monitored in terms of DCW, glucose consumption and butanol production for 96 h in the presence of OPEFB-derived TOCNs (op-TOCN), and compared with the results using wood-derived TOCNs (w-TOCN), and in the absence of TOCNs (control) (**Fig. 3.6**). The cells drastically increased by 48 h and then stayed in a stationary phase until 96 h in the presence of both op-TOCN and w-TOCN; in contrast, cell growth was almost negligible over 96 h in the absence of TOCNs (**Fig. 3.6A**). An increase of cell density in the presence of op-TOCN and w-TOCN is in good accordance with the glucose consumption, in which fed glucose was efficiently consumed over 48 h in the presence of op- and w-TOCNs (**Fig. 3.6B**). Glucose consumption became slower after 48 h of fermentation, corresponding to the stationary phase of the cultures. In contrast, very little glucose was consumed in the absence of TOCNs. Butanol production was drastically improved in the presence of both op- and w-TOCNs, reaching 30 g/L total butanol concentration after 96-h fermentation, while the butanol concentration was almost negligible in the absence of TOCNs (**Fig. 3.6C**). It is noteworthy that the total butanol concentrations in the presence of op- and w-TOCNs were higher (28.8 and 30.3 g/L-broth after 96 h, respectively) than that reported in previous work (24.2 g/L-broth) [64] in which extractive fermentation was carried out by the free cell method using a large ratio of extractant to broth ($V_e/V_b = 5.0$) and *C. saccharoperbutylacetonicum* N1-4 was used as butanol-producing strain. The distribution coefficients of butanol (K_d) in our TOCN systems were also higher (3.98 for op-TOCN and 4.97 for w-TOCN) than in the previous work ($K_d = 3.14$).

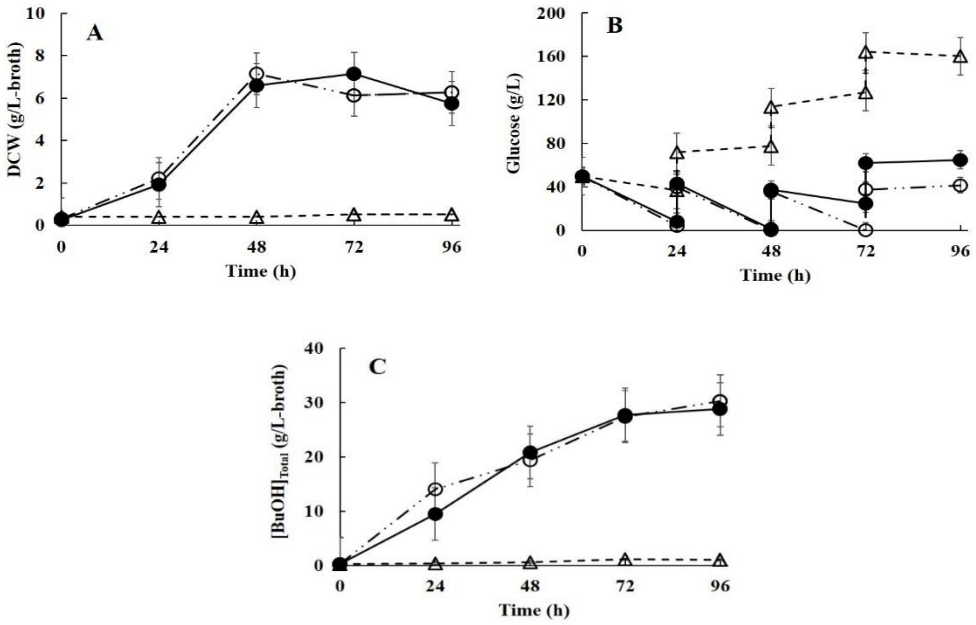

Figure 3.6. Time course of extractive fermentation using free *Clostridium saccharoperbutylacetonicum* N1-4 cells. Glucose was fed every 24 h. (A) Dry cell weight (DCW), (B) glucose concentration, and (C) total butanol concentration. Filled circles: oil palm empty fruit bunches (OPEFB)-derived TOCNs (op-TOCN); open circles: wood-derived TOCNs (w-TOCN); triangles: control, no TOCNs.

The time course of cell growth is in good accordance with the general features of the metabolic pathway of butanol production by *C. saccharoperbutylacetonicum* N1-4, which consists of two phases, acidogenesis and solventogenesis [69]. The growth behavior in the first 48 h corresponds to acidogenesis, during which cells rapidly grow while producing acetic acid and butyric acid. Solventogenesis occurs in the stationary phase, during which the cells reassimilate the previously excreted acids to acetone, butanol and ethanol [70].

Enhancement of butanol production with TOCNs could be explained by increased dispersibility of bacteria during fermentation, which improves the

microenvironment of cells. According to Derjaguin–Landau–Verwey–Overbeek theory, dispersibility of suspended solids like bacteria is dominated by repulsive electrical double layer forces [31]. The surface of both TOCNs and bacterial cells are negatively charged through carboxylate and phosphate groups, respectively. Therefore, their anionic nature causes improved colloidal stability of the bacterial system by preventing flocculation between bacteria [30]. In this work, such increased dispersibility presumably enhanced bacterial growth, resulting in higher butanol production.

3.2.3.3. Extractive fed-batch fermentation using immobilized cells

The present strategy of TOCN-enhanced butanol production was further explored in immobilized-cell fermentation. This method has great advantages since immobilized cells can be elaborated into practical flow-reactor systems, easily separated to obtain products from cell suspension, and protected from toxic products [71]. Alginate hydrogels have demonstrated high applicability as a support for cell immobilization, because they provide mild gelation conditions, transparency for microscopic observation, a gel pore network that allows the diffusion of nutrients, and a gentle environment for the entrapped materials [72,73].

Cell immobilization in alginate beads was applied to our present extractive fermentation for biobutanol production by introducing bacterial cells and TOCNs together into alginate beads. Fermentation was conducted using cells immobilized with op- and w-TOCNs, and cells immobilized without TOCNs as a control. The time courses of DCW, glucose consumption and butanol production for immobilized-cell fermentation are shown in **Fig. 3.7**. Interestingly, the DCW with op-TOCN continued to increase for 72 h, and remained at a high level up to 96 h. However, DCW with w-

TOCN and in controls decreased after 48 h of fermentation (**Fig. 3.7A**). The residual glucose was lower with op-TOCN than with w-TOCN and in controls even after 96 h, implying satisfactory cell growth. Higher glucose accumulation inhibits the fermentation process, which is related to catabolic flux [69]. The higher glucose accumulation for w-TOCN and TOCN-free conditions indicated that the substrates were not completely used. Therefore, to operate at the best glucose use efficiency, appropriate dilution ratios and concentration control of glucose feedstock are required [74]. The lower amount of residual glucose in op-TOCN conditions can be attributed to a greater number of active cells in alginate beads, resulting in higher consumption of glucose (**Table 3.1**) as the energy source in butanol-producing bacterial metabolism. Besides, solvent extraction generally enhances glucose consumption, and the solvent production (butanol) in the presence of op-TOCNs appears to be the highest among the conditions tested (**Figs. 3.7A–C**) [41].

The total butanol concentrations in the immobilized-cell treatments were 36.59 g/L-broth for op-TOCN, 31.58 g/L-broth for w-TOCN, and 23.71 g/L-broth for controls (TOCN-free) (**Fig. 3.7C**). These results were comparable with, but higher than, those for the free-cell method, which ranged from 29–30 g/L-broth in the presence of TOCNs. The slight increase of total butanol concentration after 96-h fermentation indicated that immobilization contributed to the extractive fermentation by altering cell density (in the alginate beads), but did not alter the metabolic pathway [74]. It is noteworthy that the total butanol production in the presence of TOCNs (V_e/V_b = 2.0) was higher than that reported for an immobilization method using a large ratio of extractant, V_e/V_b = 5 (30.9 g/L-broth) [64].

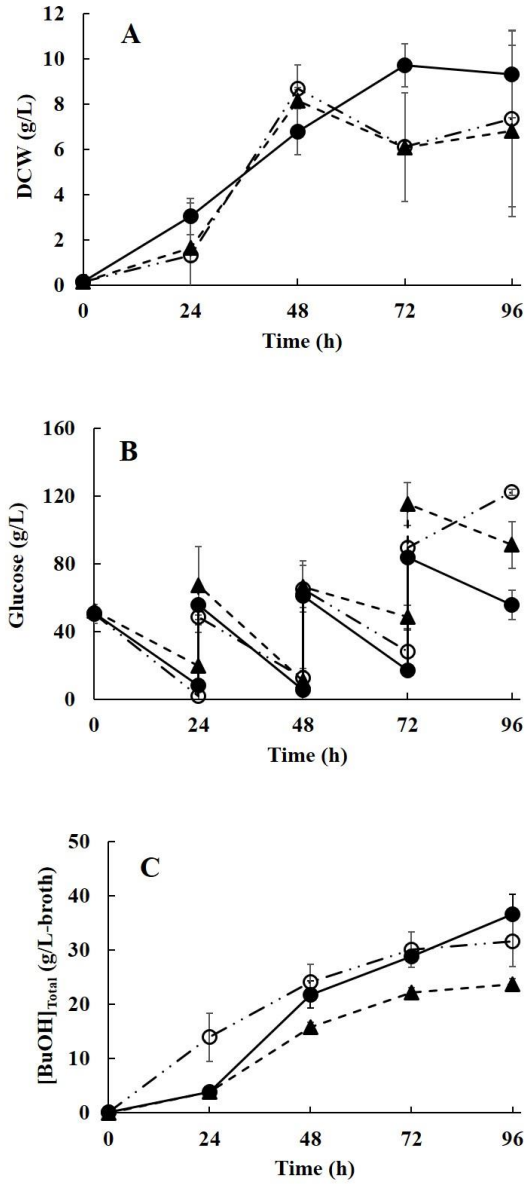

Figure 3.7. Time course of extractive fermentation using immobilized *C. saccharoperbutylacetonicum* N1-4 cells. Glucose was fed every 24 h. (A) DCW, (B) glucose concentration and (C) total butanol concentration. Filled circles: op-TOCN; open circles: w-TOCN; triangles: control without TOCNs.

Table 3.1. Extractive fermentation properties for free cells and immobilized cells

	Free cell			Immobilized cell		
Parameter	op-TOCN	w-TOCN	Control	op-TOCN	w-TOCN	Alginate without TOCNs (control)
Total butanol concentration (g/L)	28.82	30.30	1.04	36.59	31.58	23.71
Total consumed glucose (g)	2.97	2.54	0.17	3.30	2.60	3.27
Butanol yield to consumed substrate (C-mol/C-mol)	0.39	0.48	0.23	0.45	0.49	0.29

The K_d of butanol (extractant to aqueous phase) for immobilized cells using alginate beads with op-TOCN with w-TOCN, and without TOCN, was 4.45, 5.10 and 4.68, respectively (**Fig. 3.8**). These values are significantly higher than the K_d in the free cell method, which was related to the higher total butanol production obtained from immobilized cells. The higher total butanol production by immobilized cells was achieved by continuous extraction from the aqueous phase by extractant, which maintained the butanol concentration in the aqueous phase at a low level. Nevertheless, fermentation yields mainly depend on the strain and the culture conditions, which affect ABE metabolism [75]. In addition, the immobilization method would also increase plasmid stability by creating a protective microenvironment for bacterial cells [76]. This advantage is important for the growth of butanol-producing strain.

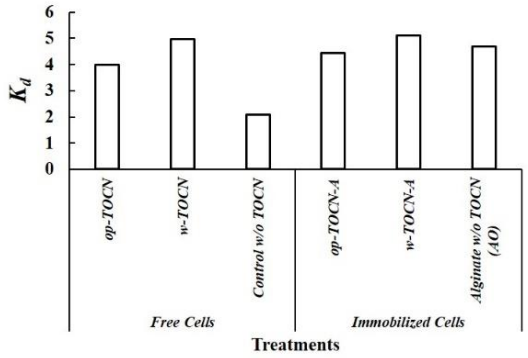

Figure 3.8. Distribution coefficient (K_d) of butanol between the extractant and the aqueous phase.

Statistical analysis revealed that immobilized cells produced significantly more butanol in the presence of TOCNs (op-TOCN and w-TOCN) compared with alginate only (i.e. no TOCNs) ($P < 0.01$). Immobilized cells in alginate (in the absence of TOCNs) are protected from the disturbance of the cellular metabolic activity such as an inhibitory effect of produced butanol [77]. In addition, the diffusion of butanol into the beads is strongly affected by the pore size. Effective pore size may be modified by electrostatic interaction of the negatively charged alginate matrix with other charged species [73], including TOCNs which have a high density of anionic carboxylate groups. The presence of TOCNs safeguard the alginate beads from swelling, prevent the loss of calcium ions because of the tightly packed nanofibrous structure, maintain the spherical shape of beads, retain a high level of cell viability, and preserve the ability of the cells to proliferate [78]. In addition, carboxylate groups in TOCNs were possibly involved in calcium binding. A schematic image of the crosslinking among TOCNs, alginates and Ca^{2+} ions (from $CaCl_2$) is provided in **Fig. 3.9**.

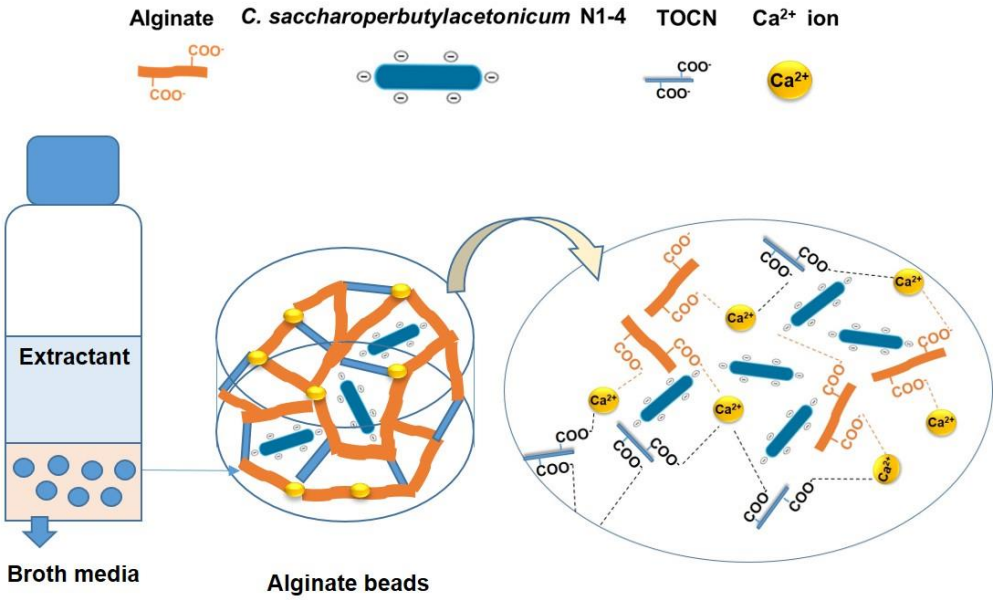

Figure 3.9. Schematic image of the crosslinking among TOCNs, alginates and Ca^{2+} ions in extractive fed-batch fermentation using immobilized cells

The free-cell and immobilized-cell methods were significantly different in terms of butanol yield ($P < 0.01$) in the presence of op-TOCN and w-TOCN (**Fig. 3.10**). To the best of our knowledge, this is the first report of TOCN addition in extractive fermentation, and we showed that TOCNs enhance microbial biobutanol production.

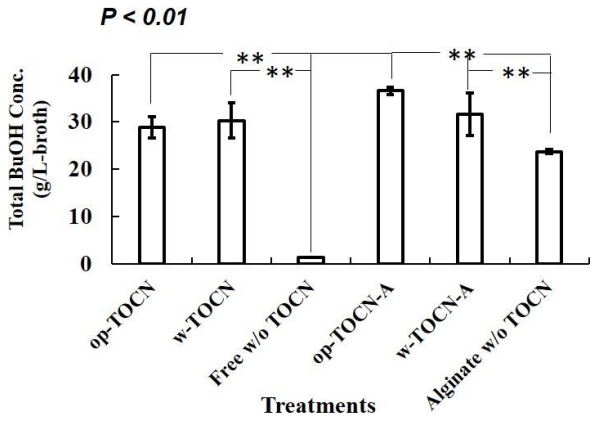

Figure 3.10. Statistical analysis for different TOCN treatments in microbial biobutanol production.

3.2.3.4. Enzyme assay

The results of enzyme assay of butanol dehydrogenase (BDH) as described in **Table 3.2**. The BDH activity was higher for alginate without TOCN at 48 h fermentation. However, the addition of op-TOCN and w-TOCN induced enzyme activity of BDH after 72 h of fermentation in immobilized cell method. In this study, the BDH activity was observed based on spectrometer analysis by observing NADPH consumption with the presence of crude extract. Further analysis using protein kit needed to support these results. However, this analysis is an approach to support that the addition of TOCN enhanced extractive fermentation of microbial butanol production.

Table 3.2. Enzyme activity analysis (butanol dehydrogenase/BDH)

Sample	**48 h (U)***	**72 h (U)***
op-TOCN free cells	0.0039 ± 0.0024	n.d
op-TOCN immobilized cells	0.0059 ± 0.0027	0.0076 ± 0.00084
w-TOCN immobilized	0.0065 ± 0.0039	0.0049 ± 0.0045
Alginate w/o TOCN	0.0071 ± 0.00082	0.0024 ± 0.0016

Remarks:* Average with standard deviation based on duplicate, DCW ~ 5.6 g/L ;U is the unit of enzyme activity where describe the amount of enzyme oxidation of 1 µmol of NADPH/min ; n.d = not determined

3.2.3.5. Microscopic analysis

Microscopic analysis was conducted to observe the morphological differences in cultures in the presence and absence of TOCNs (**Fig. 3.11**). The TOCN network was similar to a spider's web after drying, as reported previously [79]. The spider-

web-like structure was not seen in **Fig. 3.11A**, which shows material from the broth for free cells without TOCNs. In contrast, the presence of the spider-web-like structure was clearly observed in **Figs. 3.11B** and **3.11C**, when bacterial cells were cultured in the presence of TOCNs. Incorporation of alginate and TOCNs possibly contributed to the mechanical and chemical stability of alginate beads. Cells which were immobilized in the alginate beads in the presence of op- and w-TOCN were more viable and proliferated better compared with the control (without TOCNs), due to the 3D fibrous TOCNs, which would be expected to perform as an extracellular matrix with morphological similarity to nanofibrous collagen, glycoproteins and acidic polysaccharides [78].

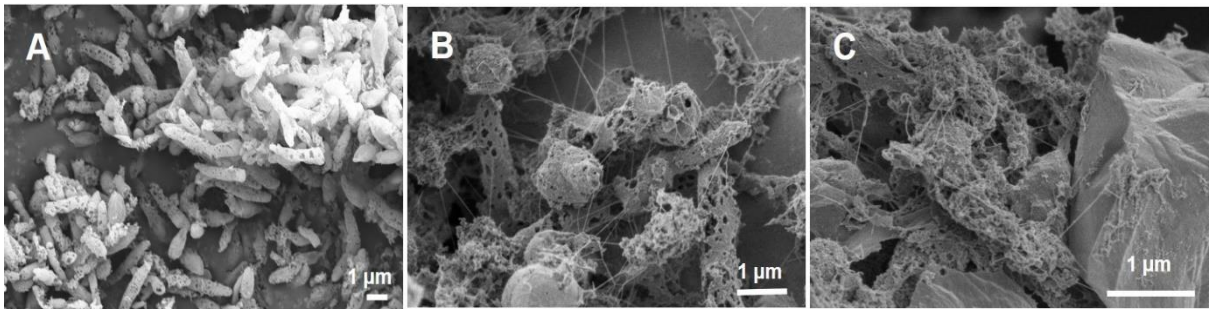

Figure 3.11. Scanning electron microscopy images of *C. saccharoperbutylacetonicum* N1-4 cells cultured (A) without TOCNs, (B) with op-TOCN, and (C) with op-TOCN in immobilized cells conditions.

Optical microscopic images of *C. saccharoperbutylacetonicum* N1-4 cells were acquired using a confocal laser scanning microscope after staining by DAPI in order to compare morphological differences between living cells. The blue fluorescence of single bacteria appeared to be aggregated to some extent in free cells without TOCNs

(**Fig. 3.12A**). In contrast, bacterial cells were dispersed in the presence of TOCNs (**Fig. 3.12B**).

Figs. 3.12D and **3.12E** showed that immobilized cells in alginate beads (in the presence of TOCNs) were trapped compared with those in alginate beads without TOCNs (**Fig. 3.12C**). One problem of cell entrapment inside the porous matrix of a polysaccharide gel like alginate is the ability of cells on the outer surface of the beads to multiply and be released from the beads, as shown by **Fig. 3.12C** [80]. The presence of TOCNs in alginate beads overcomes this disadvantage by interactions between the alginate and TOCNs. The carboxyl groups on the surfaces of TOCNs can participate in the formation of a crosslinked network in alginate beads through Ca^{2+} ions, and add structural and mechanical stability to the beads. Both cellulose and alginate belong to the polysaccharide family, and their chemical structures should provide good compatibility for the resultant crosslinked beads [81]. This crosslinking reduced cell release from the beads. The cells entrapped in the alginate–TOCN beads retained a high level of viability and ability to proliferate.

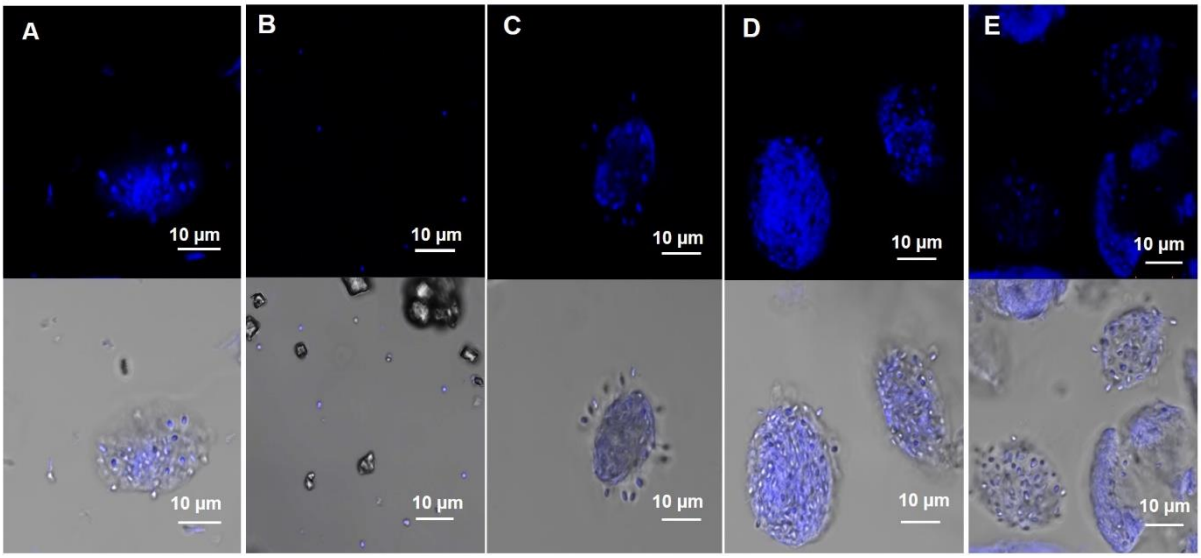

Figure 3.12. Fluorescent (top) and phase contrast (bottom) images of bacterial cells in (A) aqueous medium without TOCNs (free cells); (B) in aqueous medium in the presence of op-TOCN (free cells); (C) in alginate beads without TOCNs; (D) in alginate beads in the presence of op-TOCN; and (E) in alginate beads in the presence of w-TOCN.

The presence of TOCNs with free cells or immobilized cells during extractive fermentation has been demonstrated. In the free-cell method, the presence of TOCNs induced bacterial dispersibility by electrostatic repulsion among anionic carboxylate groups of TOCNs and negatively-charged *C. saccharoperbutylacetonicum*. This dispersibility induced higher contact of bacteria with substrate and yielded a higher total butanol concentration. The presence of TOCNs in the immobilization method induced mechanical and structural stability of alginate as a cell immobilizer by crosslinking of the acidic groups of TOCNs and alginate *via* Ca^{2+} ions, resulting in the formation of a 3D network for cell entrapment while maintaining high viability of bacteria. An increase of butanol concentration, particularly in the presence of op-TOCN, indicated that the op-TOCN contributed to the formation of a better

microenvironment without altering the metabolic pathway of the butanol-producing strain. This finding opens up the advanced use of low-cost agricultural residues in bioalcohol production.

3.3 Application of OPEFB Nanocellulose in Alginate Membrane for Water-Ethanol Mixture Separation

3.3.1 Materials

Bleached kraft pulp of oil palm empty fruit bunches (OPEFB) was kindly supplied from Biomaterial Research Institute, Indonesian Institute of Sciences (Bogor, Indonesia). 2,2,6,6-Tetramethylpiperidine 1-oxyl (TEMPO), sodium bromide, sodium hypochlorite, and sodium borohydride were purchased from Sigma-Aldrich (Tokyo, Japan) and used without further purification. Sodium alginate (500cps) was purchased from Nacalai Tesque (Kyoto, Japan), calcium chloride ($CaCl_2$) was purchased from Wako Pure Chemical (Osaka, Japan). The water used in this study was purified with an Arium Ultrapure Water System (Sartorius Co., Ltd., Tokyo, Japan). The filter holder set up for pervaporation system was purchased from Toyo Roshi Kaisha Ltd. (Tokyo, Japan) with the diameter of filter was 47 mm. Commercial membrane, PTFE Advantec Membrane Filter (Toyo Roshi Kaisha, Tokyo, Japan) with the pore size 0.5 µm was used for comparison and denoted as PTFE membrane. Ethanol (99.5%) was purchased from Fujifilm Wako Pure Chemical, Osaka, Japan, and used without further purification.

3.3.2 Method

3.3.2.1 Preparation and Characterization of OPEFB-derived TOCNs (op-TOCN)

Preparation of TOCNs from OPEFB as described in previous section (See section 3.2.2.1.) and denoted as op-TOCN. Menwhile, TOCNs from Nippon Paper Company made from wood was used as comparison and denoted as w-TOCN. The carboxylate contents were measured by conductometric titration [11]. The carboxylate content of op-TOCN was 1.50 mmol/g and w-TOCN was 1.59 mmol/g.

3.3.2.2 Preparation and Characterization of TOCNs-Alginate Membrane Cross-linked with $CaCl_2$

About 300 mg of sodium alginate was dissolved in 30-mL deionized water (DI) by vigorous stirring at room temperature to get completely dissolved. A 25-mL of 0.4 wt% of op-TOCN suspension (100 mg of dry weight) was added and the mixture was stirred for 2 h and poured into PTFE petri dish. Membranes were dried at room temperature for 2-3 days. The dried membranes then were peeled off carefully. The obtained membranes were cross-linked with $CaCl_2$, by immersing the membranes in 5% (v/v) of calcium chloride ($CaCl_2$) for 3 h, rinsed with DI water and dried in ambient air for 2 days. The obtained membrane composed of alginate and op-TOCN then denoted as op-TOCN-A. The same preparation was applied to alginate with TOCN from company (w-TOCN) and denoted as w-TOCN-A. Membranes made of alginate without TOCNs (alginate w/o TOCN) was prepared as a control. Commercial membrane, hydrophobic PTFE membrane (Advantec Membrane Filter, Toyo Roshi Kaisha Ltd., Tokyo, Japan) was used as comparison. The scheme of research experimental as described on **Fig 3.13**.

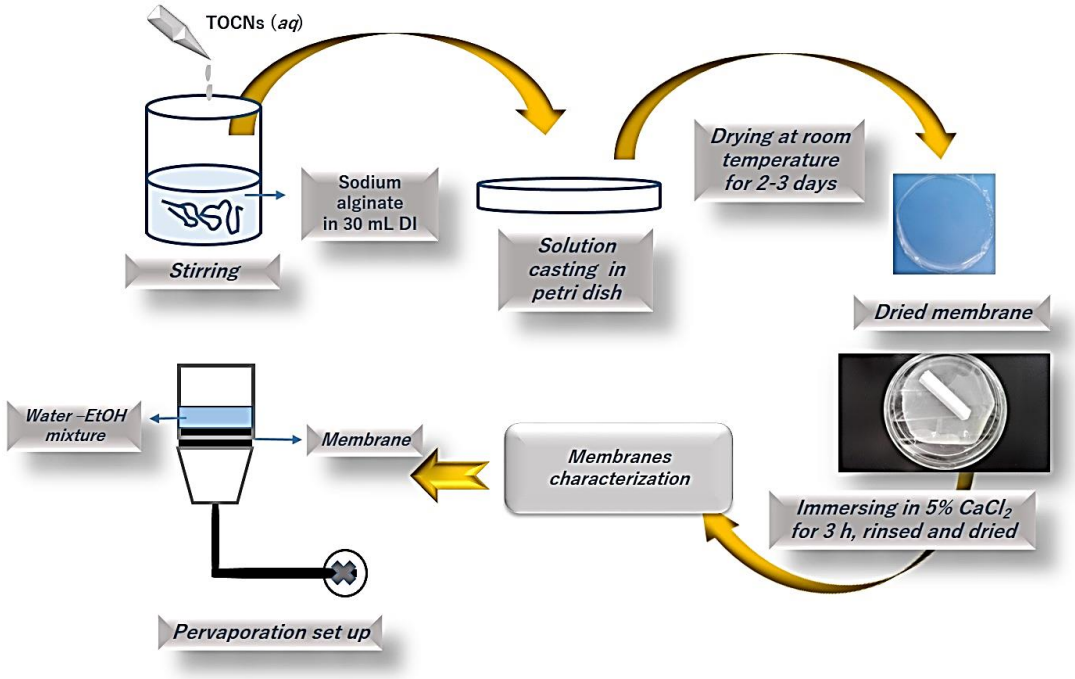

Figure 3.13. Experimental scheme of alginate-TOCNs membrane for water ethanol separation

Membrane characteristic including microscopic observation, membrane thickness, density and water content. Microscopic observation was examined by taking cross sectional as well as surface images by Scanning Electron Microscopy (Zeiss ULTRA 55, USA) at the Ultramicroscopy Research Center, Kyushu University, Japan. The observation was conducted at acceleration voltage 5 kV. Thin gold layer was coated on the surface of the samples before observation using JEOL JFC-1600 Autofine Coater (Japan Electronic Corporation Ltd., Tokyo, Japan) at 30 mA for 10 s. Membrane thickness was measured by Digital Micrometer (Series 406-Non Rotating Spindle Type 406-250, Mitutoyo Corp., Kawasaki, Japan). Membrane densities were determined by dividing weight by volume. Water contents were calculated by following equation:

$$Water\ content\ (\%) = (W_{initial} - W_{dry})/W_{inital} \quad (5)$$

Where $W_{initial}$ is the weight of membrane at initial condition (before drying) and W_{dry} is the weight of dried membrane after exposure at 103°C for 1 h. All membranes were kept on desiccator after cooling and then weighed.

Fourier Transfrom Infrared (FTIR) analysis was conducted using FTIR spectrometer (JASCO FT/IR-680 TypeA, Japan) at Center of Advanced Instrumental Analysis, Kyushu University, Japan. The analysis was conducted at spectral range 400-4000 cm^{-1}.

Contact angles of resultant membranes were observed using Drop Master 300 K. Samples were made by cutting the membranes into approximately 10 x 50 mm sheet. The contact angles were measured at four different spots by dropping a droplet (1 µL) of DI water on each membrane sample and the values averaged.

Absorption capacities of membranes in water and absolute ethanol were determined by immersing the dried membrane (dry weight W_d) in the appropriate liquid until equilibrium condition. The liquid-hydrated membranes were weighed (W_w) and the absorption capacity was calculated using Eq. 6:

$$Absorption\ \ capacity\ \ (\%) = \frac{Ww - Wd}{Wd} x\ \ 100 \quad (6)$$

Surface area and average pore sizes were measured using Brunauer-Emmett-Teller (BET) method under nitrogen atmosphere. Each sample was dewatering and degassed at 105°C for 4 h before BET analysis.

Tensile tests of obtained membranes were performed using Material Testing Instruments (STA-1225, ORIENTEC Co., Ltd., Tokyo, Japan) equipped with a 100 N load cell. Membrane sample cut into 40-50 mm x 0.7-10 mm sheet. Measurement was carried out at 20 mm of active length at 10% min^{-1} [82].

3.3.2.3 Pervaporation Experiment

The pervaporation set up which systematically shown in **Fig. 3.14,** consisted of feed glass tube, membrane filter holder, cold trap for permeate and vacuum pump. Due to the difficulties to control the desired pressure, the pressure during experimental was recorded and it ranged from 30-40 hPa. The feed across the membrane and the permeate was collected in cold trap and the collecting time was recorded. The water content was measured using hybrid titration method by Karl Fischer Moisture Titrator Kyoto-Chem MKH-700 (Kyoto Denshi Kogyo, Kyoto, Japan). The flux (*J*) and selectivity (α) were calculated using the equation of mass-time data as follows:

$$J = \frac{Q}{At} \qquad (7)$$

Because the thickness of obtained membranes were not similar, then the obtained flux values were normalized by following equation:

$$\textit{Normalized flux} = J \text{ x (membrane thickness/50 µm)} \qquad (8)$$

Selectivity of membrane and was calculated using the following equation:

$$\alpha = \left(\frac{Wp}{Ep}\right) / \left(\frac{Wf}{Ef}\right) \qquad (9)$$

Where *Q* is the mass of permeate collected in cold trap in time *t. A* is the effective membrane surface area. Sorption selectivity denoted as α, and W_p and E_p are weight fraction of water and ethanol, respectively, in permeate, and W_f and E_f are weight fraction of water and ethanol, respectively, in feed. The pervaporation was applied on membrane area of 19.625 cm^2.

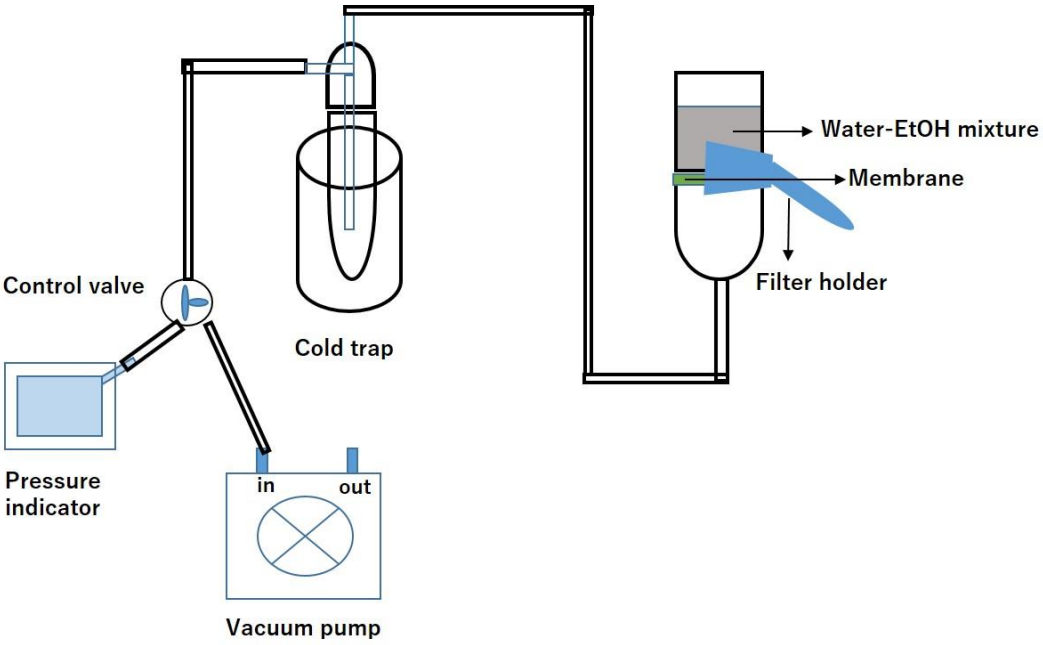

Figure 3.14. Schematic representation of experimental membrane set-up.

3.3.3 Results and Discussion

3.3.3.1 Membrane characteristic

Morphology of obtained membranes were observed using Scanning Electron Microscope (SEM), by observing the surface and cross section area. The complete images of SEM analysis as shown in **Fig. 3.15**. The presence of TOCNs in alginate-TOCNs membrane was confirmed by fibrous layer appearance on cross section images (**Fig. 3.15B-C**). This appearance was absence on control membrane (alginate w/o TOCN). The results of SEM images were in a good agreement to those of previous reported study [48]. In addition, surface morphology of alginate membrane in the presence of TOCNs showed rougher surface compared to the control membrane.

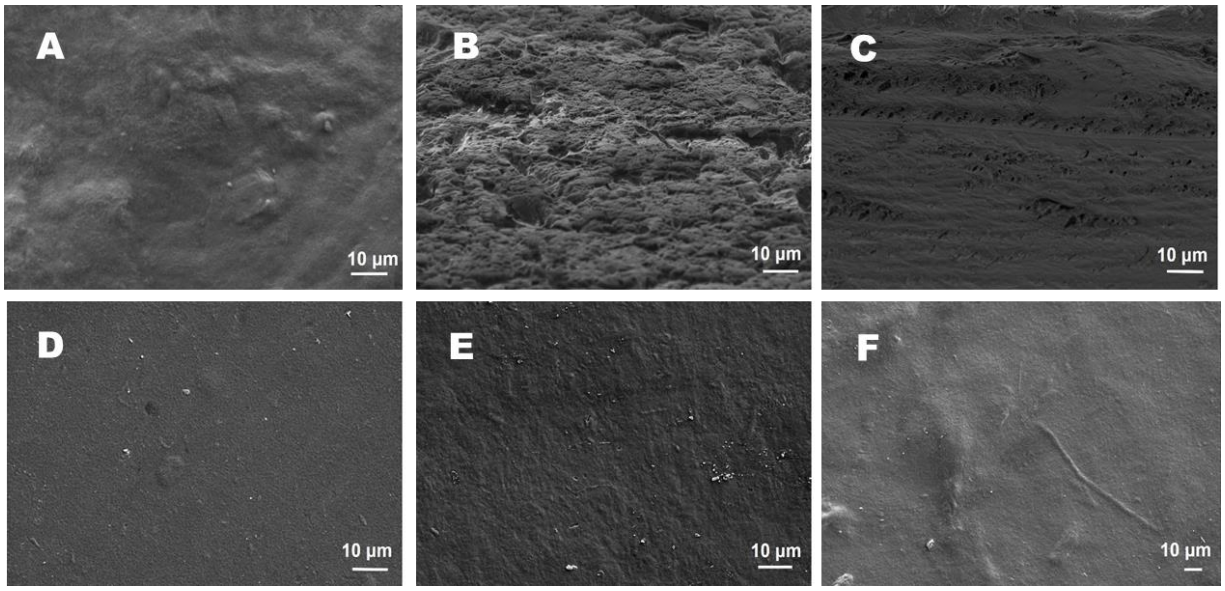

Figure 3.15. SEM images of cross section (upper) and surface morphology (bottom) of: (A,D) alginate w/o TOCN; (B,E) op-TOCN-A membrane; (C,F) w-TOCN-A membrane

The membrane thickness of alginate w/o TOCN, op-TOCN-A and w-TOCN-A were: 52 µm, 82 µm and 78 µm, respectively. In addition, the water content of alginate w/o TOCN, op-TOCN-A and w-TOCN-A were: 6.2 %; 5.8 % and 3.6%, respectively. The densities of obtained membranes were 0.81 for alginate w/o TOCN, 0.96 for op-TOCN-A and 0.73 for w-TOCN-A.

3.3.3.2 Fourier Transfrom Infrared (FTIR) analysis

The FTIR spectra as described in **Fig. 3.16**. The spectra op-TOCN showed the important adsorbance at 1720 $cm^{-1}$and 1600 cm^{-1}, which correspond to functional carboxylate groups -COOH and –COONa, respectively [83]. The spectra of op-TOCN-A at ~1602 cm^{-1} were sharper than op-TOCN. The similar appearance also was found for w-TOCN-A spectra. These peaks were assumed that the crosslinking with

alginate and $CaCl_2$ was occurred, they have exclusively the carboxylates structures of $(TOCN\text{-}COO)_2Ca$ [84]. In the absence of TOCN, the spectra of alginate w/o TOCN at 1600 cm^{-1} was broader.

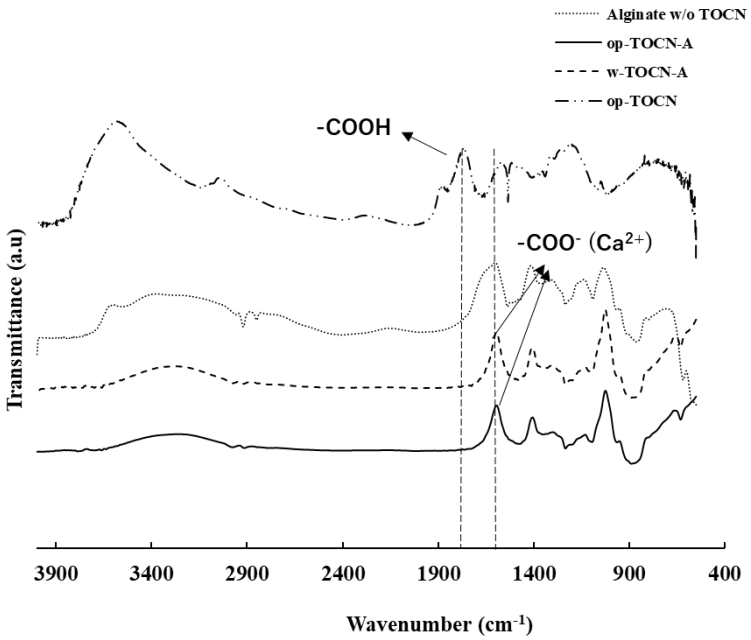

Figure 3.16. FTIR spectra of TOCN-alginate membranes and the original TOCN from OPEFB

3.3.3.3 Morphology analysis after pervaporation

The surface morphology after pervaporation was observed to check whether micro-cracks were occurred during the experimental (**Fig. 3.17D-F**). Interestingly, the micro-cracks were not observed for op-TOCN-A and w-TOCN-A. The rougher surface appeared after treatment due to the vacuum pressure applied during the pervaporation set-up. However, op-TOCN-A showed lower roughness surface compared with w-TOCN-A and alginate w/o TOCN. The optical images of membranes after treatment showed that the morphology change can be detected distinctly on w-TOCN-A than op-TOCN-A. It is assumed that the re-arrangement of

polymers chain of w-TOCN-A might occurred intensively than op-TOCN-A due to the vacuum applied during the pervaporation.

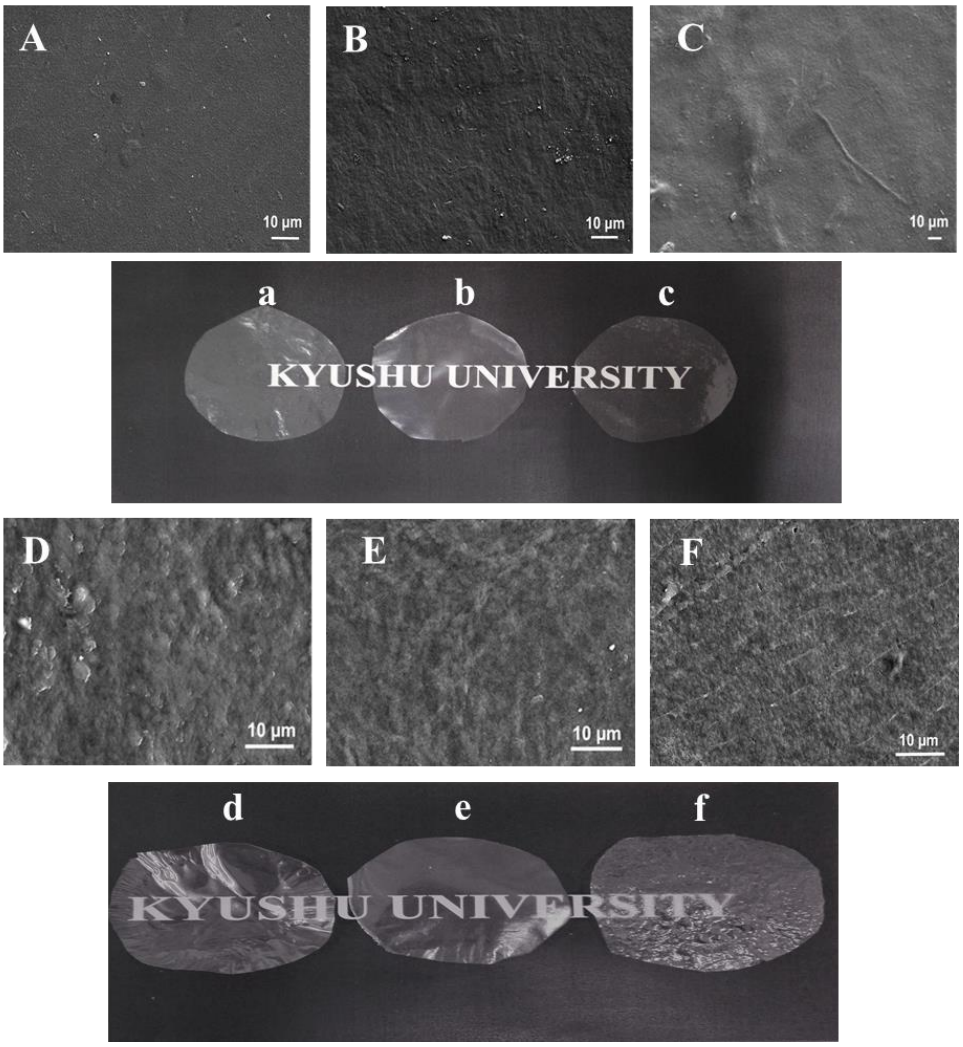

Figure 3.17. SEM images of membrane surface *before* (A: alginate w/o TOCN; B: op-TOCN-A; C: w-TOCN-A) and *after* treatment (D: alginate w/o TOCN; E: op-TOCN-A; C: w-TOCN-A) and optical images of its representative in lowercase letters

3.3.3.4 Contact angle

Contact angle measurement was applied on water and mixture of water-ethanol. Actually, measuring contact angle using absolute ethanol on the surface of

membrane was difficult because the ethanol would spread immediately on the membrane surface after dropping. Therefore, the contact angle measurement was conducted in the mixture of water and ethanol (80% water 20% ethanol and 60% water and 40% ethanol) as shown in **Fig 3.18**.

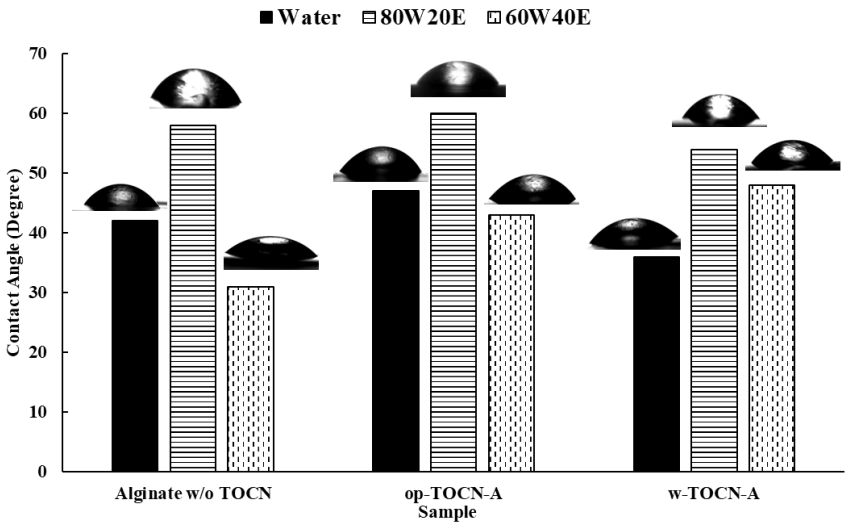

Figure 3.18. Contact angle measurement in water and water–ethanol mixtures

The contact angle is the angle at the interface where water, air and solid meet, and its value is a measure of how likely the surface is to be wetted by the water. Low contact-angle values demonstrate a tendency of the water to spread and adhere to the surface, whereas high contact-angle values show the surface's tendency to repel water [85]. The increase of ethanol concentration the contact angle decrease. It caused by the surface tension of ethanol, which determine contact angles, is smaller than that of water. The surface tension of the aqueous solution decrease with the increase of the alcohol concentrations [86]. Contact angle of PTFE membrane was difficult to be captured in both of water and water-ethanol mixtures. The contact angle of the liquid on the solid surface is a key parameter reflecting the wettabilities. Based on the figure

above (**Fig. 3.18**) the wettabilities of alginate membrane almost unchanged in the presence of TOCN.

3.3.3.5 Flux, selectivity and surface analysis

Flux analysis was conducted for the feed containing 80% ethanol and 20% water (*v/v*) and denoted as 80E20W; and 90% ethanol and 10% water (*v/v*) denoted as 90E10W. The results as described in **Fig. 3.19**.

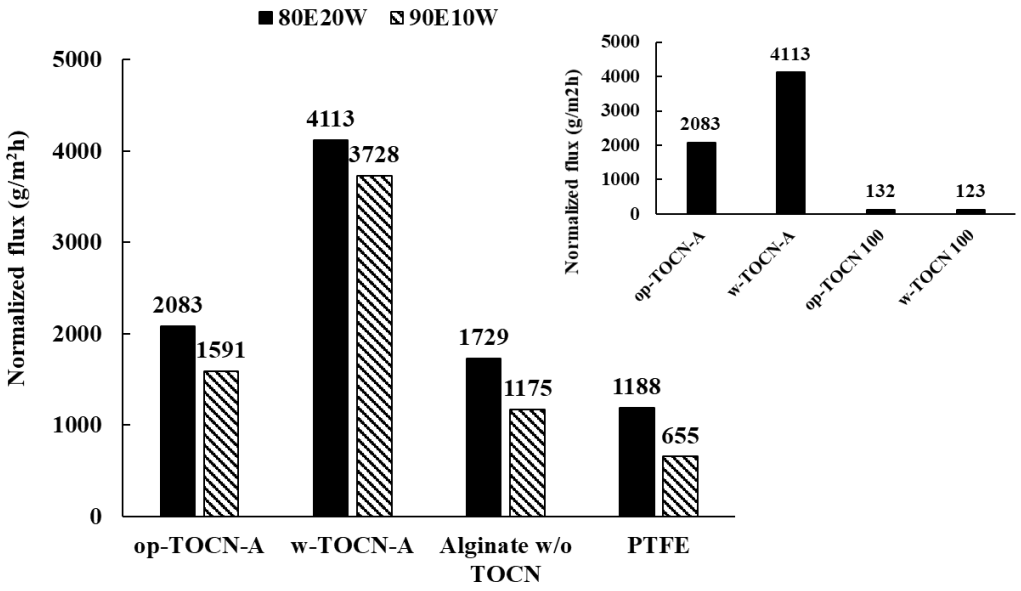

Figure 3.19. Normalized flux of alginate, alginate-TOCN membrane and PTFE in water-ethanol mixture

Figure 3.19 showed that the addition of TOCN in alginate membrane increased the flux capacity. The crosslinking between TOCN, alginate and ion Ca^{2+} increased the surface area and induced the pore size formation and affected the flux. The surface area of alginate membrane become larger in the presence of w-TOCN in w-TOCN-A membrane (**Table 3.3**), resulting highest flux compared to op-TOCN-A and alginate

w/o TOCN. During the pervaporation, the first constructive step in transporting permeating component through the membrane is sorption of the permeating component from the feed liquid into the membrane. Therefore, larger surface area was preferred to get more contact or sorption of permeating component occurred on the membrane surface [87].

Table 3.3. Adsorption capacity, water selectivity and surface analysis

Sample	Adsorption capacity (%)		Water content in permeate (%)[a]		Selectivity[b]		Surface area, $a_{s\ BET}$ (m^2g^{-1})[c]	Average pore size (nm)[c]
	Water	EtOH	80E20W[b]	90E10W[b]	80E20W	90E10W		
op-TOCN-A	87	8	23.8	11.7	53	56	0.73	37
w-TOCN-A	78	8	17.5	13.1	60	54	1.18	23
Alginate w/o TOCN	66	35	23.8	15.3	45	40	0.90	30
PTFE	32	47	24.3	14.9	42	42	4.69	5000[d]

Remarks: [a] initial water content at 80E20W was 25.5% and initial water content at 90E10W was: 15.62% measured by Karl Fischer titrator; [b] selectivity is correspond to water; collecting time was adjusted for 1 h; [c] based on BET surface analyzer with weight of measured sample ~0.1 g; [d] determined by company/supplier

In addition, op-TOCN-A and alginate w/o TOCN have lower surface area but larger in pore size compared to w-TOCN-A (**Table 3.3**). Pores size plays an important role during the second, which is diffusion of permeating component through the membrane; and third constructive step of pervaporation which is desorption of permeating component on the downstream of membrane. Therefore, the flux of op-TOCN-A was slightly higher compared to the control membrane (alginate w/o TOCN), because larger pore size of op-TOCN-A increased the diffusion and desorption rate, while the surface area of the two membranes is not too different (**Table 3.3**). However,

the mass transfer analysis was conducted by Phattaranawik and co-authors revealed that the influence of pore size was insignificant [88]. Alginate and alginate–TOCN membranes have mesopore size (2-50 nm) according to IUPAC pore size classification, while PTFE membrane classified as macropore size (> 50 nm) [89].

Comparison with the control positive membranes (op-TOCN100 and w-TOCN100) was conducted at the feed with 80% ethanol and 20% water (**inserted picture in Fig. 3.19**). The results revealed that the self-standing membrane of TOCN (op-TOCN and w-TOCN) had very low and distinct flux capacity. It is assumed that the use of self-standing film TOCN was not effective as pervaporation membrane. Nanocellulose prepared by TEMPO mediated oxidation is hydrophilic. The self-standing TOCN film had been reported to have a high water vapor permeability of approximately 70 g μm m^{-2} day^{-1} kPa^{-1} at 30% RH [56]. This property need to be combined with other hydrophilic polymers, such as alginate, for use in pervaporation membrane. Sodium alginate membrane was acknowledged to have high water solubility and sorption selectivity [90]. Hydrophilic groups absorb water molecules preferentially, which leads to both high flux and high separation factors. However, the introduction of hydrophilic groups sometimes swells the membrane significantly due to its plasticization action which results in low selectivity [55].

Figure 3.19 showed that the increase of mass percentage of water in the feed increased the flux capacity. This is because with an increase the mass percentage of water in the feed, membrane swelling increases, and this create more free volume, which results in an increase the permeate flux [91]. The flux capacity is not only affected by the mass of water transferred from the feed but also the shrinkage of internal pores of membrane in resulting flow viscosity and thus total permeation flux [92].

Hydrophobic membrane, PTFE, showed highest surface area and largest pore size which determined from the supplier. However, hydrophobic properties of PTFE membrane caused water affinity of this membrane was very low, resulting low water adsorption and flux. The large pore size make diffusion rate was too fast and caused low in water sorption and selectivity.

3.3.3.6 Tensile Test

Mechanical properties of obtained membranes as described in **Fig. 3.20**. The self-standing of alginate membrane (alginate w/o TOCN) showed lower mechanical properties. Yang and co-authors reported that alginate membrane cross-linked with cellulose and Ca^{2+} had high mechanical properties. The presence of cellulose and Ca^{2+} had tensile strength up to 47 MPa and elongation at break of 23%; while alginate with the absence of cellulose and Ca^{2+} revealed low tensile strength only about 4.2 MPa and elongation at break of 17% [93]. This study revealed that in the presence of TOCN, both of op-TOCN and w-TOCN, the tensile strength of alginate membrane improved by 2 times higher and elongation break improved 5 times higher. The higher improvement of w-TOCN than that of op-TOCN might be caused by the differences of cellulose content of woody and non woody of nanocellulose starting materials. However, this result emphasized the potential utilization of low cost agricultural residue as enhancer in membrane composite.

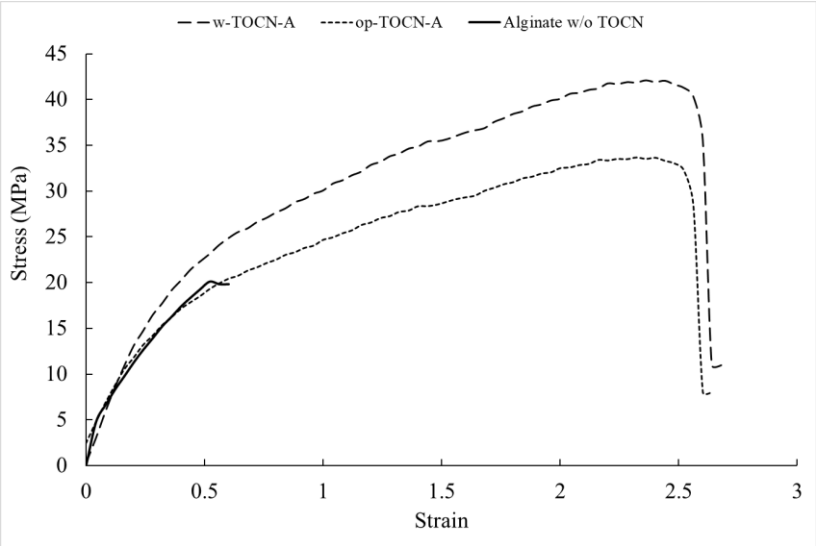

Figure 3.20. Tensile strength of alginate and alginate-TOCN

3.4 Conclusion

Nanocellulose, having carboxylate groups on its surface, was successfully applied in extractive fermentation in microbial biobutanol production. TEMPO-oxidized cellulose nanofibers (TOCNs) from OPEFB (op-TOCN) and wood (w-TOCN) resulted in better microenvironmental conditions during fermentation because of electrostatic repulsion between anionic carboxylate groups on the surface of TOCNs and negatively-charged bacterial cells. This induced good bacterial dispersibility in the medium, improving the total butanol production in broth. Higher DCW and higher total butanol concentration were achieved, up to 28–30 g/L-broth for free cells and 32–37 g/L-broth for immobilized cells, in the presence of TOCNs. Microscopic analysis revealed that the presence of TOCNs improved physical cell entrapment when alginate beads were used as an immobilizer. This finding opens up the advanced use of nanomaterials derived from low-value agricultural residues in wider applications in microbial systems.

Utilization of OPEFB-derived nanocellulose, prepared by TEMPO-mediated oxidation in pervaporation membrane (op-TOCN-A) revealed that the addition of OPEFB-derived nanocellulose in alginate matrix followed by cross-linking with Ca^{2+} induced pore size formation and slightly increased the flux capacity. However, its performance was lower but still comparable if compared with the performance of woody TOCN in alginate matrix (w-TOCN-A) in flux capacity, water selectivity and mechanical properties. The addition of hydrophilic materials such as TOCN in alginate improved the flux capacity, water sorption and selectivity in pervaporation membrane. Furthermore, membrane engineering (including membrane composition and its preparation) and pervaporation condition (pressure applied, temperature, the flow rate of feed) might determine the membrane performance. Therefore, further study for utilizing nanocellulose as pervaporation membrane is still needed to be explored to obtain the optimum condition of nanocellulose application in membrane composite in regard to achieving optimum membrane permeability and selectivity.

3.5 References

[1] BPS-Statistics Indonesia, Indonesian Oil Palm Statistics, BPS-Statistics Indonesia, Jakarta, 2018.

[2] Directorat General of Estate Crops, Tree Crop Estate Statistics of Indonesia 2014-2016, Jakarta, 2015. doi:http://ditjenbun.pertanian.go.id/tinymcpuk/gambar/file/statistik/2016/SAWIT 2014-2016.pdf.

[3] M.S. Umikalsom, A.B. Ariff, H.S. Zulkifli, C.C. Tong, M.A. Hassan, M.I.A. Karim, The treatment of oil palm empty fruit bunch fibre for subsequent use as

substrate for cellulase production by Chaetomium globosum Kunze, Bioresour. Technol. 62 (1997) 1–9. doi:10.1016/S0960-8524(97)00132-6.

[4] K. Myrtha, H. Onggo, A.D. Abdullah, A. Syampurwadi, Effect of oil palm empty fruit bunch fiber on the physical and mechanical properties of fiber glass reinforced polyester resin, J. Biol. Sci. 8 (2008) 101–106.

[5] Z.A.Z. Azrina, M.D.H. Beg, M.Y. Rosli, R. Ramli, N. Junadi, A.K.M.M. Alam, Spherical nanocrystalline cellulose (NCC) from oil palm empty fruit bunch pulp via ultrasound assisted hydrolysis, Carbohydr. Polym. 162 (2017) 115–120. doi:10.1016/j.carbpol.2017.01.035.

[6] T. Abitbol, A. Rivkin, Y. Cao, E. Abraham, Y. Nevo, T. Ben-Shalom, S. Lapidot, O. Shoseyov, Nanocellulose, a tiny fiber with huge applications, Curr. Opin. Biotechnol. 39 (2016) 76–88. doi:10.1016/j.copbio.2016.01.002.

[7] Pratima Bajpai, Pulp and Paper Industry Nanotechnology in Forest Industry, Elsevier, 2017.

[8] T. Isogai, T. Saito, A. Isogai, TEMPO electromediated oxidation of some polysaccharides including regenerated cellulose fiber, Biomacromolecules. 11 (2010) 1593–1599. doi:10.1021/bm1002575.

[9] R. Tanaka, T. Saito, A. Isogai, Cellulose nanofibrils prepared from softwood cellulose by TEMPO/NaClO/NaClO2 systems in water at pH 4.8 or 6.8, Int. J. Biol. Macromol. 51 (2012) 228–234. doi:10.1016/j.ijbiomac.2012.05.016.

[10] A. Isogai, T. Saito, H. Fukuzumi, TEMPO-oxidized cellulose nanofibers, Nanoscale. 3 (2011) 71–85. doi:10.1039/c0nr00583e.

[11] T. Saito, A. Isogai, TEMPO-mediated oxidation of native cellulose. The effect of oxidation conditions on chemical and crystal structures of the water-insoluble fractions, Biomacromolecules. 5 (2004) 1983–1989. doi:10.1021/bm0497769.

[12] Y. Okita, T. Saito, A. Isogai, Entire surface oxidation of various cellulose microfibrils by TEMPO-mediated oxidation, Biomacromolecules. 11 (2010) 1696–1700. doi:10.1021/bm100214b.

[13] Y. Li, H. Zhu, F. Shen, J. Wan, S. Lacey, Z. Fang, H. Dai, L. Hu, Nanocellulose as green dispersant for two-dimensional energy materials, Nano Energy. 13 (2015) 346–354. doi:10.1016/j.nanoen.2015.02.015.

[14] D. Cheng, Y. Wen, X. An, X. Zhu, Y. Ni, TEMPO-oxidized cellulose nanofibers (TOCNs) as a green reinforcement for waterborne polyurethane coating (WPU) on wood, Carbohydr. Polym. 151 (2016) 326–334. doi:10.1016/j.carbpol.2016.05.083.

[15] R. Endo, T. Saito, A. Isogai, TEMPO-oxidized cellulose nanofibril/poly(vinyl alcohol) composite drawn fibers, Polym. (United Kingdom). 54 (2013) 935–941. doi:10.1016/j.polymer.2012.12.035.

[16] N. Zhang, G.L. Zang, C. Shi, H.Q. Yu, G.P. Sheng, A novel adsorbent TEMPO-mediated oxidized cellulose nanofibrils modified with PEI: Preparation, characterization, and application for Cu(II) removal, J. Hazard. Mater. 316 (2016) 11–18. doi:10.1016/j.jhazmat.2016.05.018.

[17] D. Celebi, R.H. Guy, K.J. Edler, J.L. Scott, Ibuprofen delivery into and through the skin from novel oxidized cellulose-based gels and conventional topical formulations, Int. J. Pharm. 514 (2016) 238–243. doi:10.1016/j.ijpharm.2016.09.028.

[18] L. Goetz, A. Mathew, K. Oksman, P. Gatenholm, A.J. Ragauskas, A novel nanocomposite film prepared from crosslinked cellulosic whiskers, Carbohydr. Polym. 75 (2009) 85–89. doi:10.1016/j.carbpol.2008.06.017.

[19] Y. Yan, K. Wang, Z. Wang, W. Gindl-Altmutter, S. Zhang, J. Li, Fabrication of homogeneous and enhanced soybean protein isolate-based composite films via incorporating TEMPO oxidized nanofibrillated cellulose stablized nano-ZnO hybrid, Cellulose. 24 (2017) 4807–4819. doi:10.1007/s10570-017-1469-5.

[20] I. Kalashnikova, H. Bizot, B. Cathala, I. Capron, Modulation of cellulose nanocrystals amphiphilic properties to stabilize oil/water interface, Biomacromolecules. 13 (2012) 267–275. doi:10.1021/bm201599j.

[21] Z. Hu, S. Ballinger, R. Pelton, E.D. Cranston, Surfactant-enhanced cellulose nanocrystal Pickering emulsions, J. Colloid Interface Sci. 439 (2015) 139–148. doi:10.1016/j.jcis.2014.10.034.

[22] L. Jin, Q. Sun, Q. Xu, Y. Xu, Adsorptive removal of anionic dyes from aqueous solutions using microgel based on nanocellulose and polyvinylamine, Bioresour. Technol. 197 (2015) 348–355. doi:10.1016/j.biortech.2015.08.093.

[23] A.D. Dwivedi, N.D. Sanandiya, J.P. Singh, S.M. Husnain, K.H. Chae, D.S. Hwang, Y.S. Chang, Tuning and Characterizing Nanocellulose Interface for Enhanced Removal of Dual-Sorbate (AsVand CrVI) from Water Matrices, ACS Sustain. Chem. Eng. 5 (2017) 518–528. doi:10.1021/acssuschemeng.6b01874.

[24] A. Azetsu, H. Koga, L. Yuan, T. Kitaoka, Direct synthesis of gold nanocatalysts on TEMPO- oxidized pulp paper containing aldehyde groups, BioResources. 8 (2013) 3706–3717.

[25] S. Sulaiman, M.N. Mokhtar, M.N. Naim, A.S. Baharuddin, A. Sulaiman, A Review: Potential Usage of Cellulose Nanofibers (CNF) for Enzyme Immobilization via Covalent Interactions, Appl. Biochem. Biotechnol. 175 (2014) 1817–1842. doi:10.1007/s12010-014-1417-x.

[26] K.M.A. Uddin, H. Orelma, P. Mohammadi, M. Borghei, J. Laine, M. Linder, O.J. Rojas, Retention of lysozyme activity by physical immobilization in nanocellulose aerogels and antibacterial effects, Cellulose. 24 (2017) 2837–2848. doi:10.1007/s10570-017-1311-0.

[27] S. Il Yu, S.K. Min, H.S. Shin, Nanocellulose size regulates microalgal flocculation and lipid metabolism, Sci. Rep. 6 (2016) 1–9. doi:10.1038/srep35684.

[28] X. Sun, Q. Lu, Y. Boluk, Y. Liu, The impact of cellulose nanocrystals on the aggregation and initial adhesion of Pseudomonas fluorescens bacteria, Soft Matter. 10 (2014) 8923–8931. doi:10.1039/C4SM00946K.

[29] X. Sun, Y. Shao, Y. Boluk, Y. Liu, The impact of cellulose nanocrystals on the aggregation and initial adhesion to a solid surface of Escherichia coli K12: Role of solution chemistry, Colloids Surfaces B Biointerfaces. 136 (2015) 570–576. doi:10.1016/j.colsurfb.2015.09.042.

[30] X. Sun, C. Danumah, Y. Liu, Y. Boluk, Flocculation of bacteria by depletion interactions due to rod-shaped cellulose nanocrystals, Chem. Eng. J. 198–199 (2012) 476–481. doi:10.1016/j.cej.2012.05.114.

[31] M.U. Larsen, M. Seward, A. Tripathi, N.C. Shapley, Biocompatible nanoparticles trigger rapid bacteria clustering, Biotechnol. Prog. 25 (2009) 1094–1102. doi:10.1002/btpr.179.

[32] Y.N. Zheng, L.Z. Li, M. Xian, Y.J. Ma, J.M. Yang, X. Xu, D.Z. He, Problems with the microbial production of butanol, J. Ind. Microbiol. Biotechnol. 36 (2009) 1127–1138. doi:10.1007/s10295-009-0609-9.

[33] C. Xue, J. Zhao, L. Chen, S.T. Yang, F. Bai, Recent advances and state-of-the-art strategies in strain and process engineering for biobutanol production by

Clostridium acetobutylicum, Biotechnol. Adv. 35 (2017) 310–322. doi:10.1016/j.biotechadv.2017.01.007.

[34] P. Dürre, Biobutanol: An attractive biofuel, Biotechnol. J. 2 (2007) 1525–1534. doi:10.1002/biot.200700168.

[35] L.T. Mun, A. Ishizaki, S. Yoshino, K. Furukawa, Production of acetone, butanol and ethanol from palm oil waste by Clostridium saccharoperbutylacetonicum N1-4, Biotechnol. Lett. 17 (1995) 649–654. doi:10.1007/BF00129394.

[36] Y. Tashiro, K. Takeda, G. Kobayashi, K. Sonomoto, A. Ishizaki, S. Yoshino, High Butanol Production by Clostridium saccharoperbutylacetonicum N1-4 in Fed-Batch Culture with pH-Stat Continuous Butyric Acid and Glucose Feeding Method, J. Biosci. Bioeng. 98 (2004) 263–268. doi:10.1016/S1389-1723(04)00279-8.

[37] D. Jones, D.R. Woods, Acetone-butanol fermentation revisited, Microbiol. Rev. 50 (1986) 484–524. doi:3540574.

[38] W.E. Barton, A. Daugulis, Evaluation of solvents for extractive butanol fermentation with Clostridium acetobutylicum and the use of poly(propylene glycol) 1200, Appl. Microbiol. Biotechnol. 36 (1992) 632–639. doi:10.1007/BF00183241.

[39] N. Qureshi, I.S. Maddox, Reduction in butanol inhibition by perstraction: Utilization of concentrated lactose/whey permeate by Clostridium acetobutylicum to enhance butanol fermentation economics, Food Bioprod. Process. 83 (2005) 43–52. doi:10.1205/fbp.04163.

[40] N. Qureshi, I.S. Maddox, Continuous production of acetone-butanol-ethanol using immobilized cells of Clostridium acetobutylicum and integration with

product removal by liquid-liquid extraction, J. Ferment. Bioeng. 80 (1995) 185–189.

[41] A. Ishizaki, S. Michiwaki, E. Crabbe, G. Kobayashi, K. Sonomoto, S. Yoshino, Extractive acetone-butanol-ethanol fermentation using methylated crude palm oil as extractant in batch culture of Clostridium saccaharoperbutylacetonicum N1-4 (ATCC 13564), J. Biosci. Bioeng. 87 (1999) 352–356. doi:10.1016/S1389-1723(99)80044-9.

[42] S. Roffler, H. Blanch, C. Wilkey, In-situ recovery of butanol during fermentation, Bioprocess Eng. 2 (1987) 1–12.

[43] S.S. de Jesus, G.F. Ferreira, M.R. Wolf Maciel, R. Maciel Filho, Biodiesel purification by column chromatography and liquid-liquid extraction using green solvents, Fuel. 235 (2019) 1123–1130. doi:10.1016/j.fuel.2018.08.107.

[44] S. Ishii, M. Taya, T. Kobayashi, Production of butanol by Clostridium acetobutylicum in extractive fermentation system, J. Chem. Eng. Japan. 18 (1985) 125–130. doi:10.1252/jcej.18.125.

[45] F. Napoli, G. Olivieri, M.E. Russo, A. Marzocchella, P. Salatino, Butanol production by Clostridium acetobutylicum in a continuous packed bed reactor, J. Ind. Microbiol. Biotechnol. 37 (2010) 603–608. doi:10.1007/s10295-010-0707-8.

[46] A.P. Pereira, A. Mendes-Ferreira, J.M. Oliveira, L.M. Estevinho, A. Mendes-Faia, Effect of Saccharomyces cerevisiae cells immobilisation on mead production, LWT - Food Sci. Technol. 56 (2014) 21–30. doi:10.1016/j.lwt.2013.11.005.

[47] H. Fukuzumi, T. Saito, T. Iwata, Y. Kumamoto, A. Isogai, Transparent and high gas barrier films of cellulose nanofibers prepared by TEMPO-mediated oxidation, Biomacromolecules. 10 (2009) 162–165. doi:10.1021/bm801065u.

[48] T. Suratago, S. Taokaew, N. Kanjanamosit, K. Kanjanaprapakul, V. Burapatana, M. Phisalaphong, Development of bacterial cellulose/alginate nanocomposite membrane for separation of ethanol-water mixtures, J. Ind. Eng. Chem. 32 (2015) 305–312. doi:10.1016/j.jiec.2015.09.004.

[49] L. Ansaloni, J. Salas-Gay, S. Ligi, M.G. Baschetti, Nanocellulose-based membranes for CO2capture, J. Memb. Sci. 522 (2017) 216–225. doi:10.1016/j.memsci.2016.09.024.

[50] P. Hadi, M. Yang, H. Ma, X. Huang, H. Walker, B.S. Hsiao, Biofouling-resistant nanocellulose layer in hierarchical polymeric membranes: Synthesis, characterization and performance, J. Memb. Sci. 579 (2019) 162–171. doi:10.1016/j.memsci.2019.02.059.

[51] J. Torstensen, R.M.L. Helberg, L. Deng, Ø.W. Gregersen, K. Syverud, PVA/nanocellulose nanocomposite membranes for CO 2 separation from flue gas, Int. J. Greenh. Gas Control. 81 (2019) 93–102. doi:10.1016/j.ijggc.2018.10.007.

[52] O. Nechyporchuk, M.N. Belgacem, J. Bras, Production of cellulose nanofibrils: A review of recent advances, Ind. Crop. Prod. 93 (2016) 2–25. doi:10.1016/j.indcrop.2016.02.016.

[53] P. Wei, L.H. Cheng, L. Zhang, X.H. Xu, H.L. Chen, C.J. Gao, A review of membrane technology for bioethanol production, Renew. Sustain. Energy Rev. 30 (2014) 388–400. doi:10.1016/j.rser.2013.10.017.

[54] U.S. Toti, T.M. Aminabhavi, Pervaporation separation of water-isopropyl alcohol mixtures with blend membranes of sodium alginate and poly(acrylamide)-grafted guar gum, J. Appl. Polym. Sci. 85 (2002) 2014–2024. doi:10.1002/app.10816.

[55] G. Young Moon, R. Pal, R.Y.M. Huang, Novel two-ply composite membranes of chitosan and sodium alginate for the pervaporation dehydration of isopropanol and ethanol, J. Memb. Sci. 156 (1999) 17–27. doi:10.1016/S0376-7388(98)00322-6.

[56] H. Fukuzumi, T. Saito, A. Isogai, Influence of TEMPO-oxidized cellulose nanofibril length on film properties, Carbohydr. Polym. 93 (2013) 172–177. doi:10.1016/j.carbpol.2012.04.069.

[57] M. Giacinti Baschetti, M. Minelli, J. Catalano, G.C. Sarti, Gas permeation in perflurosulfonated membranes: Influence of temperature and relative humidity, Int. J. Hydrogen Energy. 38 (2013) 11973–11982. doi:10.1016/j.ijhydene.2013.06.104.

[58] G.Q. Chen, C.A. Scholes, G.G. Qiao, S.E. Kentish, Water vapor permeation in polyimide membranes, J. Memb. Sci. 379 (2011) 479–487. doi:10.1016/j.memsci.2011.06.023.

[59] Y.J. Han, K.H. Wang, J.Y. Lai, Y.L. Liu, Hydrophilic chitosan-modified polybenzoimidazole membranes for pervaporation dehydration of isopropanol aqueous solutions, J. Memb. Sci. 463 (2014) 17–23. doi:10.1016/j.memsci.2014.03.052.

[60] M. Nawawi, M Ghazali, R.Y.M. Huang, Pervaporation dehydration of isopropanol with chitosan membranes, J. Memb. Sci. 124 (1997) 53–62. doi:10.1016/S0376-7388(96)00216-5.

[61] T. Uragami, T. Saito, T. Miyata, Pervaporative dehydration characteristics of an ethanol/water azeotrope through various chitosan membranes, Carbohydr. Polym. 120 (2015) 1–6. doi:10.1016/j.carbpol.2014.11.032.

[62] N. Hastuti, K. Kanomata, T. Kitaoka, Hydrochloric Acid Hydrolysis of Pulps from Oil Palm Empty Fruit Bunches to Produce Cellulose Nanocrystals, J. Polym. Environ. 0 (2018) 0. doi:10.1007/s10924-018-1248-x.

[63] T. Yoshida, Y. Tashiro, K. Sonomoto, Novel high butanol production from lactic acid and pentose by Clostridium saccharoperbutylacetonicum, J. Biosci. Bioeng. 114 (2012) 526–530. doi:10.1016/j.jbiosc.2012.06.001.

[64] R.F. Darmayanti, Y. Tashiro, T. Noguchi, M. Gao, K. Sakai, K. Sonomoto, Novel biobutanol fermentation at a large extractant volume ratio using immobilized Clostridium saccharoperbutylacetonicum N1-4, J. Biosci. Bioeng. 126 (2018) 750–757. doi:10.1016/j.jbiosc.2018.06.006.

[65] R. Kuramae, T. Saito, A. Isogai, TEMPO-oxidized cellulose nanofibrils prepared from various plant holocelluloses, React. Funct. Polym. 85 (2014) 126–133. doi:10.1016/j.reactfunctpolym.2014.06.011.

[66] H. Fukuzumi, T. Saito, Y. Okita, A. Isogai, Thermal stabilization of TEMPO-oxidized cellulose, Polym. Degrad. Stab. 95 (2010) 1502–1508. doi:10.1016/j.polymdegradstab.2010.06.015.

[67] M. Shimizu, H. Fukuzumi, T. Saito, A. Isogai, Preparation and characterization of TEMPO-oxidized cellulose nanofibrils with ammonium carboxylate groups, Int. J. Biol. Macromol. 59 (2013) 99–104. doi:10.1016/j.ijbiomac.2013.04.021.

[68] T. Saito, S. Kimura, Y. Nishiyama, A. Isogai, Cellulose nanofibers prepared by TEMPO-mediated oxidation of native cellulose, Biomacromolecules. 8 (2007) 2485–2491. doi:10.1021/bm0703970.

[69] D.T. Jones, D.R. Woods, Acetone-butanol fermentation revisited., Microbiol. Rev. 50 (1986) 484–524. doi:3540574.

[70] H. Shinto, Y. Tashiro, M. Yamashita, G. Kobayashi, T. Sekiguchi, T. Hanai, Y. Kuriya, M. Okamoto, K. Sonomoto, Kinetic modeling and sensitivity analysis of acetone-butanol-ethanol production, J. Biotechnol. 131 (2007) 45–56. doi:10.1016/j.jbiotec.2007.05.005.

[71] P.M. Gotovtsev, E.Y. Yuzbasheva, K. V. Gorin, V. V. Butylin, G.U. Badranova, N.I. Perkovskaya, E.B. Mostova, Z.B. Namsaraev, N.I. Rudneva, A. V. Komova, R.G. Vasilov, S.P. Sineokii, Immobilization of microbial cells for biotechnological production: Modern solutions and promising technologies, Appl. Biochem. Microbiol. 51 (2015) 792–803. doi:10.1134/S0003683815080025.

[72] T. Andersen, P. Auk-Emblem, M. Dornish, 3D Cell Culture in Alginate Hydrogels, Microarrays. 4 (2015) 133–161. doi:10.3390/microarrays4020133.

[73] O. Smidsrod, G. Skjak-Braek, Alginate as immobilization matrix for cells, Trends Biotechnol. 8 (1990) 71–78. doi:10.1016/0167-7799(90)90139-O.

[74] H.W. Yen, R.J. Li, The effects of dilution rate and glucose concentration on continuous acetone-butanol-ethanol fermentation by Clostridium acetobutylicum immobilized on bricks, J. Chem. Technol. Biotechnol. 86 (2011) 1399–1404. doi:10.1002/jctb.2640.

[75] Y. Tashiro, K. Sonomoto, Advances in butanol production by clostridia, in: A. Mendez-Villaz (Ed.), Curr. Res. Educ. Top. Appl. Microbiol. Microb. Technol., 2nd ed., Formatex Research Center, Badajoz, 2010: pp. 1383–1394.

[76] R.G. Willaert, Cell Immobilization and Its Applications in Biotechnology: Trends and Future Prospects, in: E. El-Mansi, C. Bryce, A. Demain, A. Allman

(Eds.), Ferment. Microbiol. Biotechnol., 2nd ed., Taylor & Francis Group, Boca Raton, 2007: pp. 313–368.

[77] L. Häggström, N. Molin, Calcium alginate immobilized cells of clostridium acetobutylicum for solvent production, Biotechnol. Lett. 2 (1980) 241–246. doi:10.1007/BF01209440.

[78] M. Park, D. Lee, J. Hyun, Nanocellulose-alginate hydrogel for cell encapsulation, Carbohydr. Polym. 116 (2015) 223–228. doi:10.1016/j.carbpol.2014.07.059.

[79] J. Nemoto, T. Soyama, T. Saito, A. Isogai, Nanoporous networks prepared by simple air drying of aqueous TEMPO-oxidized cellulose nanofibril dispersions, Biomacromolecules. 13 (2012) 943–946. doi:10.1021/bm300041k.

[80] Y. Kourkoutas, A. Bekatorou, I.M. Banat, R. Marchant, A.A. Koutinas, Immobilization technologies and support materials suitable in alcohol beverages production: a review, Food Microbiol. 21 (2004) 377–397. doi:10.1016/j.fm.2003.10.005.

[81] N. Lin, C. Bruzzese, A. Dufresne, TEMPO-oxidized nanocellulose participating as crosslinking aid for alginate-based sponges, ACS Appl. Mater. Interfaces. 4 (2012) 4948–4959. doi:10.1021/am301325r.

[82] K. Tsuboi, S. Yokota, T. Kondo, Difference between bamboo- and wood-derived cellulose nanofibers prepared by the aqueous counter collision method, Nord. Pulp Pap. Res. J. 29 (2014) 69–76. doi:10.3183/npprj-2014-29-01-p069-076.

[83] S. Fujisawa, Y. Okita, H. Fukuzumi, T. Saito, A. Isogai, Preparation and characterization of TEMPO-oxidized cellulose nanofibril films with free

carboxyl groups, Carbohydr. Polym. 84 (2011) 579–583. doi:10.1016/j.carbpol.2010.12.029.

[84] M. Shimizu, T. Saito, A. Isogai, Water-resistant and high oxygen-barrier nanocellulose films with interfibrillar cross-linkages formed through multivalent metal ions, J. Memb. Sci. 500 (2016) 1–7. doi:10.1016/j.memsci.2015.11.002.

[85] T. Huhtamäki, X. Tian, J.T. Korhonen, R.H.A. Ras, Surface-wetting characterization using contact-angle measurements, Nat. Protoc. 13 (2018) 1521–1538. doi:10.1038/s41596-018-0003-z.

[86] L.T. Fan, X.G. Yuan, C.X. Zhou, A.W. Zeng, K.T. Yu, M. Kalbassi, K. Porter, Contact angle of ethanol and n-propanol aqueous solutions on metal surfaces, Chem. Eng. Technol. 34 (2011) 1535–1542. doi:10.1002/ceat.201000474.

[87] Y.K. Ong, G.M. Shi, N.L. Le, Y.P. Tang, J. Zuo, S.P. Nunes, T.S. Chung, Recent membrane development for pervaporation processes, Prog. Polym. Sci. 57 (2016) 1–31. doi:10.1016/j.progpolymsci.2016.02.003.

[88] J. Phattaranawik, R. Jiraratananon, A.G. Fane, Effect of pore size distribution and air flux on mass transport in direct contact membrane distillation, J. Memb. Sci. 215 (2003) 75–85. doi:10.1016/S0376-7388(02)00603-8.

[89] B.D. Zdravkov, J.J. Čermák, M. Šefara, J. Janků, Pore classification in the characterization of porous materials: A perspective, Cent. Eur. J. Chem. 5 (2007) 385–395. doi:10.2478/s11532-007-0017-9.

[90] C.K. Yeom, J.G. Jegal, K.H. Lee, Characterization of relaxation phenomena and permeation behaviors in sodium alginate membrane during pervaporation separation of ethanol-water mixture, J. Appl. Polym. Sci. 62 (1996) 1561–1576.

doi:10.1002/(SICI)1097-4628(19961205)62:10<1561::AID-APP8>3.0.CO;2-M.

[91] M.D. Kurkuri, T.M. Aminabhavi, Pervaporation separation of water and dioxane mixtures with sodium alginate-g-polyacrylamide copolymeric membranes, J. Appl. Polym. Sci. 89 (2003) 300–305. doi:10.1002/app.12087.

[92] X. Shu, X. Wang, Q. Kong, X. Gu, N. Xu, High-flux MFI zeolite membrane supported on ysz hollow fiber for separation of ethanol/water, Ind. Eng. Chem. Res. 51 (2012) 12073–12080. doi:10.1021/ie301087u.

[93] G. Yang, L. Zhang, T. Peng, W. Zhong, Effects of Ca2+ bridge cross-linking on structure and pervaporation of cellulose/alginate blend membranes, J. Memb. Sci. 175 (2000) 53–60. doi:10.1016/S0376-7388(00)00407-5.

Chapter 4

Characterization of Oil Palm Empty Fruit Bunches Nanocellulose in Film Composite

4.1 Introduction

Currently, the utilization of nanocellulose (NC) has increasingly gained attention from various research fields, particularly the field of polymer nanocomposites owing to the growing environmental risks of petroleum based-fiber products [1]. Polymer nanocomposites based on nanofillers from natural materials also have attracted interest ranging from scientific community to industry because of remarkable improvement in properties [2]. Compared to regular cellulose substrates, much smaller NC have higher mechanical strength, better optical transparence, and smoother surface. These properties combined with their low cost, light weight, flexibility, and environmental friendliness, make NC are promising candidates for fabrication of novel composites [3]. Nanocelluloses are often added to improve the mechanical, rheological, and barrier properties of many polymeric systems [4]. Existing literatures has suggested that the addition of NC in lower amount increased mechanical properties, but up to certain level (higher concentration), NC addition causes development of weaker section in polymer/NC composite, increase brittleness and causing fracture [5,6]. The utilization of NC in polymers matrix is not only to improve mechanical properties but also to improve antibiofouling, thermal and high gas barrier properties [7–10]. Key properties of NC such as structural morphology, crystallinity, aspect ratio and surface chemistry affected NC performance in polymers matrix [11–14]. In addition, NC properties are generally depend on the source of natural fibers and NC extraction condition [3,15]. Nanocellulose preparation from softwood pulp requires less mechanical treatment than

hardwood [16]. Furthermore, non-wood plants are receiving a lot of interest as NC raw materials due to the lignin content is lower and delignification become easier in NC extraction process [17].

The utilization of NC from oil palm empty fruit bunches (OPEFB) as reinforcing agent is still limited to be explored. Nevertheless, NC extraction and characterization from OPEFB has been intensively reported by a few researchers [18–20]. Extraction of cellulose nanocrystals (CNC) from microcrystalline cellulose of OPEFB by sulfuric acid hydrolysis revealed high crystallinity and thermal stability [21]. Furthermore, NC extraction of OPEFB by hydrochloric acid was effective to yield crystalline CNC with long term nanodispersibility showing clear birefringence [22]. Due to the high crystalline of NC OPEFB, their utilization to be used as reinforcing agent is preferred. Utilization of NC as reinforcing agent from other non-wood fibers also has been reported by Chen and co-authors. The study revealed that bamboo nanofibers had the greatest reinforcing effect on the starch film, due to it had largest aspect ratio, although it had lower degree of crystallinity compared to cotton linter and sisal [23]. The different type of NC added into polymer matrix also had been reported and showed different performances. CNC and cellulose nanofibrils (CNFs) addition as reinforcing agent into poly (hydroxybutyrate-co-hydroxyvalerate)/PHBV matrix showed that both increased the tensile properties of PHBV composite, moreover CNC revealed stronger reinforcing effect than CNFs [24]. Furthermore, CNFs made by TEMPO oxidation which denoted as TEMPO-oxidized cellulose nanofibrils (TOCNs) also revealed high tensile modulus and thermal stability in poly (vinyl alcohol) matrix [10].

In this study, utilization of CNC and TOCNs from OPEFB as reinforcing agent in poly (methyl vinyl ether maleic acid)/PMVEMA and poly (ethylene glycol)/PEG was investigated. In the previous study, the use of NC as reinforcing fillers in

PMVEMA-PEG matrix was in high concentration (25-75 wt%) [25,26]. In addition, high amount of NC addition drive NC aggregation due to the presence of hydroxy groups on their surface. Meanwhile, the addition of NC did not follow linier pattern of "the more the better|"; with the increase of the amount of nanocellulose, the thermal stability and elongation at break of the composite films were reduced, and the tensile force remained unchanged or even weakened after reaching maximum value [23]. PMVEMA is biocompatible water soluble polymer and PEG is most used as hydrophilic additive. In addition, by blending polymer matrix with hydrophilic additives is one easily method to get good compatibility and permeability [26]. Therefore, in this study, the NC of OPEFB was added into PMVEMA/PEG matrix in lower amount than previously reported. Comparison on performance of NC from other non-wood raw materials as reinforcing agent in polymers matrix also discussed.

4.2 Nanocellulose Composite Films with PMVEMA/PEG Cross-linkers

4.2.1 Materials

Poly (methyl vinyl ether maleic acid)/PMVEMA, Mw 1.980.000 (Sigma Aldrich, USA) (Mw 1.980.000) and PEG (Wako Pure Chemical Industries, Osaka, Japan) (Mw 20.000) were used in this study. Hydrochloric acid 0,1 M was used to obtain the solution in pH 2. The water used in this study was purified with an Arium Ultrapure Water System (Sartorius Co., Ltd., Tokyo, Japan). Bleached kraft pulp of oil palm empty fruit bunches (OPEFB) was kindly supplied from Biomaterial Research Institute, Indonesian Institute of Sciences (Bogor, Indonesia) and used as raw materials to produce CNC and TOCNs as described in Chapter 2. Here, NC derived from OPEFB, CNC OPEFB and TOCN OPEFB were denoted as CO and TO, respectively. The CO used in this study was CNC-A with the highest crystallinity index (65%), aspect ratio

23±18. The TO used in this study was TO produced using 20 mmol/g of NaClO and having carboxylate content of 1.5 mmol/g; crystallinity index 55%, aspect ratio 41±14. Meanwhile, NC from Nippon Paper Company, Japan, for a comparison were denoted as TCS and TCL for short TOCNs and long TOCNs, respectively. The carboxy contents and aspect ratio for TCS and TCL were: 1.61 mmol/g; 24±7; and 1.43 mmol/g; 44±16, respectively.

4.2.2 Method

4.2.2.1 PMVEMA-PEG film reinforced by nanocellulose

A 6.7:1 mass ratio of PMVEMA:PEG (1.5 g) was added in 40 mL of deionized water (DI) preheated at 68°C and acidified with HCl 0.1 M to reach pH 2. At first, PMVEMA was poured into the heated and acidified DI to get it dissolved completely, then followed by PEG and 5 wt% NC of OPEFB addition (0.4 wt%; 20 mL; carboxylate content 1.50 mmol/g cellulose). The 5 wt% addition of NC in PMVEMA-PEG matrix was chosen because the addition of NC OPEFB below 6% to the PVA considerably results enhancements in tensile strength and modulus as reported by Asad and co-authors [27]. Furthermore, the samples were denoted as P100 for PMVEMA-PEG only, CO100 for CNC OPEFB 100%, TO100 for 100%TOCN OPEFB , TCS100 for 100% short TOCN from company and TCL100 for 100% long TOCN from company. Similar type denotation was applied for 5 wt% addition of NC (CO5; TO5; TCS5 and TCL5). The solution was continuously stirred to get all the components mixed completely. Then the solution was homogenized by electrical homogenizer for 2–3 min, poured on teflon Petri dish, cured at 135°C for 5 min and dried at 40°C for 3–4 days. The dried films were peeled off carefully and characterized.

4.2.2.2 Film characterization

The optical transmittance (T%) was observed using UV-Vis spectrophotometer UH5300 (Hitachi, Tokyo, Japan) at 250–800 nm wavelength.

Surface analysis was observed using Atomic Force Microscopy (AFM) in mode Scanning Probe Microscope/Dimension Icon with ScanAsyst function, the results were analyzed by NanoScope Analysis Version 1.80.

Fourier Transform Infrared Spectroscopy (FTIR) analysis was conducted using FT/IR -620 (JASCO, Tokyo, Japan) at wavelength 400-4000 cm^{-1} at the Center of Advanced Instrumental Analysis, Kyushu University.

Contact angles were measured using Drop Master 300 K (Kyowa Interface Science Co, Ltd., Saitama, Japan) by dropping a 1μL of water droplet in four different spots on film surface at room temperature.

Surface color of the films was measured using handy colorimeter NR-3000 (Nippon Denshoku Industries Co., Ltd., Tokyo, Japan). A white standard color plate (L = 97.75, a = −0.49 and b = 1.96) was used as a background for color measurements. Hunter color (L, a, and b) values were averaged from three readings from each sample. Color values were expressed as L* (whiteness or brightness/darkness), a* (redness/ greenness), and b* (yellowness/blueness) [28]. *The total color difference* (ΔE) was calculated as follows:

$$\Delta E = \sqrt{(\Delta L)^2 + (\Delta a)^2 + (\Delta b)^2} \qquad (1)$$

Thermal stability was observed using thermogravimetric analyzer (TG/DTA 7300, Hitachi, Tokyo, Japan). A 0.7–1-mg portion of the specimens was scanned from

30 to 500°C at a rate of 20°C/min under a nitrogen atmosphere at the Center of Advanced Instrumental Analysis, Kyushu University.

Tensile tests were observed using Material Testing Instruments (STA-1225, ORIENTEC Co., Ltd., Tokyo, Japan) equipped with a 100 N load cell. Sample specimens were prepared by cutting the film sheets into 40–50 x 10 mm strips. Measurement was conducted at 10% min^{-1} strain rate in 20 mm span length [29]. The sample were kept at 50% humidity for 2–3 days before testing. Sample thickness were measured using Digital Micrometer (Mitutoyo Corp., Kawasaki, Japan); length and width of films was measured using TACKLife Digital Caliper DC01 (Shenzen Take Tools. Co.Ltd., Guangdong, China).

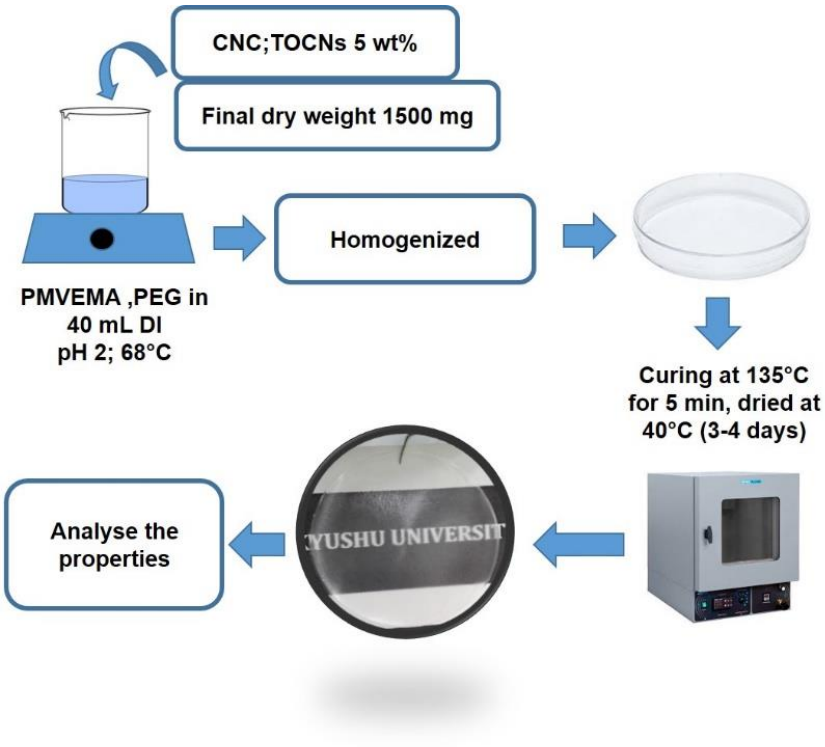

Figure 4.1. Research experimental scheme

4.2.3 Results and Discussion

4.2.3.1 Surface analysis

Surface morphology of obtained PMVEMA-PEG-NC films were observed using Atomic Force Microscopy (AFM) (**Fig. 4.2**). Microscopy images of AFM showed that the nanocelluloses have been well dispersed in PMVEMA-PEG matrix. This images were clearly showed the presence of NC in lower amount (5 wt%) of addition compared to the previous study conducted by Goetz and co-authors which used higher amount of NC about 25–75% [25]. The fibrous appearance of TOCNs from OPEFB and paper company was easier to be observed than the rod-like appearance of CNC OPEFB. AFM images confirmed the multiphase of obtained film.The cross-linking of naocellulose with PMVEMA and PEG through estrification reaction which previously reported [25] and described in **Fig. 4.3**.

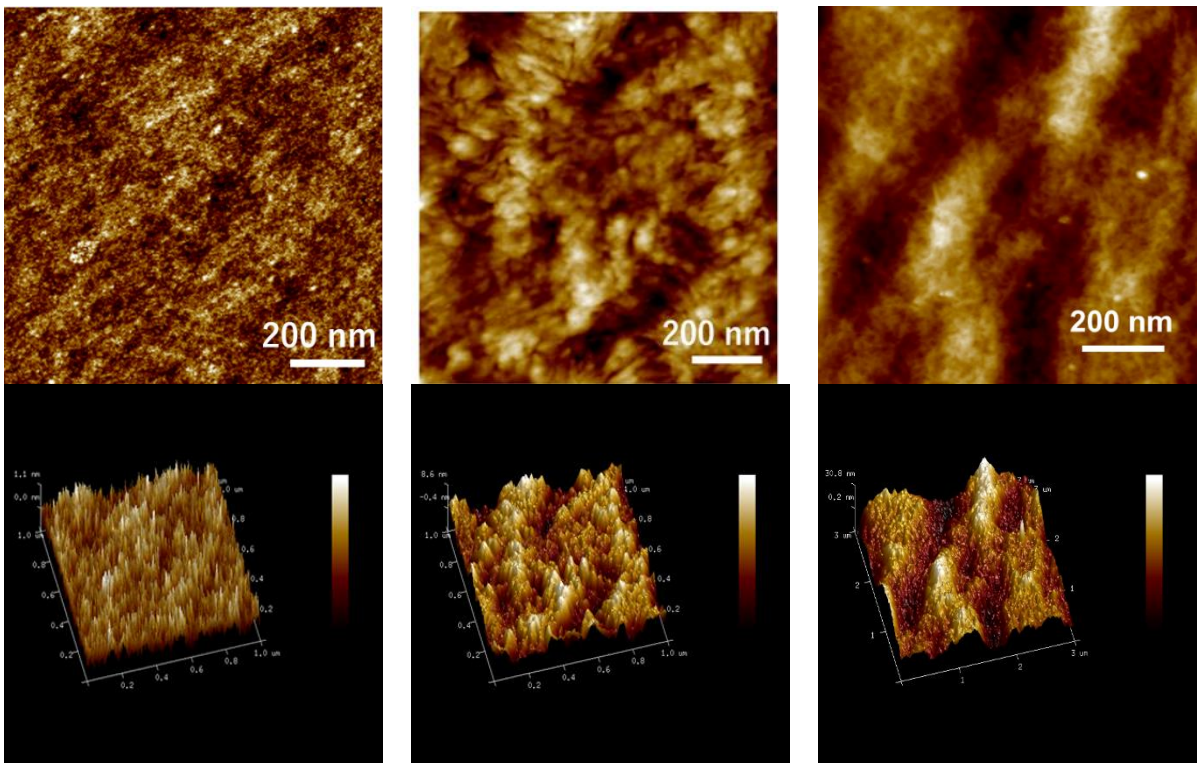

P100	CO100	TO100
Rq: 0.297 nm	Rq: 2.67 nm	Rq: 8.83 nm
Ra: 0.235 nm	Ra: 2.15 nm	Ra: 7.05 nm

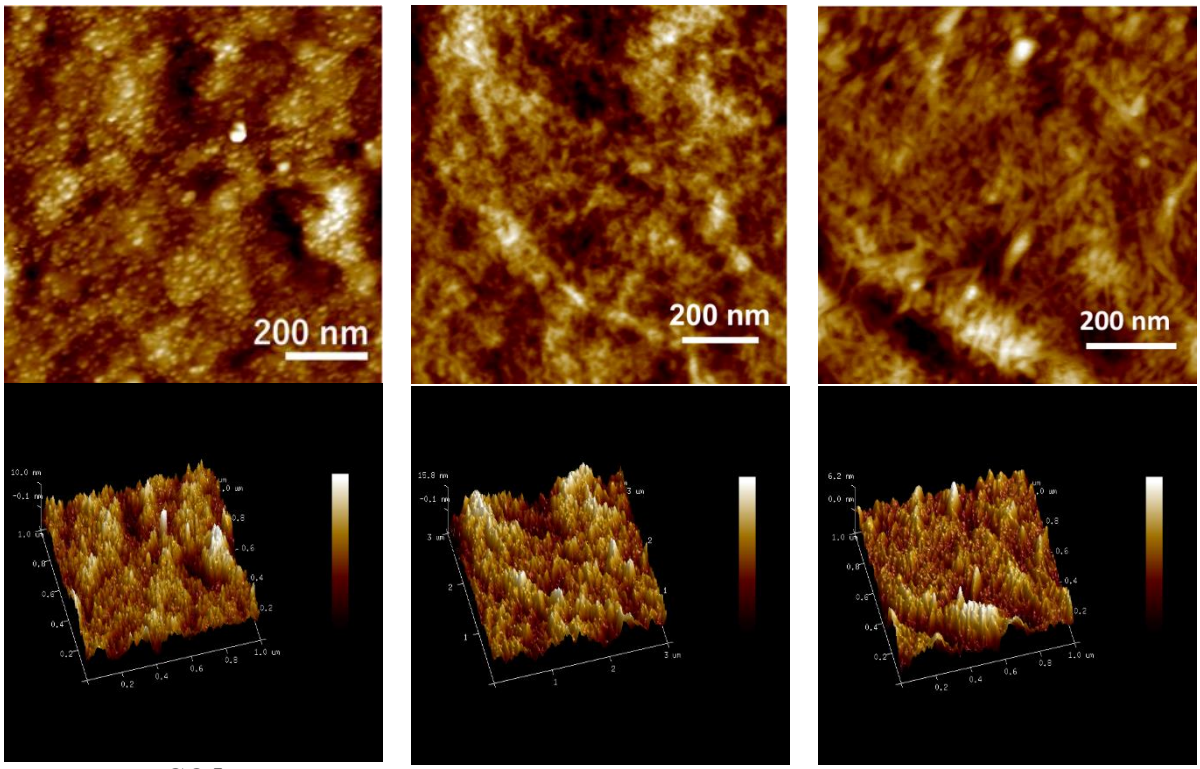

CO5
Rq: 2.64 nm
Ra: 2.02 nm

TO5
Ra: 4.40 nm
Rq: 3.50 nm

TCS100
Rq: 1.56 nm
Ra: 1.17 nm

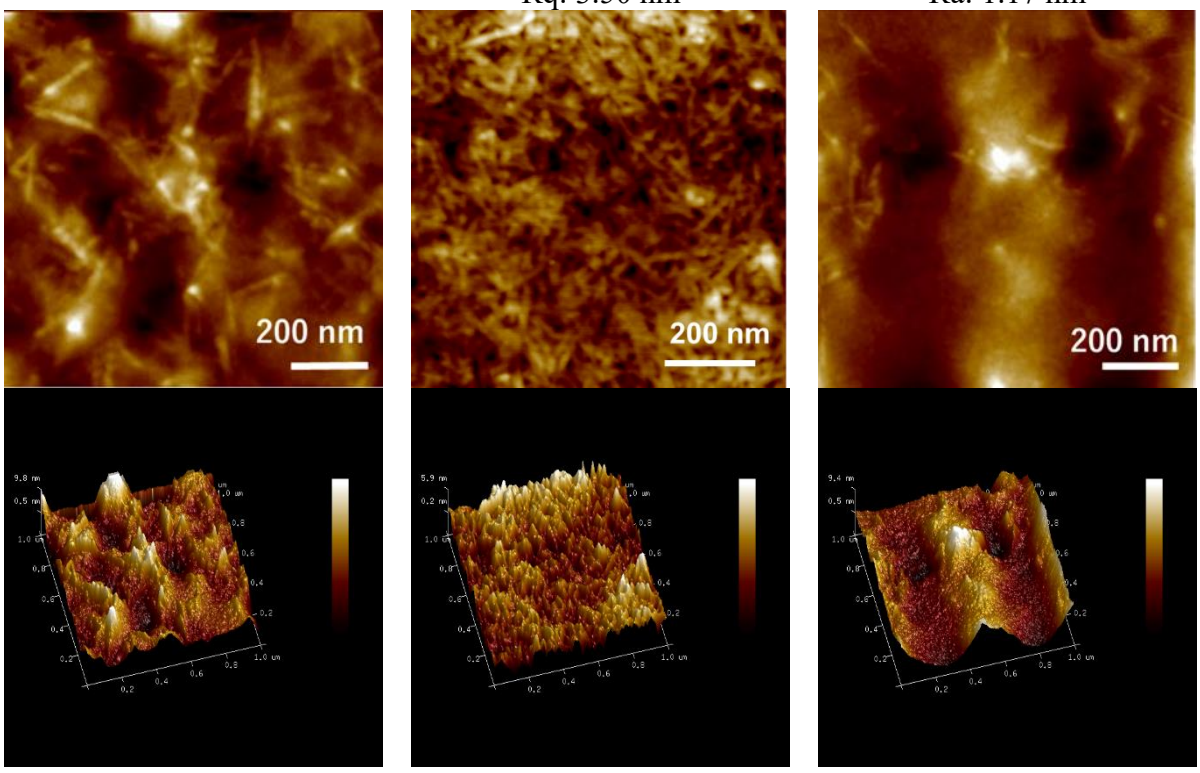

TCS5
Rq: 2.46 nm
Ra: 1.86 nm

TCL100
Ra:1.55 nm
Rq: 1.23 nm

TCL5
Rq: 2.51 nm
Ra: 2.02 nm

Figure 4.2 AFM analysis of PMVEMA-PEG-nanocellulose films

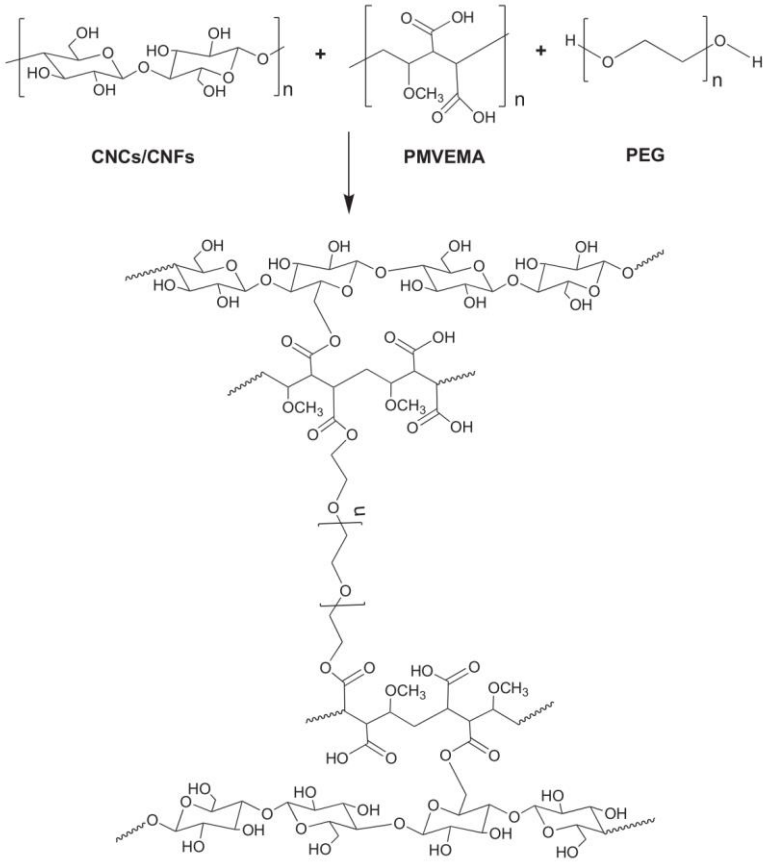

Figure 4.3. Nanocellulosics, PMVEMA and PEG cross-linking mechanism.

Reprinted from Ref 21 with the license from Elsevier

4.2.3.2 Optical transmittance

Light transmittances of PMVEMA-PEG film only/P100, 100% of nanocellulose and 5% of nanocellulose in PMVEMA-PEG matrix were observed using UV-Vis spectrophotometer (**Fig 4.4**). Control film (P100) had light transmittance of 72% at 600 nm. Meanwhile, a light transmittance of CO100 was 92%; TO100 was 79%; TCS100 was 82% and TCL100 was 84%. Furthermore, all PMVEMA-PEG films by nanocellulose addition had higher light transmittance compared to the control in the order of T% were CO5 > TCL5 > TO5 > TCS5.

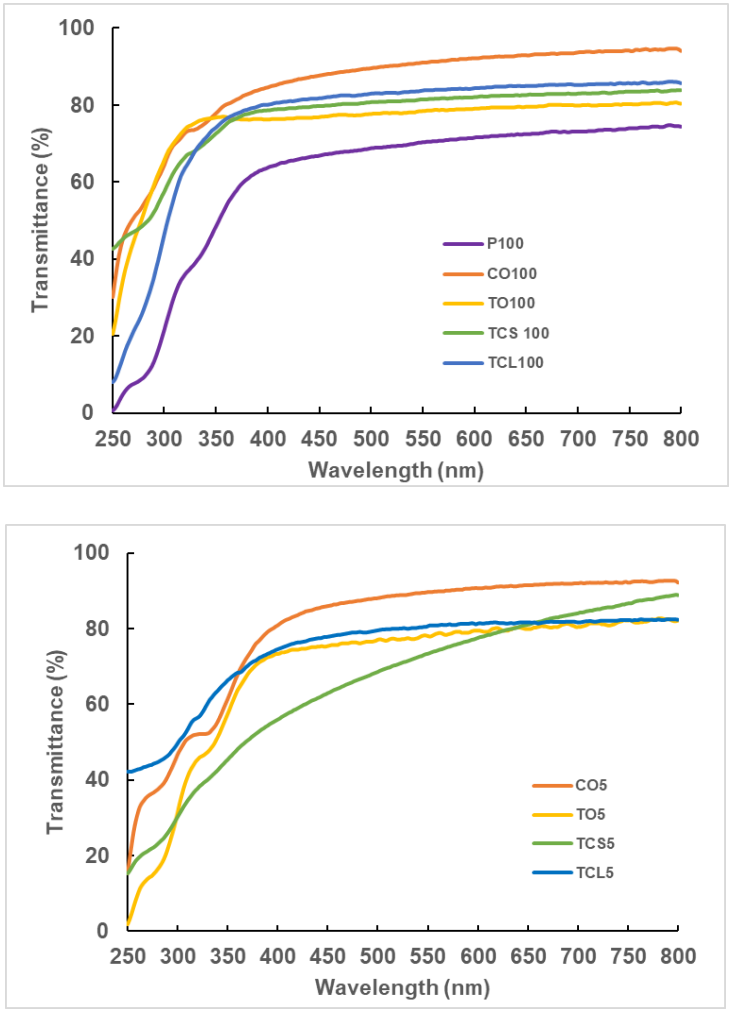

Figure 4.4. Ligth transmittance of control and 100% NC films (upper) and 5% of NC in PMVEMA-PEG matrix.

The high light transmittance may indicate that nanocellulose had high dispersibility in the water. It was in agreement with the previous study which stated that the rod-like CNC OPEFB which produced by HCl hydrolysis revealed long term nanodispersibility and showed clear birefringence [22]. The interference near infrared region indicates high smoothness on the film surface and the uniformity of film thickness [30]. All TOCNs films, both of TOCN of OPEFB (TO100) and TOCN from company (TCS 100 and TCL100) had light transmittance close to or more 80% at 600 nm which is in good agreement with those previously reported [31]. Lower

transmittance of TO100 it may be related to a lower fibrillation of TOCN OPEFB. In addition, lower transmittance of PMVEMA-PEG-NC films might be caused by drying factor and some opaque areas caused by bubbles. In higher drying temperature (at this study was 40°C), the films consolidated faster, limiting a homogeneous redistribution of the nanofibrillated material [32]. Furthermore, native PMVEMA-PEG film (P100) also showed lower transmittance. Nanocellulose fibers orientation in PMVEMA-PEG matrix also influence the optical transmittance. Films with 100% of NC were densely packed and the interstices between the fibers all small enough to avoid light scattering [33]. In contrast, in PMVEMA-PEG matrix, cross-linking between NC and the matrix made wider spaces and caused light scattering. Component rearrangement in the film matrix during the film drying, which defines its internal and surface structure, has an important role in the film optical properties [34].

4.2.3.3 FTIR analysis

Infrared spectroscopy analysis of PMVEMA-PEG film in the presence of nanocellulose was employed using Fourier Transform Infrared Spectroscopy/FT-IR (**Fig. 4.5**). The sharp peak at 1734 cm^{-1} can be attributed to the formation of ester linkage between the PMVEMA carboxylic acid and nanocellulose or PEG [25].

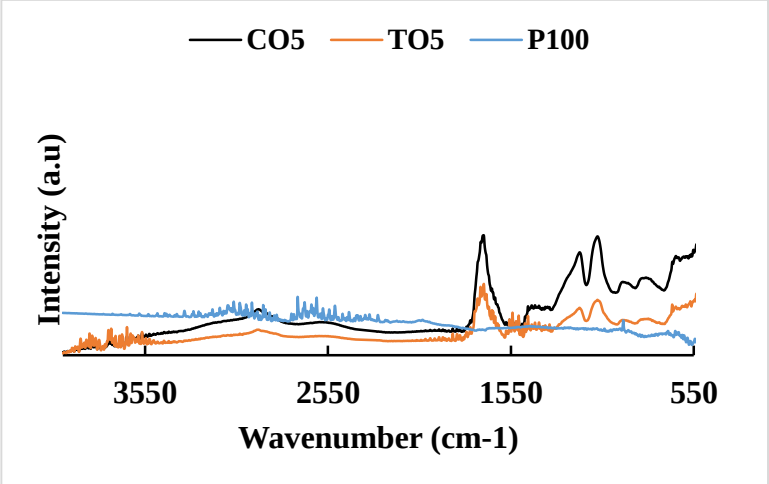

Figure 4.5. FTIR analysis of PMVEMA-PEG-nanocellulose film

4.2.3.4 Contact angles

The contact angles of obtained films were observed to identify the wettabilities of surfaces film (**Fig. 4.6)**. All films from 100% of NC showed the contact angles lower than P100 (<65°). It indicates that films made by 100% of NC were more hydrophilic compared to P100. Meanwhile, the addition of NC in PMVEMA-PEG matrix slightly increased the contact angle, which mean that surface wettability become lower compared to the control. Esterification occurred during the cross-linking between NC and PMVEMA-PEG might reduced the hydrogen bonds which reactive to the water molecules.

Surface roughness also contributed to the contact angles performance. Surface roughness analysis can be analyzed through *Ra* and *Rq* parameters by AFM analysis (**See section 4.2.3.1.**). Rougher surfaces tends to exhibit more water adsorption than smoother surface [35]. The contact angles of obtained films were in good agreement with the surface analysis using AFM. The lower roughness (lower *Rq*) was film of P100, resulting the highest contact angle which longer time for water adsorption. In contrast, TO100 had the roughest surface (highest *Rq*) and supposed to adsorp more amount of water and had lower contact angle. However, the changes of relative humidity (RH %) also have a significant influences in water adsoprtion behavior in the solid surface [35,36].

In case of fibrils length, it seemed that shorter fibrils yielded higher contact angle compared to the longer one. The length of nanocellulose had a great influence on surface structure. Shorter nanofibers was easier to derive micro-particles with more compact more even rough structure and better superhydrophobicity compared with the longer nanofibers [37]. Therefore, in this study showed that a film made by shorter CNC OPEFB (CO100) revealed higher contact angle compared to TOCNs

OPEB/TO100 (longer fibers). In addition, a film made by short TOCNs company (TCS100) had higher contact angle compared to long TOCNs company (TCL100).

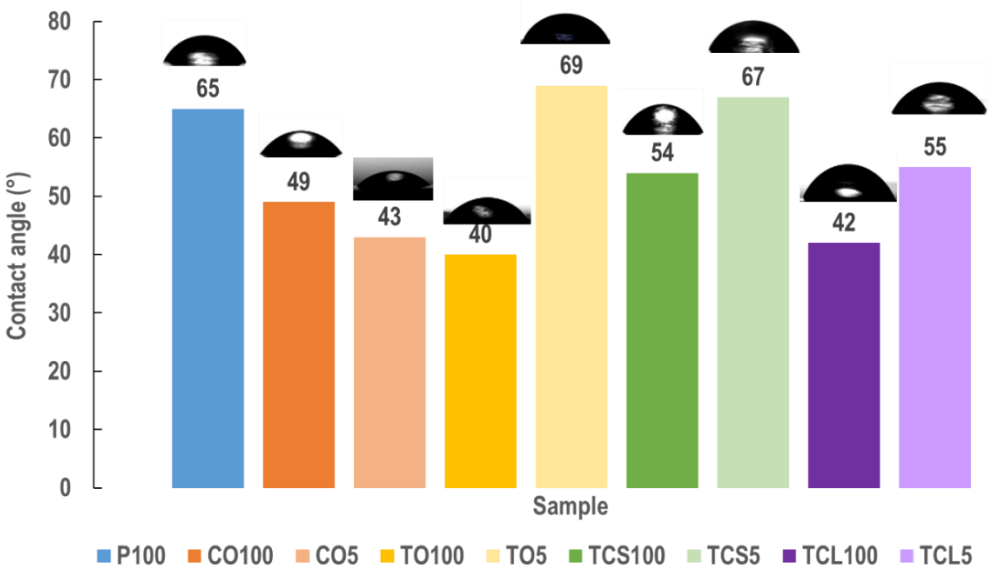

Figure 4.6. Contact angle of control film (P100) and PMVEMA-PEG-NC films

4.2.3.5 Color differentiation

The optical images of obtained films were transparent and clear (**Fig. 4.7)**. Furthermore, films of nanocellulose from OPEFB in PMVEMA-PEG matrix were more opaque compared to film made by 100% of nanocellulose OPEFB.

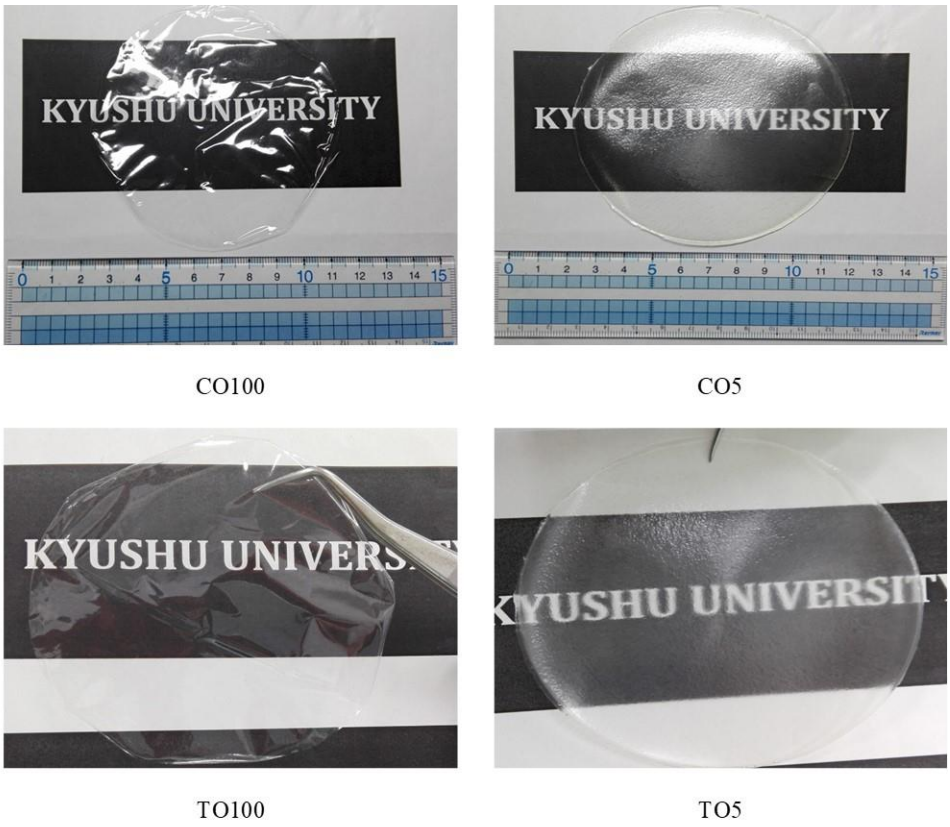

Figure 4.7. Optical images of films made by 100% of NC-OPEFB (left) and films made by 5 wt% of NC-OPEFB in PMVEMA-PEG matrix (right)

In addition, the color differentiation of obtained films can be calculated by total colour difference (TCD), denoted as △E, using equation (1) . In this study, colour differentiation referred to colour coordinate system developed by *Commision Internationale de l'Eclairage's* (CIE) L*a*b*. The results of TCD as described on **Table 4.1.**

Table 4.1. Color differentiation of obtained films of NC in PMVEMA-PEG matrix

Sample	**$(\triangle L^*)^2$**	**$(\triangle a^*)$**	**$(\triangle b^*)^2$**	**△E (to P100)**
P100	88.86	-0.55	18.61	n.d
CO100	92.47	-0.28	3.75	15.30

Sample	$(\triangle L^*)^2$	$(\triangle a^*)$	$(\triangle b^*)^2$	$\triangle E$ (to P100)
TO100	92.89	0.97	1.00	18.13
TCS100	91.76	-0.45	3.91	14.99
TCL100	92.89	0.97	1.00	18.13
CO5	90.58	0.24	4.03	14.70
TO5	90.59	0.56	3.77	14.99
TCS5	92.34	-0.33	3.46	15.55
TCL5	91.07	0.51	2.56	16.24

Total color difference (TCD) indicate the magnitude of color difference between sonicated and control samples. Differences in perceivable color can be analytically classified as very distinct (TCD > 3), distinct (1.5 < TCD < 3), and small differences (TCD < 1.5). Therefore, based on TCD values the color differences among the obtained films were very distinct [28,38]. Longer fibrils of TOCNs revealed higher TCD compared to the short fibrils. According to Rheddy and co-author, the TCD increased linierly with increase of NC content [39].

4.2.3.6 Thermal stability

Thermal properties of obtained films was analyzed by thermogravimetric (TG) and derivative thermogravimetic (DTG) (**Fig. 4.8)**. The figures showed that film of P100 had lower thermal stability compared to all 100% of nanocellulose film (CO100, TO100, TCL100 and TCS100). A slight weight loss observed in all films at below 150ºC which was attributed to the evaporated water.

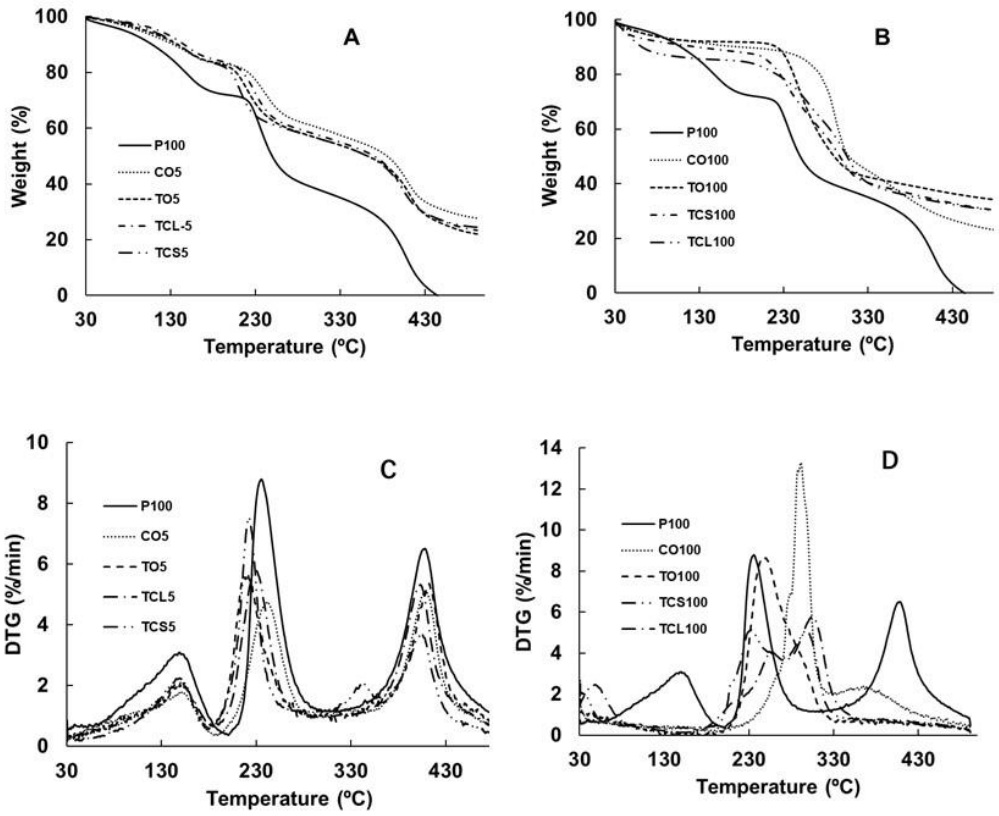

Figure 4.8. TG curves (A,B) and DTG curves (C,D) of obtained films

The derivative weight curve of NC-PMVEMA-PEG (CO5, TO5, TCS5, TCL5) and P100 films showed three distinct peaks of T_{max} (**Fig. 4.8 C**). The first peak is associated with the dehydration of the diacids of the PMVEMA. The second peak is associated with the combined decomposition of PMVEMA and PEG and third peak is attributed to the polymer chain degradation [40]. The length of TOCNs contributed to the thermal stability. The results showed that longer TOCNs in PMVEMA-PEG matrix slightly increased thermal stability of film by having higher maximum degradation temperatures (T_{max}).. The onset temperetures (T_{on}) and maximum degradation temperatures (T_{max}) as summarized in **Table 4.2**.

Table 4.2. Summary of T_{on} and T_{max} of NC-PMVEMA-PEG

	P100	CO100	TO100	TCL100	TCS100	CO5	TO5	TCL5	TCS5
T_{on} (°C)	107	179	217	63	128	126	132	143	134
T_{max} (°C)	151[a]	291	232	260	235	151[a]	146[a]	149[a]	145[a]
	235[b]					243[b]	221[b]	229[b]	222[b]
	408[c]					409[c]	412[c]	403[c]	348[c]
									404[d]

Remarks : [a]First peak, [b]second peak; [c]third peak; [d] fourth peak

The lower thermal stability was observed in TOCNs films compared to CNC film. CO100 and CO5 had higher T_{max} compared to the films containing TOCNs. The presence of sodium carboxylate groups in TOCNs decreased thermal stability because decarboxylation takes place at lower temperature [41]. Thermal stability is associated with the high crystalline of NC. Film of CO100 showed higher thermal stability **(Fig. 4.8B and D**) than TO100 because CNC OPEFB had higher crystallinity index (60%) [22] than TOCN OPEFB (55%). Furthermore, the increase of T_{max} with the presence of NC can be attributed to the efficient cross-linking between NC and PMVEMA-PEG matrix [40].

4.2.3.7 Tensile tests

Mechanical properties of obtained films can be interpreted from tensile stress-strain curves (**Fig. 4.9**). Film made of CO and TO revealed high mechanical properties with stress strenght up to 97 MPa (**Table 4.3)**. Control film which made of PMVEMA/PEG only showed low tensile strength with the stress only 6 MPa (**Table 4.3)**. The addition of OPEFB-derived nanocellulose in PMVEMA-PEG matrix

increased maximum stress up to 33 % and 67 % by the addition of 5 wt% of CO and TO, respectively. Tensile strenghts of obtained films were higher compared to the previously reported study which made of PMVEMA-PEG foam and used high concentration of nanocellulose (> 5%) as additive using directional freezing method [26]. By comparing the results, TO5 showed higher reinforcing effect rather than CO5; eventhough CO had higher crystallininity than TO. It is emphasized the hypothese that cellulose nanofibers had greater reinforcing effect than cellulose nanocrystals. Previous study had reported that the addition of CNF yielded higher modulus than CNC at the same concentration of addition in PMVEMA-PEG foam via directional freezing [26]. This fact leads to the suggestion that fiber length is a critical factor in determining film properties, particularly in tensile strength. During gelation, long fiber tends to entangled and increased surface area of film. Furthermore, larger surface area caused distribution of force applied on film surface was wider than short fiber. Longer fibers showed higher tensile strenght compared to short fibers. This result was in a good accordance with the results previously reported by Fukuzumi and co-authors [42].

Table 4.3. Physical properties of obtained films

Sample	Modulus Young (MPa)	Tensile strengh (MPa)	Strain-to failure (%)	Water content (%)	Density (g/cm^3)
P100	45 ± 4	6 ± 2	0.3	8.8 ± 0.9	0.88 ± 0.2
CO100	69 ± 15	52 ± 11	0.8	8.1 ± 0.1	0.60 ± 0.4
TO100	75 ± 19	73 ± 28	1.2	15.3 ± 0.1	0.78 ± 0.1
TCS100	68 ± 10	46 ± 6	0.7	10.4 ± 0.4	0.76 ± 0.1
TCL100	55 ± 19	97 ± 29	1.8	6.4 ± 0.5	1.16 ± 0.5
CO5	70 ± 19	8 ± 4	0.15	8.8 ± 0.9	0.94 ± 0.2
TO5	72 ± 22	12 ± 9	0.2	8.4 ± 0.6	0.66 ± 0.1
TCS5	63 ± 9	10 ± 1	0.2	10.4 ± 0.4	0.77 ± 0.1
TCL5	82± 37	14 ± 7	0.2	7.6 ± 0.9	0.57 ± 0.3

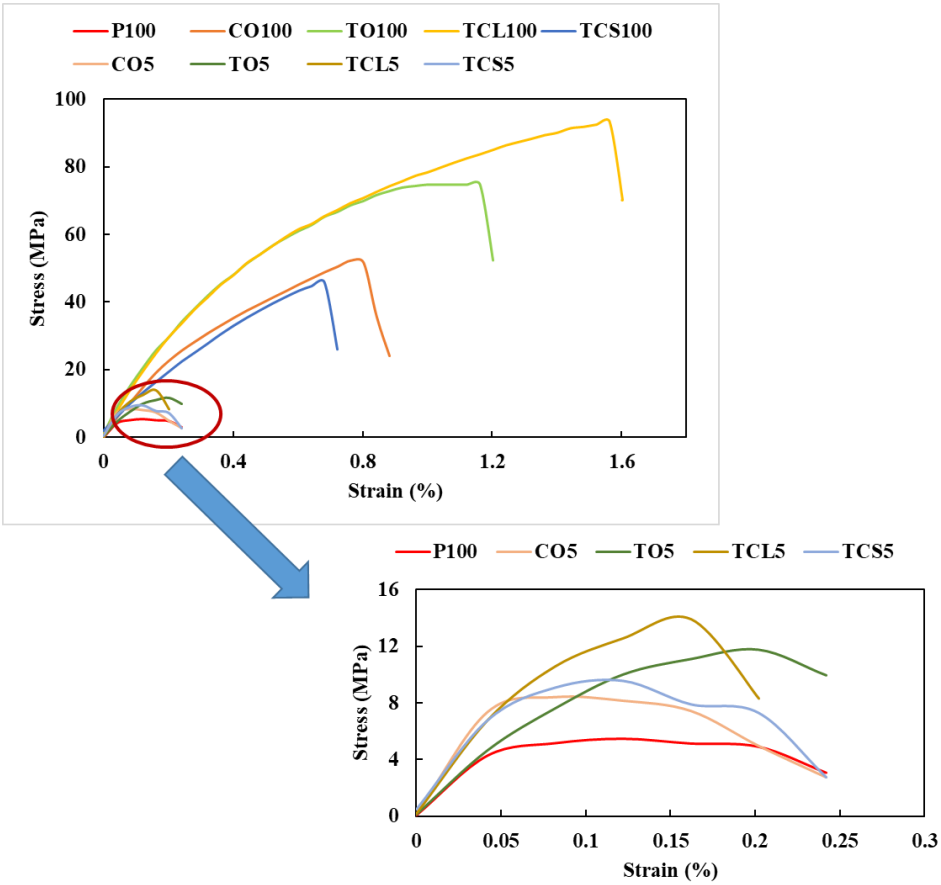

Figure 4.9. Tensile strength curves of PMVEMA-PEG-OPEFB nanocellulose

Mechanical properties of PMVEMA-PEG-nanocellulose film is relative low compared to nanocellulose film. Previous study reported the use of PMVEMA-PEG film in ratio 1:1 with low concentration of PMVEMA (5%) showed relatively low stress about 31 MPa and Young Modulus about 9 MPa [43].

Nanocellulose of OPEFB prepared using TEMPO-mediated oxidation (TO) revealed higher reinforcing effect than nanocellulose prepared by acid hydrolysis (CO). The formation of the reactive carboxyl groups on its surface due the mediated oxidation of OH groups is expected to increase the interactions with the polymeric matrix at the interfacial region, therefore TOCN had been examined as interfacial

strengthener in continuous fiber-reinforced polymer composite [44]. In addition, higher tensile properties of nanocellulose-loaded PMVEMA-PEG film due to higher structural integrity owing to molecular strain restriction and higher mechanical interlocking in the microstructure [6].

4.3 Comparison with Nanocellulose from Other Agricultural Residues as Reinforcing Agent

The rising interest towards environmental issue, the need more versatile polymer-based materials had led to increasing interest about polymer composites filled with natural organic fillers [45]. The interest of organic fillers increased because the use of inorganic fillers face the limitation in their processability, biocompatibility and biodegradability [46]. Nanocellulose (NC) is one of natural organic fillers that has been used in polymeric matrixes including polycaprolactone (PCL) [11], polypropylene [47], $LiClO_4$ doped ethylene oxide-epichlorohydrin (EO-EPI) copolymers [48], polyvinyl alcohol and polyacrilamide [49]. Interestingly, all nanocellulose used in those reported studies derived from non-wood materials such as from rami fibers; tunicate, sugarcane baggase and still revealed high mechanical properties improvement [11,47–49]. Utilization of nanocellulose as reinforcing agent gained significant research interest due to the possibility of exploring the stiffness and strength of cellulose crystals [50]. Therefore, the utilization of non-wood materials as raw material of nanocellulose, such as agricultural residue, is interesting to be explored.

4.3.1 Nanocellulose derived from sugarcane baggase

Isolation and characterization nanocellulose from sugarcane baggase (SCB) had been reported by a few researchers [51–54]. Nanocellulose produced by steam explosion followed by mechanical distengration yielded CNF-SCB with diameter 20–

40 nm [51]. Cellulose nanocrystals of SCB (CNC-SCB) produced by sulfuric acid hydrolysis had aspect ratio of 12 ± 15 [52]. Futhermore, other reported study revealed CNC-SCB produced by 64% sulfuric acid hydrolysis had length, diameter and aspect ratio of 247 nm; 10 nm and 24, respectively. This CNC-SCB then used as reinforcing filler of 3 wt% in starch film revealed water barrier properties and induced higher mechanical properties with the tensile strength reached 17 MPa and Young's modulus about 520 MPa [55]. In addition, the use of CNC-SCB produced by the same method in poly(vynil alcohol)/PVA and polyacrylamide (PCA) demonstrated an optimized mechanical properties by the addition of 5 wt% CNC-SCB yielding 90 MPa of tensile strenght and more than 3500 MPa of Young's Modulus [49].

4.3.2 Nanocellulose derived from oat husk

Isolation and characterization of oat husk-derived nanocellulose (OH-NC) had been reported be a few researchers [7,56,57]. Cellulose nanocrystals from oat husk (CNC-OH) produced by 65% of H_2SO_4 at 45°C for 45 minutes revealed crystallinity index of 62%, which is higher than its original pulp as 53% [7]. In addition, other study reported that CNC-OH produced by enzymatic scheme yielded higher crystallinity up to 90% [58]. Paschoal and co-authors reported that cellulose nanofibrils of oat husk (CNF-OH) produced using 64% of H_2SO_4 at 45°C for 30 min and 60 min showed negligible crytallinity [56]. TEMPO-mediated oxidation had been used to produce OH-NC, yielded TEMPO-oxidized cellulose nanofibrils of oat husk (TOCN-OH) with the carboxy content 0.70 mmol/g and used as film. The study reported that film made by 100% of TOCN-OH showed the highest surface roughness compared to the film made by 100% of TOCN from corn husk [57].

4.3.3 Nanocellulose from corn husk

Corn husk-derived nanocellulose (CH-NC) had been reported by several researchers [59–61]. Mendes and co-authors reported that the lower ratio of acid to corn husk fibers with longer time of acid hydrolysis (120 min) yielded highest crystallinity index compared with the higher ratio of acid to fiber in short time of hydrolysis [59]. Nanocellulose from corn husk made by 64 wt % of H_2SO_4 revealed lowest aspect ratio and crystallinity index (47%) compared to nanocellulose produced from TEMPO-mediated oxidation (83%) and high ultra sonication method (72%) [60]. In addition, CN-NC produced by high ultrasonication yielded high aspect ratio up to 394 with crystallinity index of 65%. The use of 1 wt% of thus CH-NC in poly(vynil alcohol) films revealed tensile strenght of 56 MPa and elongation 336% at break [61].

4.3.4 Nanocellulose from pineapple leaf fibers

Isolation and characterization of pineapple leaf fibers-derived nanocellulose (PLF-NC) was reported by a few researchers [62–65]. Pineapple leaf fibers-derives nanocellulose (PLF-NC) produced using 5% oxalic acid followed by steam explosion and sonication yielded high crystalline nanocellulose of 89% [62]. Cherian and co-authors reported that PLF-NC produced by 11% oxalic acid yielded cyrstallinity index about 74% with aspect ratio of 50 [63]. Nanocellulose from pineapple leaf fibers (PLF-NC) produced using acid hyrolysis 3.5 M HCl followed by high shear homogenization and ultrasonication had crystallinity index of 69% and 62%, respectively [64]. The use of 3 wt% of thus PLF-NC in potato starch matrix showed highest reinforcing efficiency and it becomes lower at 4 wt% of PLF-NC addition [66]. In addition, utilization of PLF-NC (5 wt%) in polyurethane matrix revealed highest tensile strenght (53 MPa) and Young modulus (992 MPa) [67].

4.3.5 Nanocellulose from barley straw and husk

Barley straw and husk-derived nanocellulose (BS-NC and BH-NC) extracted using enzymatically pre-treated and hydrolyzed using H_2SO_4 64 wt % at 45 °C. The resultant cellulose nanocrystals showed 270 nm in lenght and 15 nm in diameter for CNC barley straw (CNC-BS); and 150-250 nm in length and 10 nm in diameter for CNC barley husk (CNC-BH). Utilization of 3 wt% those CNCs in PVA and chitosan matrices revealed high tensile strenght, elongation break and Young's Modulus [68].

4.3.6 Nanocellulose from corncob

Isolation of corncob-derived nanocellulose (CC-NC) had been reported by a few researchers [69–71]. Nanocellulose of conrcob produced using H_2SO_4 62 wt% at 44 °C revealed high crystallinity about 71 % with needle-like shape [72]. In addition, CC-NC produced using TEMPO-mediated oxidation (CC-TOCN) had lower crystallinity of 49% but highest aspect ratio about 210 [70]. Corncob-cellulose nanocrystals (CC-CNC) produced by H_2SO_4 9.17 M for 60 had aspect ratio 53; used as a filler in PVA film. The ultimate tensile strenght increased by increasing the CC-CNC and reached 50 MPa, but the water vapor permeability was decreased [71].

The comparison of reinforcing performance of OPEFB-derived nanocellulose and other agricultural reasidues-derived nanocellulose were summarized in Table 4.4

Table 4.4. Comparison between NC of OPEFB and NC other agricultural residues

No	Source of nanocellulose	Preparation method	Properties	% Reinforcement	Matrix reinforced	Performance	Ref.
1	Sugarcane baggase	64% H_2SO_4	Cr.I: n.d AR: 24	3%	Starch+ glycerol	T: 17 MPa ε: 9% *Y*: 520 MPa	[55]
		60% H_2SO_4	Cr.I: 93% L: 170 nm D:35 nm	5%	PVA/PAAm	T: 90 MPa ε: 5% *Y:* 3500 MPa	[49]
2	Oat husk	65% H_2SO_4	Cr.I: 62% D:76 nm	5%	Whey protein isolate (WPI)	T: 4.2 MPa ε: 10% *Y:* 100 MPa	[7]

No	Source of nanocellulose	Preparation method	Properties	% Reinforcement	Matrix reinforced	Performance	Ref.
3	Corn husk	High ultrasonication	Cr.I:65% AR:394	1%	PVA	T: 56 MPa ε: 336% *Y:* n.d	[61]
4	Pineapple leaf fibres	11% oxalic acid followed by steam explosion	Cr.I:74% AR: 30	5%	Poly-urethane	T: 53 MPa ε: n.d *Y:* 992 MPa	[67]
5	Barley straw Barley husk	64% H_2SO_4+ultrasonication	Cr.I: n.d L 280±70 nm D 30±10 nm	1%	PVA+ chitosan	Barley straw T: 47 MPa ε: 160 % *Y:* 680 MPa Barley husk T: 63 MPa ε: 200% *Y:* 830 MPa	[68]
6	Corncob	9.17 M H_2SO_4 + ultrasonication	Cr.I 84% AR 53	9%	PVA	T: 50 MPa ε: n.d *Y:* n.d	[71]
7	Oil Palm Empty Fruit Bunches (OPEFB)	3M HCl	Cr.I 60% AR: 24±19	5%	PMVEMA/ PEG	T: 8 MPa ε: 0.15% *Y:* 70 MPa	This study
		TEMPO-mediated oxidation	Cr.I: 55% AR: 41±14	5%	PMVEMA/ PEG	T: 12 MPa ε: 0.2 % *Y:* 72 MPa	This study

Remarks:Cr.I=crystallinity index; AR= aspect ratio; L= length; D= diameter; PVA= poly(vinyl alcohol); PAAm=poly acrylamide; PMVEMA= poly(methyl vinyl-co-maleic acid); PEG= poly(ethylene glycol); T= tensile strength; ε= strain; *Y*= Young Modulus

Table 4.4 showed that OPEFB-derived nanocellulose had comparable performance with sugarcane baggase and oat husk, although it was lower compared to other agricultural residues. However, the use of nanocellulose as reinforcing agent in polymeric matrix greatly affected by the amount of loaded-nanocellulose, its dispersion and compatibility with the polymeric matrix. Better dispersion of individual cellulose nanofibers in the polymer matrix may improve composite properties [50]. Variation in width and length of resultant nanocellulose also affected the nanocellulose performance. The fiber dimension is depending on the starting materials, pre-treatments, apparatuses of mechanical fibrillation, which have explicit influence on the resultant nanocellulose-containing composite materials [73].

4.4 Conclusion

Nanocellulose from OPEFB had been successfully applied as reinforcing fillers in PMVEMA-PEG matrix. The OPEFB-derived nanocellulose addition improved the light transmittance, thermal stability and mechanical properties in low concentration (5 wt%). This finding provide other view of point for previous studies which used higher concentration (25%-75%) of nanocellulose in PMVEMA-PEG matrix. Comparison with other agricultural residues which applied in different matrix showed that OPEFB-derived nanocellulose had comparable mechanical properties with sugarcane baggase produced by acid hydrolysis and even higher from oat husk. However, the reinforcing performance of nanocellulose in polymeric matrix is greatly affected by the starting material and nanocellulose extraction condition. This study revealed that low cellulose content of non-wood starting material, OPEFB, had a potential utilization as reinforcing filler by improving the composite properties, particularly in light transmittance, thermal stability and mechanical properties.

4.5 References

[1] L.K. Kian, N. Saba, M. Jawaid, M.T.H. Sultan, A review on processing techniques of bast fibers nanocellulose and its polylactic acid (PLA) nanocomposites, Int. J. Biol. Macromol. 121 (2019) 1314–1328. doi:10.1016/j.ijbiomac.2018.09.040.

[2] C.J. Chirayil, L. Mathew, P.A. Hassan, M. Mozetic, S. Thomas, Rheological behaviour of nanocellulose reinforced unsaturated polyester nanocomposites,

Int. J. Biol. Macromol. 69 (2014) 274–281. doi:10.1016/j.ijbiomac.2014.05.055.

[3] R.J. Moon, A. Martini, J. Nairn, J. Simonsen, J. Youngblood, Cellulose nanomaterials review: structure, properties and nanocomposites., 2011. doi:10.1039/c0cs00108b.

[4] H. Kargarzadeh, M. Mariano, J. Huang, N. Lin, I. Ahmad, A. Dufresne, S. Thomas, Recent developments on nanocellulose reinforced polymer nanocomposites: A review, Polymer (Guildf). 132 (2017) 368–393. doi:10.1016/j.polymer.2017.09.043.

[5] S. Butylina, S. Geng, K. Oksman, Properties of as-prepared and freeze-dried hydrogels made from poly(vinyl alcohol) and cellulose nanocrystals using freeze-thaw technique, Eur. Polym. J. 81 (2016) 386–396. doi:10.1016/j.eurpolymj.2016.06.028.

[6] R. Pramanik, B. Ganivada, F. Ram, K. Shanmuganathan, A. Arockiarajan, Influence of nanocellulose on mechanics and morphology of polyvinyl alcohol xerogels, J. Mech. Behav. Biomed. Mater. 90 (2019) 275–283. doi:10.1016/j.jmbbm.2018.10.024.

[7] Z. Qazanfarzadeh, M. Kadivar, Properties of whey protein isolate nanocomposite films reinforced with nanocellulose isolated from oat husk, Int. J. Biol. Macromol. 91 (2016) 1134–1140. doi:10.1016/j.ijbiomac.2016.06.077.

[8] P. Hadi, M. Yang, H. Ma, X. Huang, H. Walker, B.S. Hsiao, Biofouling-resistant nanocellulose layer in hierarchical polymeric membranes: Synthesis,

characterization and performance, J. Memb. Sci. 579 (2019) 162–171. doi:10.1016/j.memsci.2019.02.059.

[9] H. Fukuzumi, T. Saito, S. Iwamoto, Y. Kumamoto, T. Ohdaira, R. Suzuki, Pore size determination of TEMPO-oxidized cellulose nanofibrils films by positron annihilation lifetime spectroscopy, Biomacromolecules. 12 (2011) 4057–4062. doi:10.1021/bm201079n.

[10] R. Endo, T. Saito, A. Isogai, TEMPO-oxidized cellulose nanofibril/poly(vinyl alcohol) composite drawn fibers, Polymer (Guildf). 54 (2013) 935–941. doi:10.1016/j.polymer.2012.12.035.

[11] Y. Habibi, A. Dufresne, Highly filled bionanocomposites from functionalized polysaccharide nanocrystals, Biomacromolecules. 9 (2008) 1974–1980. doi:10.1021/bm8001717.

[12] Y. Han, M. Yu, L. Wang, Soy protein isolate nanocomposites reinforced with nanocellulose isolated from licorice residue: Water sensitivity and mechanical strength, Ind. Crops Prod. 117 (2018) 252–259. doi:10.1016/j.indcrop.2018.02.028.

[13] M.B.K. Niazi, Z. Jahan, S.S. Berg, Ø.W. Gregersen, Mechanical, thermal and swelling properties of phosphorylated nanocellulose fibrils/PVA nanocomposite membranes, Carbohydr. Polym. 177 (2017) 258–268. doi:10.1016/j.carbpol.2017.08.125.

[14] J.D. Rusmirović, J.Z. Ivanović, V.B. Pavlović, V.M. Rakić, M.P. Rančić, V. Djokić, A.D. Marinković, Novel modified nanocellulose applicable as

reinforcement in high-performance nanocomposites, Carbohydr. Polym. 164 (2017) 64–74. doi:10.1016/j.carbpol.2017.01.086.

[15] B. Deepa, E. Abraham, N. Cordeiro, M. Mozetic, A.P. Mathew, K. Oksman, M. Faria, S. Thomas, L.A. Pothan, Utilization of various lignocellulosic biomass for the production of nanocellulose: a comparative study, Cellulose. 22 (2015) 1075–1090. doi:10.1007/s10570-015-0554-x.

[16] W. Stelte, A. Anandi, Preparation and and characterization of cellulose nanofibers from two commercial hardwood and softwood pulps, Ind. Eng. Chem. Res. 48 (2009) 11211–11219. doi:10.1021/ie9011672.

[17] O. Nechyporchuk, M.N. Belgacem, J. Bras, Production of cellulose nanofibrils: A review of recent advances, Ind. Crop. Prod. 93 (2016) 2–25. doi:10.1016/j.indcrop.2016.02.016.

[18] Z.A.Z. Azrina, M.D.H. Beg, M.Y. Rosli, R. Ramli, N. Junadi, A.K.M.M. Alam, Spherical nanocrystalline cellulose (NCC) from oil palm empty fruit bunch pulp via ultrasound assisted hydrolysis, Carbohydr. Polym. 162 (2017) 115–120. doi:10.1016/j.carbpol.2017.01.035.

[19] F. Fahma, S. Iwamoto, N. Hori, T. Iwata, A. Takemura, Isolation , preparation , and characterization of nanofibers from oil palm empty-fruit-bunch (OPEFB), Cellulose. 17 (2010) 977–985. doi:10.1007/s10570-010-9436-4.

[20] M. Jonoobi, A. Khazaeian, P.M. Tahir, S.S. Azry, K. Oksman, Characteristics of cellulose nanofibers isolated from rubberwood and empty fruit bunches of

oil palm using chemo-mechanical process, Cellulose. 18 (2011) 1085–1095. doi:10.1007/s10570-011-9546-7.

[21] M.K.M. Haafiz, A. Hassan, Z. Zakaria, I.M. Inuwa, Isolation and characterization of cellulose nanowhiskers from oil palm biomass microcrystalline cellulose, Carbohydr. Polym. 103 (2014) 119–125. doi:10.1016/j.carbpol.2013.11.055.

[22] N. Hastuti, K. Kanomata, T. Kitaoka, Hydrochloric Acid Hydrolysis of Pulps from Oil Palm Empty Fruit Bunches to Produce Cellulose Nanocrystals, J. Polym. Environ. 26 (2018) 3698–3709. doi:10.1007/s10924-018-1248-x.

[23] Q. Chen, Y. Liu, G. Chen, A comparative study on the starch-based biocomposite films reinforced by nanocellulose prepared from different non-wood fibers, Cellulose. 26 (2019) 2425–2435. doi:10.1007/s10570-019-02254-x.

[24] D. Jun, Z. Guomin, P. Mingzhu, Z. Leilei, L. Dagang, Z. Rui, Crystallization and mechanical properties of reinforced PHBV composites using melt compounding: Effect of CNCs and CNFs, Carbohydr. Polym. 168 (2017) 255–262. doi:10.1016/j.carbpol.2017.03.076.

[25] L. Goetz, A. Mathew, K. Oksman, P. Gatenholm, A.J. Ragauskas, A novel nanocomposite film prepared from crosslinked cellulosic whiskers, Carbohydr. Polym. 75 (2009) 85–89. doi:10.1016/j.carbpol.2008.06.017.

[26] L. Liang, C. Huang, N. Hao, A.J. Ragauskas, Cross-linked poly(methyl vinyl ether-co-maleic acid)/poly(ethylene glycol)/nanocellulosics foams via

directional freezing, Carbohydr. Polym. 213 (2019) 346–351. doi:10.1016/j.carbpol.2019.02.073.

[27] M. Asad, N. Saba, A.M. Asiri, M. Jawaid, E. Indarti, W.D. Wanrosli, Preparation and characterization of nanocomposite films from oil palm pulp nanocellulose/poly (Vinyl alcohol) by casting method, Carbohydr. Polym. 191 (2018) 103–111. doi:10.1016/j.carbpol.2018.03.015.

[28] B.K. Tiwari, K. Muthulumarappan, C.P. O'Donnell, P.J. Cullen, Effects of sonication on the kinetics of orange juice quality parameters, J Agric Food Chem. 56 (2008) 2423–2428. doi:10.1021/jf073503y.

[29] K. Tsuboi, S. Yokota, T. Kondo, Difference between bamboo- and wood-derived cellulose nanofibers prepared by the aqueous counter collision method, Nord. Pulp Pap. Res. J. 29 (2014) 69–76. doi:10.3183/npprj-2014-29-01-p069-076.

[30] M. Takahashi, K. Iyoda, T. Miyauchi, S. Ohkido, M. Tahashi, K. Wakita, Preparation and characterization of Eu:Ti codoped LiNbO3 films prepared by the sol–gel method, J. Appl. Phys. 106 (2009) 044102. doi:10.1063/1.3204023.

[31] H. Fukuzumi, T. Saito, A. Isogai, Influence of TEMPO-oxidized cellulose nanofibril length on film properties, Carbohydr. Polym. 93 (2013) 172–177. doi:10.1016/j.carbpol.2012.04.069.

[32] K. Syverud, G. Chinga-Carrasco, J. Toledo, P.G. Toledo, A comparative study of Eucalyptus and Pinus radiata pulp fibres as raw materials for

production of cellulose nanofibrils, Carbohydr. Polym. 84 (2011) 1033–1038. doi:10.1016/j.carbpol.2010.12.066.

[33] M. Nogi, S. Iwamoto, A.N. Nakagaito, H. Yano, Optically Transparent Nanofiber Paper, Adv. Mater. 21 (2009) 1595–1598. doi:10.1002/adma.200803174.

[34] R. Villalobos, J. Chanona, P. Hernández, G. Gutiérrez, A. Chiralt, Gloss and transparency of hydroxypropyl methylcellulose films containing surfactants as affected by their microstructure, Food Hydrocoll. 19 (2005) 53–61. doi:10.1016/j.foodhyd.2004.04.014.

[35] N.D. A Manaf, K. Fukuda, Z.A. Subhi, M.F. Mohd Radzi, Influences of surface roughness on the water adsorption on austenitic stainless steel, Tribol. Int. 136 (2019) 75–81. doi:10.1016/j.triboint.2019.03.014.

[36] Z.A. Subhi, T. Morita, K. Fukuda, Analysis of humidity effects on early stage of sliding, Procedia Eng. 68 (2013) 199–204. doi:10.1016/j.proeng.2013.12.168.

[37] X. Zheng, S. Fu, Reconstructing micro/nano hierarchical structures particle with nanocellulose for superhydrophobic coatings, Colloids Surfaces A Physicochem. Eng. Asp. 560 (2019) 171–179. doi:10.1016/j.colsurfa.2018.10.005.

[38] A. Patras, N.P. Brunton, B.K. Tiwari, F. Butler, Stability and Degradation Kinetics of Bioactive Compounds and Colour in Strawberry Jam during

Storage, Food Bioprocess Technol. 4 (2011) 1245–1252. doi:10.1007/s11947-009-0226-7.

[39] J.P. Reddy, J.W. Rhim, Characterization of bionanocomposite films prepared with agar and paper-mulberry pulp nanocellulose, Carbohydr. Polym. 110 (2014) 480–488. doi:10.1016/j.carbpol.2014.04.056.

[40] S.S. Nair, J. Zhu, Y. Deng, A.J. Ragauskas, Hydrogels prepared from cross-linked nanofibrillated cellulose, ACS Sustain. Chem. Eng. Eng. 2 (2014) 772–780. doi:10.1021/sc400445t.

[41] H. Fukuzumi, T. Saito, Y. Okita, A. Isogai, Thermal stabilization of TEMPO-oxidized cellulose, Polym. Degrad. Stab. 95 (2010) 1502–1508. doi:10.1016/j.polymdegradstab.2010.06.015.

[42] H. Fukuzumi, T. Saito, A. Isogai, Influence of TEMPO-oxidized cellulose nanofibril length on film properties, Carbohydr. Polym. 93 (2013) 172–177. doi:10.1016/j.carbpol.2012.04.069.

[43] T.R. Raj Singh, P.A. McCarron, A.D. Woolfson, R.F. Donelly, Physochemicql characterization of poly(ethylene glycol) plasticized poly(methyl vinyl ether-co-maleic acid) films, J. Appl. Polym. Sci. 112 (2009) 2792–2799. doi:10.1002/app.29523.

[44] B.E.B. Uribe, E.M.S. Chiromito, A.J.F. Carvalho, R. Arenal, J.R. Tarpani, TEMPO-oxidized cellulose nanofibers as interfacial strengthener in

continuous-fiber reinforced polymer composites, Mater. Des. 133 (2017) 340–348. doi:10.1016/j.matdes.2017.08.004.

[45] F.P. La Mantia, M. Morreale, Green composites: A brief review, Compos. Part A Appl. Sci. Manuf. 42 (2011) 579–588. doi:10.1016/j.compositesa.2011.01.017.

[46] M. Roohani, Y. Habibi, N.M. Belgacem, G. Ebrahim, A.N. Karimi, A. Dufresne, Cellulose whiskers reinforced polyvinyl alcohol copolymers nanocomposites, Eur. Polym. J. 44 (2008) 2489–2498. doi:10.1016/j.eurpolymj.2008.05.024.

[47] N. Ljungberg, C. Bonini, F. Bortolussi, C. Boisson, L. Heux, J.Y. Cavaillé, New nanocomposite materials reinforced with cellulose whiskers in atactic polypropylene: Effect of surface and dispersion characteristics, Biomacromolecules. 6 (2005) 2732–2739. doi:10.1021/bm050222v.

[48] M. Schroers, A. Kokil, C. Weder, Solid polymer electrolytes based on nanocomposites of ethylene oxide-epichlorohydrin copolymers and cellulose whiskers, J. Appl. Polym. Sci. 93 (2004) 2883–2888. doi:10.1002/app.20870.

[49] A. Mandal, D. Chakrabarty, Characterization of nanocellulose reinforced semi-interpenetrating polymer network of poly(vinyl alcohol) & polyacrylamide composite films, Carbohydr. Polym. 134 (2015) 240–250. doi:10.1016/j.carbpol.2015.07.093.

[50] K.Y. Lee, Y. Aitomäki, L.A. Berglund, K. Oksman, A. Bismarck, On the use of nanocellulose as reinforcement in polymer matrix composites, Compos. Sci. Technol. 105 (2014) 15–27. doi:10.1016/j.compscitech.2014.08.032.

[51] Y.H. Feng, T.Y. Cheng, W.G. Yang, P.T. Ma, H.Z. He, X.C. Yin, X.X. Yu, Characteristics and environmentally friendly extraction of cellulose

nanofibrils from sugarcane bagasse, Ind. Crops Prod. 111 (2018) 285–291. doi:10.1016/j.indcrop.2017.10.041.

[52] R.M. Leão, P.C. Miléo, J.M.L.L. Maia, S.M. Luz, Environmental and technical feasibility of cellulose nanocrystal manufacturing from sugarcane bagasse, Carbohydr. Polym. 175 (2017) 518–529. doi:10.1016/j.carbpol.2017.07.087.

[53] P.R. Sharma, A.J. Varma, Functional nanoparticles obtained from cellulose: Engineering the shape and size of 6-carboxycellulose, Chem. Commun. 49 (2013) 8818–8820. doi:10.1039/c3cc44551h.

[54] A. Mandal, D. Chakrabarty, Isolation of nanocellulose from waste sugarcane bagasse (SCB) and its characterization, Carbohydr. Polym. 86 (2011) 1291–1299. doi:10.1016/j.carbpol.2011.06.030.

[55] A.M. Slavutsky, M.A. Bertuzzi, Water barrier properties of starch films reinforced with cellulose nanocrystals obtained from sugarcane bagasse, Carbohydr. Polym. 110 (2014) 53–61. doi:10.1016/j.carbpol.2014.03.049.

[56] G.B. Paschoal, C.M.O. Muller, G.M. Carvalho, C.A. Tischer, S. Mali, Isolation and characterization of nanofibrillated cellulose from oat hulls, Quim. Nova. 38 (2015) 478–482. doi:10.5935/0100-4042.20150029.

[57] F. Valdebenito, M. Pereira, G. Ciudad, L. Azocar, R. Briones, G. Chinga-Carrasco, On the nanofibrillation of corn husks and oat hulls fibres, Ind. Crops Prod. 95 (2017) 528–534. doi:10.1016/j.indcrop.2016.11.006.

[58] J.P. de Oliveira, G.P. Bruni, S.L.M. el Halal, F.C. Bertoldi, A.R.G. Dias, E. da R. Zavareze, Cellulose nanocrystals from rice and oat husks and their

application in aerogels for food packaging, Int. J. Biol. Macromol. 124 (2019) 175–184. doi:10.1016/j.ijbiomac.2018.11.205.

[59] C.A.D.C. Mendes, N.M.S. Ferreira, C.R.G. Furtado, A.M.F. De Sousa, Isolation and characterization of nanocrystalline cellulose from corn husk, Mater. Lett. 148 (2015) 26–29. doi:10.1016/j.matlet.2015.02.047.

[60] X. Yang, F. Han, C. Xu, S. Jiang, L. Huang, L. Liu, Z. Xia, Effects of preparation methods on the morphology and properties of nanocellulose (NC) extracted from corn husk, Ind. Crops Prod. 109 (2017) 241–247. doi:10.1016/j.indcrop.2017.08.032.

[61] S. Xiao, R. Gao, L.K. Gao, J. Li, Poly(vinyl alcohol) films reinforced with nanofibrillated cellulose (NFC) isolated from corn husk by high intensity ultrasonication, Carbohydr. Polym. 136 (2015) 1027–1034. doi:10.1016/j.carbpol.2015.09.115.

[62] E. Abraham, B. Deepa, L.A. Pothan, M. Jacob, S. Thomas, U. Cvelbar, R. Anandjiwala, Extraction of nanocellulose fibrils from lignocellulosic fibres: A novel approach, Carbohydr. Polym. 86 (2011) 1468–1475. doi:10.1016/j.carbpol.2011.06.034.

[63] B.M. Cherian, A.L. Leão, S.F. de Souza, S. Thomas, L.A. Pothan, M. Kottaisamy, Isolation of nanocellulose from pineapple leaf fibres by steam

explosion, Carbohydr. Polym. 81 (2010) 720–725. doi:10.1016/j.carbpol.2010.03.046.

[64] M. Mahardika, H. Abral, A. Kasim, S. Arief, M. Asrofi, Production of Nanocellulose from Pineapple Leaf Fibers via High-Shear Homogenization and Ultrasonication, Fibers. 6 (2018) 28. doi:10.3390/fib6020028.

[65] K. Wahyuningsih, E.S. Iriani, F. Fahma, Utilization of cellulose from pineapple leaf fibers as nanofiller in polyvinyl alcohol-based film, Indones. J. Chem. 16 (2016) 181–189. doi:10.14499/ijc-v16i2p181-189.

[66] P. Balakrishnan, M.S. Sreekala, M. Kunaver, M. Huskić, S. Thomas, Morphology, transport characteristics and viscoelastic polymer chain confinement in nanocomposites based on thermoplastic potato starch and cellulose nanofibers from pineapple leaf, Carbohydr. Polym. 169 (2017) 176–188. doi:10.1016/j.carbpol.2017.04.017.

[67] B.M. Cherian, A.L. Leão, S.F. De Souza, L.M.M. Costa, G.M. De Olyveira, M. Kottaisamy, E.R. Nagarajan, S. Thomas, Cellulose nanocomposites with nanofibres isolated from pineapple leaf fibers for medical applications, Carbohydr. Polym. 86 (2011) 1790–1798. doi:10.1016/j.carbpol.2011.07.009.

[68] E. Fortunati, P. Benincasa, G.M. Balestra, F. Luzi, A. Mazzaglia, D. Del Buono, D. Puglia, L. Torre, Revalorization of barley straw and husk as precursors for cellulose nanocrystals extraction and their effect on PVA_CH

nanocomposites, Ind. Crops Prod. 92 (2016) 201–217. doi:10.1016/j.indcrop.2016.07.047.

[69] F.I. Ditzel, E. Prestes, B.M. Carvalho, I.M. Demiate, L.A. Pinheiro, Nanocrystalline cellulose extracted from pine wood and corncob, Carbohydr. Polym. 157 (2017) 1577–1585. doi:10.1016/j.carbpol.2016.11.036.

[70] C. Liu, B. Li, H. Du, D. Lv, Y. Zhang, G. Yu, X. Mu, H. Peng, Properties of nanocellulose isolated from corncob residue using sulfuric acid, formic acid, oxidative and mechanical methods, Carbohydr. Polym. 151 (2016) 716–724. doi:10.1016/j.carbpol.2016.06.025.

[71] H.A. Silvério, W.P. Flauzino Neto, D. Pasquini, Effect of incorporating cellulose nanocrystals from corncob on the tensile, thermal and barrier properties of poly(vinyl alcohol) nanocomposites, J. Nanomater. 2013 (2013). doi:10.1155/2013/289641.

[72] F.I. Ditzel, E. Prestes, B.M. Carvalho, I.M. Demiate, L.A. Pinheiro, Nanocrystalline cellulose extracted from pine wood and corncob, Carbohydr. Polym. 157 (2017) 1577–1585. doi:10.1016/j.carbpol.2016.11.036.

[73] A. Isogai, Wood nanocelluloses: Fundamentals and applications as new bio-based nanomaterials, J. Wood Sci. 59 (2013) 449–459. doi:10.1007/s10086-013-1365-z.

Chapter 5

Concluding Remarks

Nanocellulose extraction from low cost agricultural residue, oil palm empty fruit bunches (OPEFB), had been successfully conducted using hydrochloric acid to produce cellulose nanocrystals and TEMPO-mediated oxidation to produce TEMPO-oxidized cellulose nanofibrils. Microscopy analysis revealed that nanoscale dimension had been obtained based on microcopy analysis and to have comparable properties with woody CNC/TOCN. The obtained nanocellulose had been applied in bioenergy application and as reinforcing agent in polymeric matrix.

Reactive carboxylate groups of OPEFB-derived TOCN were effective to induce microenvironment of bacteria strain-producing butanol by inducing electrostatic repulsion between anionic carboxylate groups on the surface of TOCNs and negatively-charged bacterial cells. This induced good bacterial dispersibility in the medium, improving the total butanol production in broth. In the immobilized cell method, crosslinking of anionic carboxylate groups of TOCNs and alginate *via* Ca^{2+} ions to form alginate beads induced favorable 3-D networks for cell entrapment, and possibly provided better microenvironment for bacterial growth, then higher DCW and higher total butanol concentration were achieved. The addition of OPEFB-derived nanocellulose in alginate matrix followed by cross-linking with Ca^{2+} induced pore size formation and slightly increased the flux capacity in pervaporation membrane for water-ethanol separation. However, its performance was lower but still comparable compared with the performance of woody TOCN in alginate matrix (w-TOCN-A) in flux capacity, water selectivity and mechanical properties.

Utilization of OPEFB-derived nanocellulose as reinforcing filler in PMVEMA-PEG matrix showed remarkable properties in thermal stability and mechanical properties by only 5 wt% of nanocellulose addition, much lower than previous reported studies (25%–75%). Nanocellulose in form of TOCN-OPEFB exhibited higher reinforcing performance compared to CNC-OPEFB.

Evidently, the advantages of OPEFB-derived nanocellulose functionalization gained from its nanodispersion, the optimum amount of nanocellulose addition and the interfacial interaction that still remained limited to be elucidated. However, these finding open up utilization of low cost agricultural residue, OPEFB, for wider application by advanced nanocellulose technology.

Appendix

BET analysis of obtained membranes in pervaporation experimental (**Chapter 3, section 3.3).**

1. TOCN-OPEFB (op-TOCN-A)

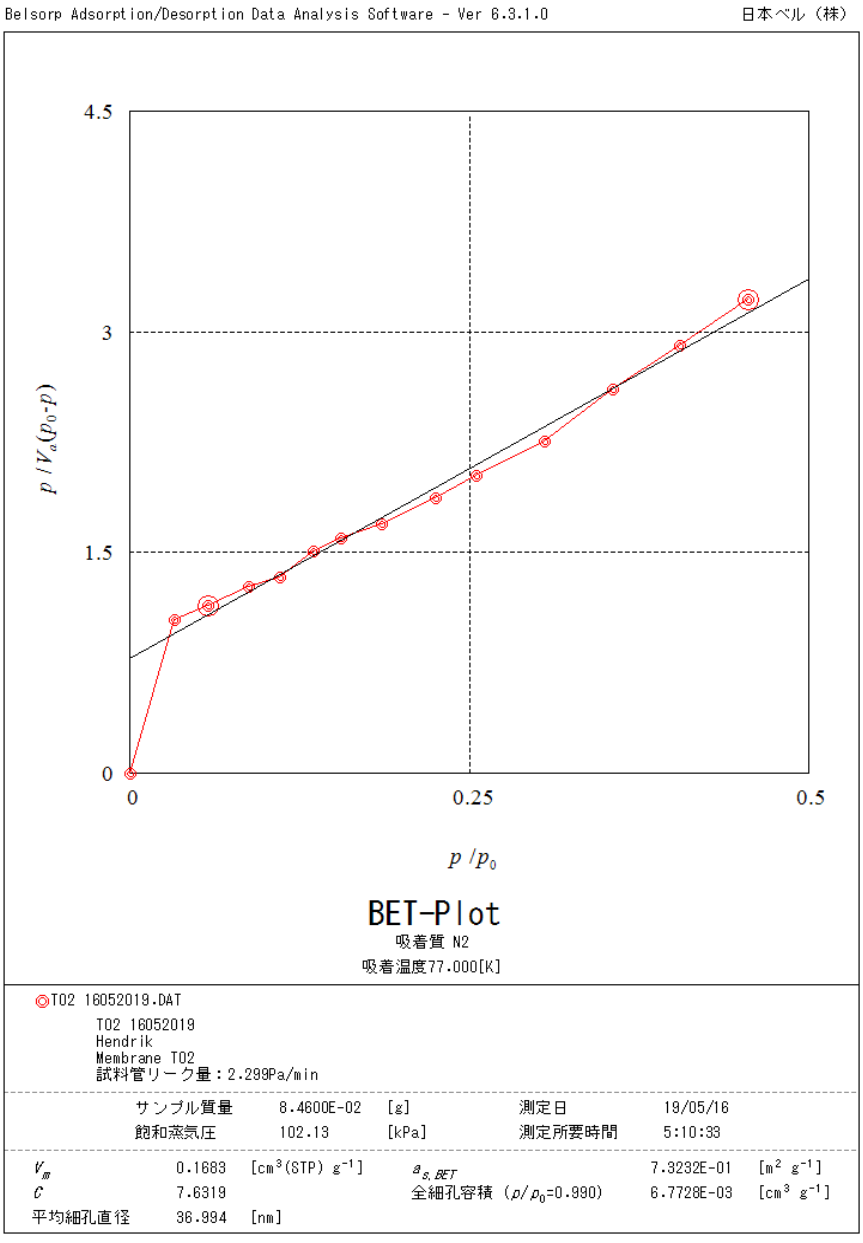

2. Woody TOCN from company (w-TOCN-A)

Belsorp Adsorption/Desorption Data Analysis Software - Ver 6.3.1.0　　日本ベル（株）

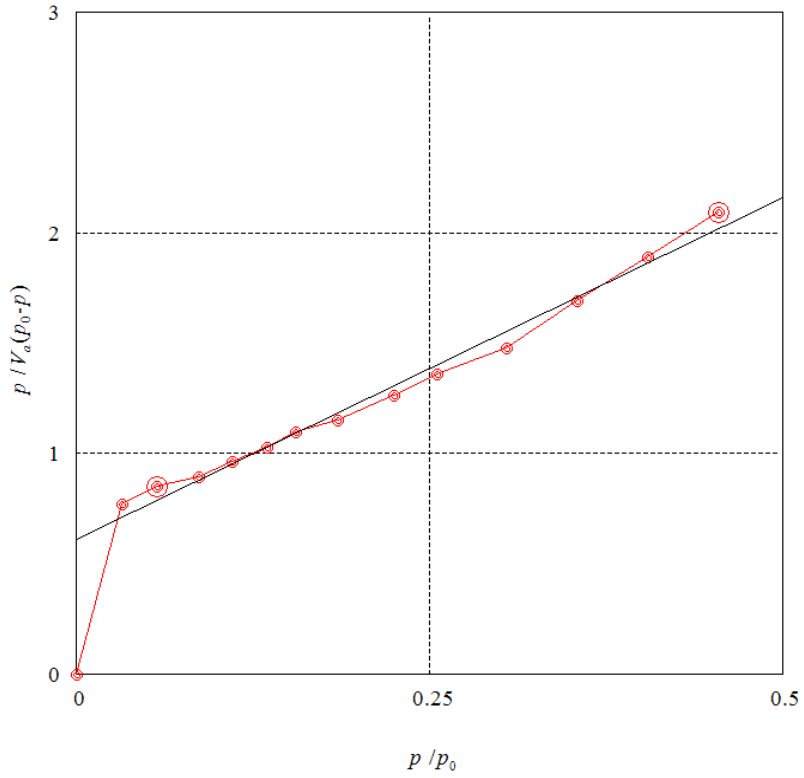

BET-Plot
吸着質 N2
吸着温度77.000[K]

◎TC 17052019.DAT
TC 17052019
Hendrik
Membrane TC Redo
試料管リーク量：3.416Pa/min

サンプル質量	8.2200E-02	[g]	測定日	19/05/17	
飽和蒸気圧	102.21	[kPa]	測定所要時間	5:17:34	

V_m	0.2701	[cm³(STP) g⁻¹]	$a_{S,BET}$	1.1758E+00	[m² g⁻¹]
C	6.0509		全細孔容積 (p/p_0=0.990)	6.7190E-03	[cm³ g⁻¹]
平均細孔直径	22.858	[nm]			

3. Control membrane (Alginate without TOCN)

Belsorp Adsorption/Desorption Data Analysis Software - Ver 6.3.1.0　　日本ベル（株）

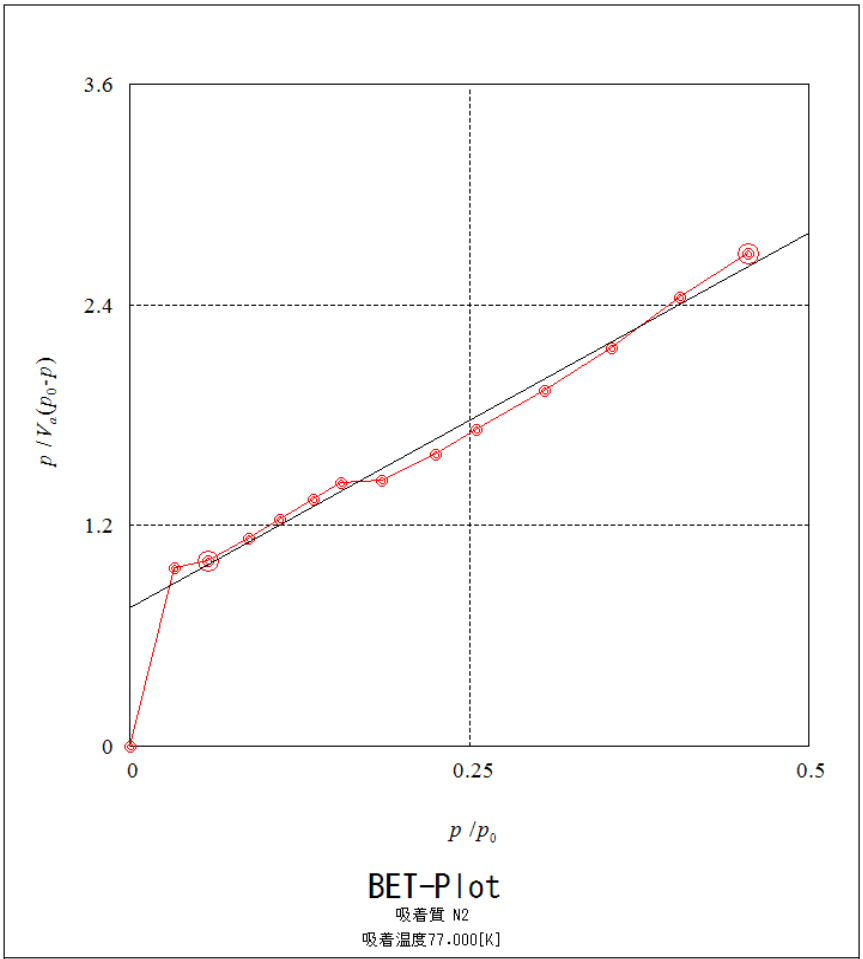

◎C 17052019.DAT

C 17052019
Hendrik
Membrane C Redo
試料管リーク量：2.111Pa/min

サンプル質量	8.1700E-02	[g]	測定日	19/05/17	
飽和蒸気圧	102.21	[kPa]	測定所要時間	5:19:54	

V_m	0.2075	[cm³(STP) g⁻¹]	$a_{S,BET}$	9.0307E-01	[m² g⁻¹]
C	6.3925		全細孔容積 (p/p_0=0.990)	6.7760E-03	[cm³ g⁻¹]
平均細孔直径	30.013	[nm]			

4. PTFE membrane

Belsorp Adsorption/Desorption Data Analysis Software - Ver 6.3.1.0　　日本ベル（株）

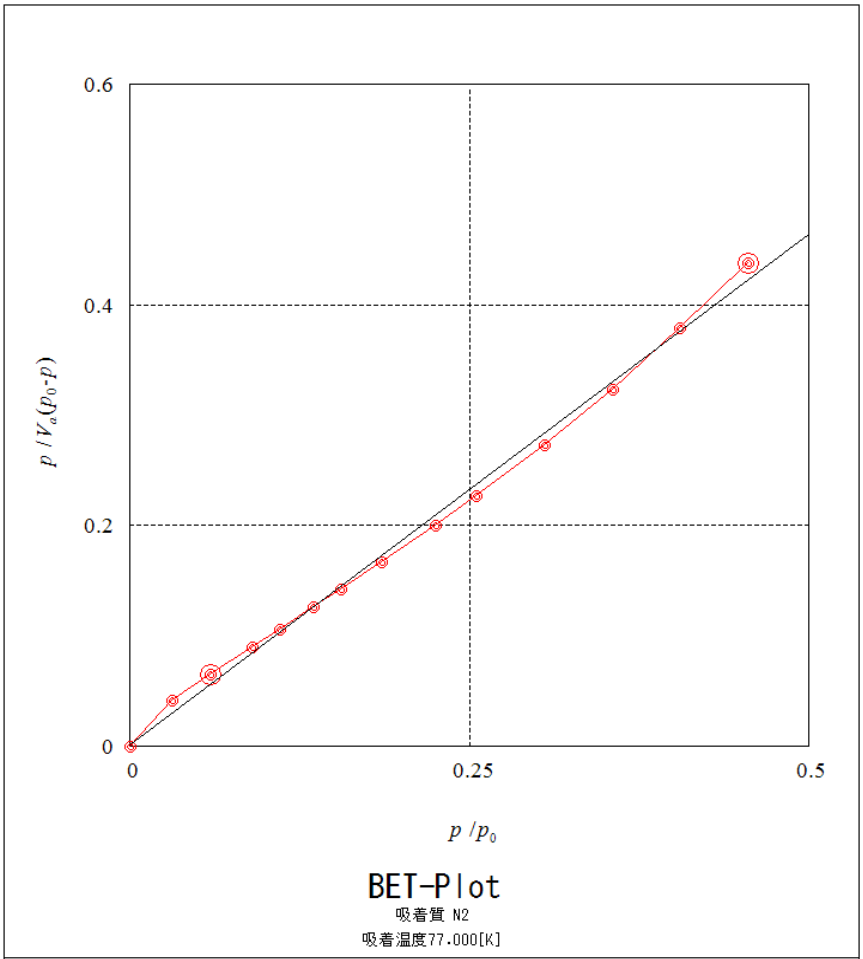

◎PTFE 01062019.DAT
PTFE
Hendrik
PTFE
試料管リーク量：2.786Pa/min

	サンプル質量	0.1147 [g]		測定日	19/06/01
	飽和蒸気圧	102.10 [kPa]		測定所要時間	7:15:55

V_m	1.0796	[cm^3(STP) g^{-1}]	$a_{S,BET}$	4.6988E+00	[m^2 g^{-1}]
C	1627.7		全細孔容積 (p/p_0=0.990)	3.2314E-02	[cm^3 g^{-1}]
平均細孔直径	27.508	[nm]			